**Author(s):** Majola, S. N. T.; Shi, Z.; Song, B. Y.; Li, Z. P.; Zhang, S. Q.; Bark, R. A.; Sharpey-Schafer, J. F.; Aschman, D. G.; Bvumbi, S. P.; Bucher, T. D.; Cullen, D. M.; Dinoko, T. S.; Easton, J. E.; Erasmus, N.; Greenlees, P. T.; Hartley, D. J.; Hirvonen, J.; Korichi, A.; Jakobsson, U.; Jones, P.; Jongile, S.; Julin, R.; Juutinen, S.; Ketelhut, S.; Kheswa, B. V.; Khumalo, N. A.; Lawrie, E. A.; Lawrie, J. J.; Lindsay, R.; Madiba, T.

**Title:** β and γ bands in N = 88, 90, and 92 isotones investigated with a five-dimensional collective Hamiltonian based on covariant density functional theory : Vibrations, shape coexistence, and superdeformation

**Year:** 2019

**Version:** Published version

# $\beta$ and $\gamma$ bands in $N = 88$, 90, and 92 isotones investigated with a five-dimensional collective Hamiltonian based on covariant density functional theory: Vibrations, shape coexistence, and superdeformation

S. N. T. Majola,[1,2,3,4] Z. Shi,[5] B. Y. Song,[6] Z. P. Li,[6] S. Q. Zhang,[7] R. A. Bark,[2] J. F. Sharpey-Schafer,[8] D. G. Aschman,[4] S. P. Bvumbi,[3] T. D. Bucher,[2,9] D. M. Cullen,[10,11] T. S. Dinoko,[2,12] J. E. Easton,[2,8] N. Erasmus,[2,8] P. T. Greenlees,[10] D. J. Hartley,[13] J. Hirvonen,[10] A. Korichi,[14] U. Jakobsson,[10] P. Jones,[2] S. Jongile,[1,2,9] R. Julin,[10] S. Juutinen,[10] S. Ketelhut,[10] B. V. Kheswa,[2,3] N. A. Khumalo,[2,8] E. A. Lawrie,[2,8] J. J. Lawrie,[2] R. Lindsay,[8] T. E. Madiba,[2,8] L. Makhathini,[2,9] S. M. Maliage,[2,8] B. Maqabuka,[2,8] K. L. Malatji,[2,9] P. L. Masiteng,[2,3,8] P. I. Mashita,[2,8] L. Mdletshe,[1,2] A. Minkova,[15] L. Msebi,[2,8] S. M. Mullins,[2] J. Ndayishimye,[2] D. Negi,[2,16] A. Netshiya,[2,8] R. Newman,[9] S. S. Ntshangase,[1] R. Ntshodu,[2] B. M. Nyakó,[17] P. Papka,[2,9] P. Peura,[10] P. Rahkila,[10] L. L. Riedinger,[18] M. A. Riley,[19] D. G. Roux,[20] P. Ruotsalainen,[10] J. J. Saren,[10] C. Scholey,[10] O. Shirinda,[2,9] M. A. Sithole,[2,8] J. Sorri,[10,21] M. Stankiewicz,[2,4] S. Stolze,[10,22] J. Timár,[17] J. Uusitalo,[10] P. A. Vymers,[2,9] M. Wiedeking,[2] and G. L. Zimba[2,3,10]

[1]*Department of Physics, University of Zululand, Private Bag X1001, Kwa Dlangezwa, 3886, South Africa*
[2]*iThemba LABS, National Research Foundation, P.O. Box 722, Somerset-West 7129, South Africa*
[3]*Department of Physics, University of Johannesburg, P.O. Box 524, Auckland Park 2006, South Africa*
[4]*Department of Physics, University of Cape Town, Private Bag X3, Rondebosch 7701, South Africa*
[5]*School of Physics and Nuclear Energy Engineering, Beihang University, Beijing 100191, China*
[6]*School of Physical Science and Technology, Southwest University, Chongqing, 400715, China*
[7]*State Key Laboratory of Nuclear Physics and Technology, School of Physics, Peking University, Beijing 100871, China*
[8]*Department of Physics, University of the Western Cape, Private Bag X17, Bellville 7535 South Africa*
[9]*Department of Physics, Stellenbosch University, Private Bag X1, Matieland, 7602, South Africa*
[10]*Department of Physics, P.O. Box 35, FI-40014 University of Jyvaskyla, Finland*
[11]*Schuster Laboratory, University of Manchester, Manchester M13 9PL, United Kingdom*
[12]*National Metrology Institute of South Africa, Private Bag x34, Lynnwood Ridge, Pretoria, 0040, South Africa*
[13]*Department of Physics, U.S. Naval Academy, Annapolis, Maryland 21402, USA*
[14]*CSNSM-IN2P3-CNRS, F-91405 Orsay Campus, France*
[15]*University of Sofia, Faculty of Physics, Sofia 1164, Bulgaria*
[16]*UM-DAE Centre for Excellence in Basic Sciences, Kalina, Mumbai 400098, India*
[17]*MTA Atomki, P.O. Box 51, H-4001 Debrecen, Hungary*
[18]*University of Tennessee, Department of Physics and Astronomy, Knoxville, Tennessee 37996, USA*
[19]*Department of Physics, Florida State University, Tallahassee, Florida 32306, USA*
[20]*Department of Physics, Rhodes University, P.O. Box 94, Grahamstown 6140, South Africa*
[21]*Sodankylä Geophysical Observatory, University of Oulu, Tähteläntie 62, FI-99600 Sodankylä*
[22]*Physics Division, Argonne National Laboratory, Argonne, Illinois 60439, USA*

(Received 4 July 2018; revised manuscript received 5 June 2019; published 30 October 2019)

A comprehensive systematic study is made for the collective $\beta$ and $\gamma$ bands in even-even isotopes with neutron numbers $N = 88$ to 92 and proton numbers $Z = 62$ (Sm) to 70 (Yb). Data, including excitation energies, $B(E0)$ and $B(E2)$ values, and branching ratios from previously published experiments are collated with new data presented for the first time in this study. The experimental data are compared to calculations using a five-dimensional collective Hamiltonian (5DCH) based on the covariant density functional theory (CDFT). A realistic potential in the quadrupole shape parameters $V(\beta, \gamma)$ is determined from potential energy surfaces (PES) calculated using the CDFT. The parameters of the 5DCH are fixed and contained within the CDFT. Overall, a satisfactory agreement is found between the data and the calculations. In line with the energy staggering $S(I)$ of the levels in the $2_\gamma^+$ bands, the potential energy surfaces of the CDFT calculations indicate $\gamma$-soft shapes in the $N = 88$ nuclides, which become $\gamma$ rigid for $N = 90$ and $N = 92$. The nature of the $0_2^+$ bands changes with atomic number. In the isotopes of Sm to Dy, they can be understood as $\beta$ vibrations, but in the Er and Yb isotopes the $0_2^+$ bands have wave functions with large components in a triaxial superdeformed minimum. In the vicinity of $^{152}$Sm, the present calculations predict a soft potential in the $\beta$ direction but do not find two coexisting minima. This is reminiscent of $^{152}$Sm exhibiting an $X(5)$ behavior. The model also predicts that the $0_3^+$ bands are of two-phonon nature, having an energy twice that of the $0_2^+$ band. This is in contradiction with the data and implies that other excitation modes must be invoked to explain their origin.

DOI: 10.1103/PhysRevC.100.044324

 

## I. INTRODUCTION

The Bohr Hamiltonian [1,2] predicts the existence of time-dependent $\beta$ and $\gamma$ quadrupole vibrations of the nuclear shape which have been associated with the first excited $K^\pi = 0_2{}^+$ and $K^\pi = 2_\gamma{}^+$ intrinsic states, respectively. The nature of these states has been studied extensively over the years [3–24]. However, despite many decades of research, a full understanding of these levels in even-even deformed nuclei remains elusive. In particular, low-lying rotational bands based on the first excited $0_2{}^+$ state, which are traditionally understood as $\beta$ vibrational bands, show properties at odds with this interpretation [15]. This may be due to the interplay of other modes of excitations contributing to their formation.

The most common competing low-lying $0_2{}^+$ configuration occurs when the nucleus exhibits shape coexistence [21]. Another mode of excitation that may further contribute to the formation of the first excited $0_2{}^+$ states is quadrupole pairing. Pairing is the well-known residual interaction that gives rise to the $0^+$ ground states in all even-even nuclei. In the simplest approximation, the strength of the interaction is independent of the orbitals near the Fermi surface, but in a more refined approximation, it is configuration dependent and may lead to the formation of low-lying first excited $0_2{}^+$ states that can compete with $\beta$ vibrations [25–32]. Experimentally, the challenge is to determine which of the three aforementioned excitations best describes the nature of the first excited $0_2{}^+$ states in the $A \approx 160$ mass region. While there is a long history of doubt being cast on the axial $\beta$ vibration interpretation of the first excited $K^\pi = 0_2{}^+$ rotational bands, the $K^\pi = 2_\gamma{}^+$ bands arise naturally due to axial symmetry breaking [33,34], be it static or dynamic.

In a search for a more accurate description of the so-called quadrupole vibrational bands, an extensive systematic method is carried out for the nuclides in the $A \approx 160$ mass region, between $N = 88$ and 92 and Sm to Yb. To this end, we have performed in-beam $\gamma$-ray spectroscopy measurements of $K^\pi = 0_2{}^+$ and $K^\pi = 2_\gamma{}^+$ bands in the even-even transitional deformed nuclei with neutron numbers $N = 88$, 90, and 92 with proton numbers $Z = 62$ to 70. In many instances, the $0_2{}^+$ bands and $\gamma$ bands have been extended or observed for the first time. The determination of a comprehensive set of level energies and branching ratios between bands allows their electromagnetic properties to be compared to nuclear models.

The theoretical approach adopted here, to come to an understanding of the properties of these bands, is to use a modern form of the Bohr Hamiltonian, a five-dimensional collective Hamiltonian (5DCH) based on the covariant density functional theory (CDFT) [35,36]. Rather than use a harmonic oscillator potential in $\beta$ and $\gamma$, a realistic potential $V(\beta, \gamma)$ is determined from the potential energy surfaces (PESs) calculated using the CDFT. Thereafter, the inertial parameters of the model are determined and a five-dimensional Bohr Hamiltonian is solved to give the resulting level scheme. The advantages of this approach are that the potential energy surfaces can automatically incorporate any shape-coexisting minima, allowing vibrational and shape-coexisting bands to be calculated on the same footing. An important point is that the parameters of pairing and the mean field are fixed.

In the next section, we present the experimental details. In Sec. III, we present our data on $K^\pi = 0_2{}^+$ and $K^\pi = 2_\gamma{}^+$ bands constituting new level schemes, $\gamma$-ray angular and polarization data, together with ratios of out-of-band to in-band $B(E2)$ ratios. These, together with literature values that fill in gaps in our data, including absolute $B(E2)$ values and $E0$ transitions rates, are then compared to the 5DCH-CDFT calculations in Sec. V.

## II. EXPERIMENTAL DETAILS

In total, data from 13 $\gamma$-$\gamma$ coincidence measurements have been analyzed to study the low spin spectroscopy of 12 different nuclides. Measurements for two species were carried out using the JUROGAM II arrays [37], while the rest were conducted using the AFRODITE array of iThemba LABS [38]. The experimental details including reactions, beam energies, statistics, and arrays are shown in Table I.

Of the 13 nuclides studied, we present here substantial revisions or additions only to the level schemes of $^{158,160}$Yb and $^{158}$Dy, with an emphasis on bands relevant to this study, namely the first excited $0^+$ (denoted as $0_2{}^+$ in this paper), ground, and $\gamma$ bands. Other level schemes deduced during the course of our investigations have been presented elsewhere [39–44]; however, in general, spectroscopic information such as directional correlation from oriented states (DCO) ratios, polarization anisotropies, and ratios of out-of-band to in-band $B(E2)$s have not previously been reported. Table II contains this spectroscopic information. In this study, the technique of DCO (or $R_{\rm DCO}$) has been used in order to assist in determining the multipolarities of new transitions and to confirm those of transitions deduced from previous studies. DCO matrices were prepared in such a way that transitions detected at a forward and/or backward angle $\theta_1$ are placed on one axis and the coincident transitions detected at an angle $\theta_2$, close to 90 °, are placed on the other axis. The $R_{\rm DCO}$ ratio is then defined by

$$R_{\rm DCO} = \frac{I(\gamma_1(\theta_2)\gamma_2(\theta_1))}{I(\gamma_1(\theta_1)\gamma_2(\theta_2))}, \tag{1}$$

where one of the transitions in the ratio is chosen to be of known stretched $E2$ character. In this work, $R_{\rm DCO}$ ratios for all three data sets give values close 0.6 and 1 when the second transition is of stretched pure dipole or quadrupole character, respectively. The DCO ratios for the JUROGAM II array were deduced using detectors in rings at 158° and 86° + 94°. Similarly, detectors at angles 135° and 90° were used to determine DCO ratios for data collected using the AFRODITE array. In order to determine the magnetic or electric nature of the transitions, linear polarization measurements have been performed. In effect, the polarization sensitivity possessed by both the AFRODITE and JUROGAM II arrays has allowed us to determine the electromagnetic nature of transitions reported in this work. In both cases, this was achieved by using clover detectors close to 90°. Here, the clovers are treated as Compton polarimeter apparatus. The polarization anisotropy

TABLE I. Experimental details showing apparatus and target-beam combinations that were used for the experiments analyzed in this work. The acquired statistics for each experiment are also shown in the table.

| Nucleus | Reaction(s) | Beam energy (MeV) | Target thickness (mg/cm$^2$) | Events $\times 10^9$ | Spectrometer(s) |
|---|---|---|---|---|---|
| $N = 88$ | | | | | |
| $^{158}$Yb | $^{144}$Sm($^{18}$O, 4$n$) | 78 | 3 | 2.0 $\gamma\gamma$ | AFRODITE |
| $^{156}$Er | $^{147}$Sm($^{12}$C, 3$n$) | 65 | 6 | 1.4 $\gamma\gamma$ | AFRODITE |
| $^{154}$Dy | $^{155}$Gd($^{3}$He, 4$n$) | 37.5 | 3.2 | 0.4 $\gamma\gamma$ | AFRODITE |
| $^{152}$Gd | $^{152}$Sm ($\alpha$, 4$n$) | 45 | 5 | 0.5 $\gamma\gamma$ | AFRODITE |
| $^{150}$Sm | $^{136}$Xe($^{18}$O, 4$n$) | 75 | 5 | 0.5 $\gamma\gamma$ | AFRODITE |
| | $^{148}$Nd($\alpha$, 2$n$) | 25 | 5 | 2.0 $\gamma\gamma\gamma$ | JUROGAM II |
| $N = 90$ | | | | | |
| $^{160}$Yb | $^{147}$Sm($^{16}$O, 3$n$) | 73 | 4 | 2.0 $\gamma\gamma$ | AFRODITE |
| $^{158}$Er | $^{150}$Sm($^{12}$C, 4$n$) | 65 | 1 | 0.4 $\gamma\gamma$ | AFRODITE |
| $^{156}$Dy | $^{155}$Gd($\alpha$, 3$n$) | 25 | 0.98 | 14 $\gamma\gamma$ | JUROGAM II |
| $^{154}$Gd | $^{152}$Sm($\alpha$, 2$n$) | 25 | 4 | 0.5 $\gamma\gamma$ | AFRODITE |
| $N = 92$ | | | | | |
| $^{162}$Yb | $^{150}$Sm($^{16}$O, 4$n$) | 83 | 3 | 7.4 $\gamma\gamma$ | AFRODITE |
| $^{160}$Er | $^{152}$Sm($^{12}$C, 4$n$) | 64 | 5 | 2.7 $\gamma\gamma$ | AFRODITE |
| $^{158}$Dy | $^{156}$Gd($\alpha$, 2$n$) | 27 | 11 | 1.1 $\gamma\gamma$ | AFRODITE |

$A_p$ can then be obtained using

$$A_p = \frac{aN_v - N_h}{aN_v + N_h}, \tag{2}$$

where $N_h$ and $N_v$ represent the number of $\gamma$ rays, which respectively scatter perpendicular or parallel to the beam direction between the crystals of a clover detector. The relative efficiency parameter $a$ is a normalization constant used to account for the asymmetry of a configuration. Pure stretched electric transitions such as $E1$s and $E2$s preferably scatter in the perpendicular direction with respect to the beam axis. As a result, a polarization anisotropy measurement $A_p$ yields a value with a positive sign for a stretched pure electric transition. Conversely, a value with a negative sign is obtained for a stretched pure magnetic dipole.

## III. LEVEL SCHEMES

### A. $N = 88$ isotones

The spectroscopy of low spin structures in $^{150}$Sm [39], $^{152}$Gd [39], and $^{154}$Dy [40,45] has been reported in our previous in-beam works. Here, a couple of levels have been added to both the odd and even spin $\gamma$ bands of $^{150}$Sm and $^{152}$Gd. In this work, only ratios of transition rates extracted for the above mentioned isotones, relating to the decays out of the $0_2{}^+$ and $2_\gamma{}^+$ bands, are reported for the first time.

For $^{158}$Yb, a completely new sequence of rotational levels built on the $(2_\gamma{}^+)$ state, as illustrated in Fig. 1, is observed. A spectrum supporting the placements of the transitions associated with this band is shown in Fig. 2(a). The spectrum gated on the 486-keV doublet, depopulating the $4^+$ and $8^+$ members, clearly shows the in-band transitions, namely the 486-, 488-, 555-, and 634-keV $\gamma$ rays. It also shows numerous interband transitions connecting this structure to the ground band. The 579- and 937-keV transitions decaying out of the 937-keV level of this band (to the $0^+$ and $2^+$ members of the ground band) confine the possible spin and parity assignments of the 937-keV level to either $I^\pi = 0^+$, $1^-$, $1^+$, or $2^+$. The DCO value for the 937-keV transition is consistent with it being a stretched $E2$ transition, and this leaves the $2^+$ as the most probable assignment for the 937-keV level. The DCO measurement that has been carried out for the 579-keV transition is indicative of this transition being a dipole, thus validating our spin and parity assignments for the 937-keV level. Similar decay patterns are observed for the transitions (i.e., 589-, 1065-, 508-, 1077-, 349-, 994-, and 903-keV transitions) decaying out of the 1423-, 1911-, and 2951-keV levels. The DCO measurements were successfully performed for most of these transitions. By applying analogous arguments used to infer spin and parity assignment for the 937-keV level, the 1423-, 1911-, 2397-, and 2951-keV levels have been respectively assigned to $I^\pi = 4^+$, $6^+$, $8^+$, and $10^+$. The 3585- and 4300-keV levels are assumed to be additional members of this sequence connected by stretched $E2$ transitions.

The spin and parity assignments and excitation energies of levels in this band relative to the ground band as well as its decay pattern identify it as the even spin sequence of the $2_\gamma{}^+$ band.

### B. $N = 90$ isotones

The spectroscopic information (such as level energies and branching ratios) of the first excited $0^+$ and $2^+$ bands in $^{152}$Sm are taken from Refs. [25,46].

The level schemes of $^{154}$Gd and $^{156}$Dy have been reported in our recent work, published in Refs. [41,47,48] and [42], respectively. Here, we report for the first time the DCO and polarization observables from some of these measurements, as well as $B(E2)$ ratios; see Table II. A detailed paper on $^{158}$Er has been completed and results will be published elsewhere [49].

A partial level scheme of low-lying positive-parity bands obtained in $^{160}$Yb is shown in Fig. 3. It is worth noting that a study of the negative-parity levels in $^{160}$Yb from the same experiment has been published in Ref. [50]. Spectra

TABLE II. Experimentally determined properties for the nuclei investigated in this study with the exception of $^{152}$Sm, $^{154}$Dy, $^{158}$Er, and $^{162}$Yb. Data include excitation levels $E_x$ (in keV), $\gamma$-ray energies $E$ (in keV), spins for the initial and final states, polarization anisotropy $A_p$, DCO ratios, and assigned multipolarities. All DCO ratios were deduced by gating on stretched $E2$ transitions with the exception of those marked with asterisks (*), which were measured by gating on $E1$ transitions. The symbol $^{\zeta}$ is used to denote DCO ratios that were deduced using the $\alpha$-induced reaction data in $^{156}$Dy. The branching ratios for out-of-band to in-band transitions, $(BE2)_{\rm out}/(BE2)_{\rm in}$, for the $0_2{}^+$ and $2^+$ bands are also listed. Empty cells refer to information that could not be obtained.

| Nucleus/band name | $E_i$ | $I_i$ | $I_f$ | $E_\gamma$(keV) | DCO | $A_p$ | Assign | $(BE2)_{\rm out}/(BE2)_{\rm in}$ |
|---|---|---|---|---|---|---|---|---|
| $^{150}$Sm | | | | | | | | |
| Ground | | | | | | | | |
| | 334 | 2 | 0 | 333.9(1) | 0.98(10) | 0.09(10) | $E2$ | |
| | 773 | 4 | 2 | 439.3(1) | 0.94(10) | 0.09(10) | $E2$ | |
| | 1279 | 6 | 4 | 505.6(1) | 0.97(10) | 0.07(10) | $E2$ | |
| | 1837 | 8 | 6 | 558.1(1) | 0.97(10) | 0.08(20) | $E2$ | |
| | 2433 | 10 | 8 | 596.1(1) | 1.09(20) | 0.08(20) | $E2$ | |
| | 3048 | 12 | 10 | 615.2(1) | 0.94(50) | 0.06(60) | $E2$ | |
| | 3676 | 14 | 12 | 627.5(1) | 0.97(11) | | $E2$ | |
| | 4305 | 16 | 14 | 629.6(2) | | | $E2$ | |
| $0_2{}^+$ band | | | | | | | | |
| | 740 | 0 | 2 | 406.5(2) | 0.67(36) | 0.07(54) | $E2$ | |
| | 1046 | 2 | 0 | 305.6(2) | 0.78(17) | 0.06(24) | $E2$ | |
| | | | 4 | 272.8(2) | | | $E2$ | |
| | | | 2 | 712.1(2) | 1.41(16) | −0.002(10) | $M1/E2$ | |
| | | | 0 | 1046.0(2) | | | $E2$ | 0.009(2) |
| | 1449 | 4 | 2 | 403.0(2) | 1.02(20) | 0.10(20) | $E2$ | |
| | | | 4 | 676.0(3) | 1.27(12) | −0.04(11) | $M1/E2$ | |
| | | | 2 | 1115.3(2) | | | $E2$ | 0.001(10) |
| | 1822 | 6 | 4 | 372.7(2) | 0.82(90) | 0.12(17) | $E2$ | |
| | | | 6 | 543.1(3) | 0.66(30) | −0.07(24) | $M1/E2$ | |
| | | | 4 | 1049.1(3) | | | $E2$ | 0.002(1) |
| | 2247 | 8 | 6 | 424.9(3) | 0.86(11) | 0.11(31) | $E2$ | |
| | | | 6 | 967.9(2) | 1.31(22) | | $E2$ | 0.003(1) |
| | 2746 | 10 | 8 | 499.0(2) | 0.64(33) | | $E2$ | |
| | 3306 | (12) | 10 | 560.3(3) | | | $E2$ | |
| (even) | | | | | | | | |
| | 1194 | 2 | 0 | 453.3(2) | | | $E2$ | |
| | | | 2 | 859.8(2) | | | $M1/E2$ | |
| | | | 0 | 1193.7(2) | | | $E2$ | |
| | 1642 | 4 | 2 | 448.9(1) | 1.24(36) | | $E2$ | |
| | | | 4 | 869.4(3) | 1.36(31) | −0.04(30) | $M1/E2$ | |
| | | | 2 | 1308.7(2) | | 0.15(76) | $E2$ | 0.033(4) |
| | 2107 | 6 | 4 | 464.8(2) | 1.31(21) | 0.39(25) | $E2$ | |
| | | | 6 | 285.6(2) | | | $M1/E2$ | |
| | | | 6 | 828.5(3) | | | $M1/E2$ | |
| | | | 4 | 1334.0(3) | | | $E2$ | 0.027(4) |
| | 2664 | (8) | 6 | 557.2(3) | | | $E2$ | |
| | | | 6 | 1385.7(3) | | | $E2$ | |
| | 3200 | 10 | (8) | 535.3(1) | | | $E2$ | |
| | | | (8) | 1362.9(1) | | | $E2$ | |
| (odd) | | | | | | | | |
| | 1505 | 3 | 4 | 731.4(2) | | | $M1/E2$ | |
| | | | 2 | 1170.7(2) | 1.08(33) | −0.00(2) | $M1/E2$ | |
| | 2020 | 5 | 3 | 515.8(1) | 0.91(48) | | $E2$ | |
| | | | 4 | 377.8(1) | | | $M1/E2$ | |
| | | | 6 | 741.8(2) | | | $M1/E2$ | |
| | | | 4 | 1247.1(1) | 1.03(36) | −0.03(21) | $M1/E2$ | 0.036(2) |
| | 2570 | (7) | 5 | 550.0(1) | 0.74(13) | 0.05(20) | $E2$ | |
| | | | (6) | 463.0(1) | | | $M1/E2$ | |
| | | | 8 | 748.6(2) | | | $M1/E2$ | |
| | | | 6 | 1291.5(2) | 1.02(62) | −0.09(27) | $M1/E2$ | 0.019(1) |
| | 3155 | (9) | (7) | 585.0(2) | 0.91(21) | | $E2$ | |

TABLE II. (*Continued.*)

| Nucleus/band name | $E_i$ | $I_i$ | $I_f$ | $E_\gamma$(keV) | DCO | $A_p$ | Assign | $(BE2)_{out}/(BE2)_{in}$ |
|---|---|---|---|---|---|---|---|---|
| $^{152}$Gd | | | | | | | | |
| Ground | | | | | | | | |
| | 345 | 2 | 0 | 344.73(10) | 1.08(1) | 0.05(1) | $E2$ | |
| | 756 | 4 | 2 | 411.58(10) | 1.05(1) | 0.06(1) | $E2$ | |
| | 1229 | 6 | 4 | 472.40(10) | 1.01(1) | 0.06(1) | $E2$ | |
| | 1749 | 8 | 6 | 520.02(10) | 1.03(1) | 0.06(1) | $E2$ | |
| | 2303 | 10 | 8 | 554.19(10) | 1.07(1) | 0.06(1) | $E2$ | |
| | 2888 | 12 | 10 | 585.2(1) | 0.98(2) | 0.05(1) | $E2$ | |
| | 3504 | 14 | 12 | 616.1(1) | 0.87(3) | 0.06(2) | $E2$ | |
| | 4147 | 16 | 14 | 642.4(2) | 0.93(7) | 0.11(4) | $E2$ | |
| $0_2^+$ band | | | | | | | | |
| | 616 | 0 | 2 | 271.50(11) | | | $E2$ | |
| | 931 | 2 | 0 | 315.54(12) | | | $E2$ | |
| | | | 2 | 586.77(13) | | | $M1/E2$ | |
| | | | 0 | 931.35(17) | | 0.16(6) | $E2$ | 0.011(1) |
| | 1283 | 4 | 2 | 352.12(13) | 1.13(4) | 0.10(2) | $E2$ | |
| | | | 4 | 527.36(13) | 1.00(3) | −0.03(3) | $M1/E2$ | |
| | | | 2 | 938.8(1) | | | $E2$ | |
| | 1669 | 6 | 4 | 386.37(13) | 1.02(3) | 0.10(3) | $E2$ | |
| | | | 6 | 441.08(16) | 1.12(5) | −0.04(5) | $M1/E2$ | |
| | 2141 | 8 | 8 | 392.2(2) | | | $M1/E2$ | |
| | | | 6 | 472.01(6) | 1.28(3) | 0.06(1) | $E2$ | |
| | 2695 | 10 | 10 | 392.1(4) | | | $M1/E2$ | |
| | | | 8 | 553.94(13) | 1.04(2) | 0.08(2) | $E2$ | |
| (even) | | | | | | | | |
| | 1110 | 2 | 2 | 765.93(16) | | | $M1/E2$ | |
| | | | 0 | 1110.3(2) | | | $E2$ | |
| | 1552 | 4 | 2 | 441.44(17) | 1.23(13) | | $E2$ | |
| | | | 4 | 795.52(10) | 0.62(13) | −0.09(10) | $M1/E2$ | |
| | | | 2 | 1207.02(15) | | | $E2$ | 0.014(10) |
| | 1999 | 6 | 4 | 448.20(11) | | | $E2$ | |
| | | | 6 | 771.33(12) | | | $M1/E2$ | |
| | | | 4 | 1243.44(23) | | | $E2$ | 0.006(2) |
| | 2464 | 8 | 6 | 464.60(12) | 1.23(11) | 0.08(7) | $E2$ | |
| | | | 6 | 1236.20(19) | | | $E2$ | 0.004(1) |
| | 2969 | 10 | 8 | 504.56(19) | | | $E2$ | |
| (odd) | | | | | | | | |
| | 1435 | 3 | 4 | 679.08(21) | 0.79(10) | −0.02(11) | $M1/E2$ | |
| | | | 2 | 1090.73(10) | | | $M1/E2$ | |
| | 1863 | 5 | 3 | 427.94(17) | 1.11(16) | 0.05(9) | $E2$ | |
| | | | 6 | 634.30(19) | 0.55(11) | −0.09(5) | $M1/E2$ | |
| | | | 4 | 1107.21(16) | | | $M1/E2$ | 0.019(11) |
| | 2304 | 7 | 5 | 440.64(15) | 1.29(14) | 0.11(9) | $E2$ | |
| | | | 6 | 1075.38(16) | | −0.02(5) | $M1/E2$ | 0.014(5) |
| | 2780 | 9 | 7 | 476.73(15) | | 0.12(9) | $E2$ | |
| | | | 8 | 1030.93(19) | | | $M1/E2$ | 0.007(5) |
| | 3299 | 11 | 9 | 519.11(19) | | | $E2$ | |
| | | | 10 | 995.96(18) | | | $M1/E2$ | |
| | 3857 | 13 | 11 | 557.9(3) | | | $E2$ | |
| $^{154}$Dy | | | | | | | | |
| Ground | | | | | | | | |
| | 335 | 2 | 0 | 334.7(1) | | | $E2$ | |
| | 747 | 4 | 2 | 412.5(1) | | | $E2$ | |
| | 1224 | 6 | 4 | 477.2(1) | | | $E2$ | |
| | 1748 | 8 | 6 | 523.7(1) | | | $E2$ | |
| | 2305 | 10 | 8 | 557.1(1) | | | $E2$ | |

TABLE II. (*Continued*.)

| Nucleus/band name | $E_i$ | $I_i$ | $I_f$ | $E_\gamma$(keV) | DCO | $A_p$ | Assign | $(BE2)_{\text{out}}/(BE2)_{\text{in}}$ |
|---|---|---|---|---|---|---|---|---|
| | 2894 | 12 | 10 | 589.1(1) | | | $E2$ | |
| | 3511 | 14 | 12 | 616.33(12) | | | $E2$ | |
| | 4175 | 16 | 14 | 664.49(12) | | | $E2$ | |
| | 4871 | 18 | 16 | 696.00(11) | | | $E2$ | |
| | 5567 | 20 | 18 | 695.81(14) | | | $E2$ | |
| $0_2{}^+$ band | | | | | | | | |
| | 661 | 0 | 2 | 326.22(12) | | | $E2$ | |
| | 905 | 2 | 0 | 245.26(13) | | | $E2$ | |
| | | | 2 | 570.71(13) | | | $M1/E2$ | |
| | | | 0 | 905.29(14) | | | $E2$ | 0.008(3) |
| | 1252 | 4 | 2 | 346.71(13) | | | $E2$ | |
| | | | 4 | 504.86(13) | | | $M1/E2$ | |
| | 1659 | 6 | 4 | 407.07(13) | | | $E2$ | |
| | | | 6 | 435.13(14) | | | $M1/E2$ | |
| | 2164 | 8 | 8 | 416.30(14) | | | $M1/E2$ | |
| | | | 6 | 504.59(13) | | | $E2$ | |
| | 2760 | 10 | 8 | 595.73(13) | | | $E2$ | |
| | 3291 | 12 | 10 | 531.54(14) | | | $E2$ | |
| | | | 10 | 985.01(15) | | | $E2$ | |
| $\gamma$ (even) | | | | | | | | |
| | 1028 | 2 | 0 | 367.1(13) | | | $E2$ | |
| | 1028 | | 2 | 692.82(15) | | | $M1/E2$ | |
| | 1443 | 4 | 2 | 415.26(16) | | | $E2$ | |
| | 1443 | | 4 | 695.82(13) | | | $M1/E2$ | |
| | 1443 | | 2 | 1108.05(15) | | | $E2$ | 0.007(1) |
| | 1886 | 6 | 4 | 443.35(13) | | | $E2$ | |
| | 1886 | | 6 | 661.60(14) | | | $M1/E2$ | |
| | 1886 | | 4 | 1138.69(16) | | | $E2$ | 0.003(1) |
| | 2371 | 8 | 6 | 485.43(13) | | | $E2$ | |
| | 2371 | | 8 | 622.81(16) | | | $M1/E2$ | |
| | 2371 | | 6 | 1147.12(19) | | | $E2$ | 0.001(1) |
| | 2913 | 10 | 8 | 541.66(14) | | | $E2$ | |
| | 3515 | 12 | 10 | 602.22(25) | | | $E2$ | |
| $\gamma$ (odd) | | | | | | | | |
| | 1334 | 3 | 4 | 587.75(14) | | | $M1/E2$ | |
| | | | 2 | 999.82(14) | | | $M1/E2$ | |
| | 1740 | 5 | 3 | 405.68(14) | | | $E2$ | |
| | | | 4 | 993.14(13) | | | $M1/E2$ | 0.025(2) |
| | 2183 | 7 | 5 | 443.47(13) | | | $E2$ | |
| | | | 6 | 959.36(14) | | | $M1/E2$ | 0.016(1) |
| | 2678 | 9 | 7 | 495.01(13) | | | $E2$ | |
| | | | 8 | 930.47(18) | | | $M1/E2$ | 0.013(1) |
| | 3223 | 11 | 9 | 545.11(14) | | | $E2$ | |
| | | | 10 | 918.12(15) | | | $M1/E2$ | |
| | 3810 | 13 | 11 | 586.63(17) | | | $E2$ | |
| $^{156}$Er | | | | | | | | |
| Ground | | | | | | | | |
| | 345 | 2 | 0 | 344.6(1) | 1.11(5) | | $E2$ | |
| | 798 | 4 | 2 | 453.1(1) | 1.30(6) | | $E2$ | |
| | 1341 | 6 | 4 | 543.5(1) | 1.16(6) | | $E2$ | |
| | 1959 | 8 | 6 | 618.2(1) | 1.17(9) | | $E2$ | |
| | 2634 | 10 | 8 | 674.31(13) | 0.98(19) | | $E2$ | |
| | 3315 | 12 | 10 | 682.02(13) | | | $E2$ | |
| | 3838 | 14 | 12 | 522.47(13) | | | $E2$ | |
| | 4383 | 16 | 14 | 544.88(13) | | | $E2$ | |

TABLE II. (*Continued.*)

| Nucleus/band name | $E_i$ | $I_i$ | $I_f$ | $E_\gamma$(keV) | DCO | $A_p$ | Assign | $(BE2)_{out}/(BE2)_{in}$ |
|---|---|---|---|---|---|---|---|---|
| $\gamma$ (even) | | | | | | | | |
| | 1221 | 2 | 2 | 876.49(11) | | | M1 | |
| | | | 0 | 1220.93(25) | | | $E2$ | |
| | 1547 | 4 | 2 | 325.71(19) | | | $E2$ | |
| | | | 4 | 749.10(16) | | | M1 | |
| | | | 2 | 1202.24(15) | | | $E2$ | 0.004(1) |
| | 1970 | 6 | 4 | 423.39(14) | | | $E2$ | |
| | | | 6 | 629.09(14) | | | M1 | |
| | | | 4 | 1172.62(15) | | | $E2$ | 0.004(1) |
| | 2482 | 8 | 6 | 511.34(13) | | | $E2$ | |
| | | | 8 | 521.80(14) | | | M1 | |
| | | | 6 | 595.91(16) | | | $E2$ | |
| | | | 6 | 1140.62(17) | | | $E2$ | 0.002(1) |
| | 3044 | 10 | 8 | 562.55(13) | | | $M1/E2$ | |
| | | | 8 | 1084.74(17) | | | $E2$ | 0.001(1) |
| | 3653 | 12 | 10 | 609.29(14) | | | $E2$ | |
| | | | 10 | 708.69(17) | | | $E2$ | |
| $0_2{}^+$ band | | | | | | | | |
| | 930 | 2 | 2 | 585.81(14) | | | $M1/E2$ | |
| | | | 0 | 930.51(13) | | | $E2$ | |
| | 1406 | 4 | 2 | 475.72(14) | | | $E2$ | |
| | | | 4 | 608.30(14) | | | $M1/E2$ | |
| | | | 2 | 1061.52(17) | | | $E2$ | 0.008(1) |
| | 1886 | 6 | 4 | 339.27(19) | | | $E2$ | |
| | | | 4 | 480.41(13) | | | $E2$ | |
| | | | 6 | 544.80(13) | | | $M1/E2$ | |
| | | | 4 | 1089.17(14) | | | $E2$ | 0.009(1) |
| | 2378 | 8 | 8 | 418.28(17) | | | $M1/E2$ | |
| | | | 6 | 490.99(13) | | | $E2$ | |
| | | | 6 | 1036.88(14) | | | $E2$ | 0.009(1) |
| | 2945 | 10 | 8 | 566.44(13) | | | $E2$ | |
| | | | 8 | 985.0(10) | | | $E2$ | 0.004(1) |
| | 3592 | 12 | 10 | 645.80(14) | | | $E2$ | |
| | 4284 | 14 | 12 | 692.32(17) | | | $E2$ | |
| $\gamma$ (odd) | | | | | | | | |
| | 1352 | 3 | 2 | 420.72(16) | | | $M1/E2$ | |
| | | | 4 | 554.1(10) | | | $M1/E2$ | |
| | | | 2 | 1006.89(15) | | | $M1/E2$ | |
| | 1836 | 5 | 3 | 484.12(14) | | | $E2$ | |
| | | | 4 | 289.3(10) | | | $M1/E2$ | |
| | | | 4 | 430.00(16) | | | $M1/E2$ | |
| | | | 4 | 1038.30(17) | | | $M1/E2$ | 0.021(2) |
| | 2369 | 7 | 5 | 533.38(14) | | | $E2$ | |
| | | | 6 | 1028.07(18) | | | $M1/E2$ | 0.007(1) |
| | 2963 | 9 | 7 | 593.66(15) | | | $E2$ | |
| | | | 8 | 1003.4(2) | | | $M1/E2$ | 0.036(3) |
| $^{158}$Yb | | | | | | | | |
| Ground | | | | | | | | |
| | 358 | 2 | 0 | 358.02(10) | | | $E2$ | |
| | 834 | 4 | 2 | 476.41(10) | | | $E2$ | |
| | 1404 | 6 | 4 | 569.36(10) | | | $E2$ | |
| | 2047 | 8 | 6 | 643.44(10) | | | $E2$ | |
| | 2744 | 10 | 8 | 697.29(10) | | | $E2$ | |
| | 3427 | 12 | 10 | 682.87(10) | | | $E2$ | |
| | 3936 | 14 | 12 | 508.67(12) | | | $E2$ | |
| | 4504 | 16 | 14 | 567.81(13) | | | $E2$ | |

TABLE II. (*Continued*.)

| Nucleus/band name | $E_i$ | $I_i$ | $I_f$ | $E_\gamma$(keV) | DCO | $A_p$ | Assign | $(BE2)_{\text{out}}/(BE2)_{\text{in}}$ |
|---|---|---|---|---|---|---|---|---|
| $\gamma$ (even) band | | | | | | | | |
| | 937 | 2 | 2 | 579.2(1) | 0.67(8) | | $M1/E2$ | |
| | | | 0 | 937.2(1) | 0.97(6) | | $E2$ | |
| | 1423 | 4 | 2 | 486.1(1) | | | $E2$ | |
| | | | 4 | 589.3(1) | 0.59(7) | | $M1/E2$ | |
| | | | 2 | 1065.3(2) | 1.15(6) | | $E2$ | 0.020(4) |
| | 1911 | 6 | 4 | 488.0(1) | | | $E2$ | |
| | | | 6 | 507.7(2) | | | $M1/E2$ | |
| | | | 4 | 1077.3(2) | 1.14(10) | | $E2$ | 0.019(2) |
| | 2397 | 8 | 8 | 350.3(1) | 0.61(11) | | $M1/E2$ | |
| | | | 6 | 485.9(2) | 0.91(8) | | $E2$ | |
| | | | 6 | 993.6(2) | 1.12(12) | | $E2$ | 0.018(2) |
| | 2951 | 10 | 8 | 554.6(2) | 1.11(19) | | $E2$ | |
| | | | 8 | 903.4(3) | | | $E2$ | 0.021(5) |
| | 3585 | 12 | 10 | 634.3(2) | | | $E2$ | |
| | | | 10 | 840.2(2) | | | $E2$ | 0.09(2) |
| | 4300 | 14 | 12 | 714.1(3) | | | $E2$ | |
| $^{154}$Gd | | | | | | | | |
| Ground | | | | | | | | |
| | 123 | 2 | 0 | 122.86(10) | 1.01(10) | | $E2$ | |
| | 370 | 4 | 2 | 247.44(10) | 1.02(11) | 0.15(10) | $E2$ | |
| | 716 | 6 | 4 | 345.9(1) | 1.01(10) | 0.15(5) | $E2$ | |
| | 1142 | 8 | 6 | 426.0(1) | 1.00(10) | 0.14(15) | $E2$ | |
| | 1634 | 10 | 8 | 491.8(1) | 1.013(20) | 0.13(10) | $E2$ | |
| | 2180 | 12 | 10 | 546.64(13) | 1.01(15) | 0.14(10) | $E2$ | |
| | 2772 | 14 | 12 | 591.98(14) | 0.97(3) | 0.12(30) | $E2$ | |
| | 3398 | 16 | 14 | 625.87(18) | 1.05(15) | | $E2$ | |
| $0_2{}^+$ band | | | | | | | | |
| | 814 | 2 | 0 | 134.80(20) | | | $E2$ | |
| | | | 4 | 443.61(14) | | | $E2$ | |
| | | | 2 | 690.97(14) | | | $M1/E2$ | |
| | | | 0 | 813.88(19) | | | $E2$ | |
| | 1045 | 4 | 2 | 231.66(14) | | | $E2$ | |
| | | | 6 | 329.20(16) | | | $E2$ | |
| | | | 4 | 675.17(13) | 0.85(12) | −0.04(10) | $M1/E2$ | |
| | | | 2 | 922.66(14) | 0.88(30) | 0.11(20) | $E2$ | 0.002(1) |
| | 1363 | 6 | 4 | 317.63(13) | 0.99(10) | 0.12(10) | $E2$ | |
| | | | 6 | 646.86(13) | | −0.05(10) | $M1/E2$ | |
| | | | 4 | 993.05(14) | 0.95(20) | 0.03(10) | $E2$ | 0.001(1) |
| | 1753 | 8 | 6 | 389.96(13) | 1.00(10) | 0.16(10) | $E2$ | |
| | | | 8 | 610.85(14) | | | $M1/E2$ | |
| | | | 6 | 1037.23(17) | | | $E2$ | 0.001(1) |
| | 2190 | 10 | 8 | 436.89(13) | 1.01(10) | | $E2$ | |
| | | | 10 | 555.90(15) | 0.86(5) | −0.01(5) | $M1/E2$ | |
| | | | 8 | 1047.98(18) | | | $E2$ | 0.001(1) |
| | 2617 | 12 | 10 | 427.11(13) | 1.00(1) | | $E2$ | |
| | | | 12 | 435.80(13) | 1.01(1) | | $M1/E2$ | |
| | | | 10 | 983.5(3) | | | $E2$ | 0.001(1) |
| | 3022 | 14 | 12 | 404.76(14) | 0.98(4) | 0.09(30) | $E2$ | |
| | 3484 | 16 | 14 | 462.73(17) | 1.11(12) | | $E2$ | |
| $\gamma$ (even) | | | | | | | | |
| | 995 | 2 | 2 | 871.42(14) | | | $M1/E2$ | |
| | | | 0 | 994.32(14) | 0.95(4) | | $E2$ | |
| | 1261 | 4 | 2 | 266.91(17) | 0.96(5) | 0.07(5) | $E2$ | |
| | | | 4 | 890.97(13) | 0.91(3) | −0.13(5) | $M1/E2$ | |
| | | | 2 | 1138.56(14) | 0.89(8) | | $E2$ | 0.008(1) |
| | 1603 | 6 | 4 | 341.96(15) | | | $E2$ | |
| | | | 6 | 886.86(13) | 0.77(20) | −0.02(1) | $M1/E2$ | |
| | | | 4 | 1233.10(15) | | | $E2$ | 0.004(1) |
| | 2014 | 8 | 6 | 411.15(14) | 0.99(5) | 0.16(5) | $E2$ | |

TABLE II. (*Continued.*)

| Nucleus/band name | $E_i$ | $I_i$ | $I_f$ | $E_\gamma$(keV) | DCO | $A_p$ | Assign | $(BE2)_{out}/(BE2)_{in}$ |
|---|---|---|---|---|---|---|---|---|
| | | | 7 | 207.8(5) | | | $M1/E2$ | |
| | | | 6 | 651.3(10) | | | $E2$ | |
| | | | 8 | 872.18(14) | | | $M1/E2$ | |
| | | | 6 | 1298.36(16) | 0.93(7) | | $E2$ | 0.004(1) |
| | 2485 | 10 | 8 | 470.97(14) | 0.97(13) | 0.19(6) | $E2$ | |
| | | | 10 | 851.21(15) | 0.6(4) | −0.13(3) | $M1/E2$ | |
| | | | 8 | 1343.55(19) | 1.04(11) | 0.19(24) | $E2$ | 0.004(1) |
| | 3005 | 12 | 10 | 519.65(12) | | | $E2$ | |
| | | | 12 | 824.7(14) | | | $M1/E2$ | |
| | | | 10 | 1372.14(18) | | | $E2$ | 0.006(1) |
| $\gamma$ (odd) | | | | | | | | |
| | 1125 | 3 | 4 | 755.20(14) | 0.88(3) | −0.05(2) | $M1/E2$ | |
| | | | 2 | 1002.78(13) | 0.93(2) | −0.05(4) | $M1/E2$ | |
| | 1429 | 5 | 3 | 303.86(17) | 1.02(7) | 0.18(5) | $E2$ | |
| | | | 6 | 713.18(14) | 0.69(5) | −0.01(5) | $M1/E2$ | |
| | | | 4 | 1059.31(13) | 0.72(1) | 0.01(2) | $M1/E2$ | 0.040(3) |
| | 1807 | 7 | 5 | 377.23(14) | | 0.24(4) | $E2$ | |
| | | | 8 | 664.45(14) | 0.92(4) | −0.11(3) | $M1/E2$ | |
| | | | 6 | 1090.65(13) | 0.53(2) | 0.06(3) | $M1/E2$ | 0.023(1) |
| | 2247 | 9 | 7 | 440.22(14) | | 0.08(4) | $E2$ | |
| | | | 10 | 613.31(18) | 0.81(5) | −0.01(4) | $M1/E2$ | |
| | | | 8 | 1104.88(14) | 0.57(1) | | $M1/E2$ | 0.017(1) |
| | 2741 | 11 | 9 | 494.13(15) | | 0.16(5) | $E2$ | |
| | | | 10 | 1107.38(18) | 0.57(1) | 0.16(8) | $M1/E2$ | 0.011(1) |
| | 3278 | 13 | 11 | 537.31(19) | 1.23(15) | 0.15(9) | $E2$ | |
| | 3278 | 13 | 12 | 1098.1(12) | 0.57(1) | | $M1/E2$ | |
| $^{156}$Dy | | | | | | | | |
| Ground | | | | | | | | |
| | 138 | 2 | 0 | 137.63(10) | 0.92(10)$^\zeta$ | | $E2$ | |
| | 404 | 4 | 2 | 266.23(10) | 1.00(10)$^\zeta$ | 0.14(10) | $E2$ | |
| | 770 | 6 | 4 | 366.07(10) | 1.02(10)$^\zeta$ | 0.13(10) | $E2$ | |
| | 1215 | 8 | 6 | 445.14(10) | 1.04(15)$^\zeta$ | 0.096(30) | $E2$ | |
| | 1724 | 10 | 8 | 508.89(10) | 1.04(10)$^\zeta$ | 0.098(12) | $E2$ | |
| | 2285 | 12 | 10 | 560.67(10) | 1.00(13)$^\zeta$ | 0.089(12) | $E2$ | |
| | 2886 | 14 | 12 | 601.84(11) | 0.90(10)$^\zeta$ | 0.06(2) | $E2$ | |
| | 3522 | 16 | 14 | 635.41(11) | 0.99(3)$^\zeta$ | 0.099(2) | $E2$ | |
| $0_2{}^+$ band | | | | | | | | |
| | 828 | 2 | 4 | 424.04(22) | | | $E2$ | |
| | | | 2 | 690.69(11) | | | $M1/E2$ | |
| | 1088 | 4 | 2 | 259.47(12) | | | $E2$ | |
| | | | 6 | 317.70(11) | | | $E2$ | |
| | | | 4 | 683.84(12) | | | $M1/E2$ | |
| | | | 2 | 950.44(12) | | | $E2$ | 0.0010(10) |
| | 1437 | 6 | 4 | 348.81(10) | 0.98(3) | | $E2$ | |
| | | | 6 | 666.70(12) | 0.68(10) | −0.05(41) | $M1/E2$ | |
| | | | 4 | 1032.91(12) | | | $E2$ | 0.0010(10) |
| | 1858 | 8 | 6 | 421.31(10) | | | $E2$ | |
| | | | 8 | 642.91(11) | 0.71(3) | −0.10(30) | $M1/E2$ | |
| | | | 6 | 1088.14(15) | | | $E2$ | 0.001(1) |
| | 2315 | 10 | 8 | 456.64(13) | | | $E2$ | |
| | | | 10 | 590.72(15) | 0.71(10) | | $M1/E2$ | |
| | | | 8 | 1099.71(14) | | | $E2$ | 0.001(1) |
| $\gamma$ (even) | | | | | | | | |
| | 891 | 2 | 2 | 752.41(14) | | | $M1/E2$ | |
| | 1168 | 4 | 2 | 277.18(21) | | | $E2$ | |
| | | | 4 | 763.92(13) | 0.708(41)$^\zeta$ | −0.060(40) | $M1/E2$ | |
| | | | 2 | 1030.40(12) | | | $E2$ | 0.004(2) |

TABLE II. (*Continued*.)

| Nucleus/band name | $E_i$ | $I_i$ | $I_f$ | $E_\gamma$(keV) | DCO | $A_p$ | Assign | $(BE2)_{\text{out}}/(BE2)_{\text{in}}$ |
|---|---|---|---|---|---|---|---|---|
| | 1524 | 6 | 4 | 356.53(15) | | | $E2$ | |
| | | | 6 | 754.45(16) | | | $M1/E2$ | |
| | | | 4 | 1120.60(17) | | | $E2$ | 0.004(1) |
| | 1956 | 8 | 6 | 431.86(14) | | 0.101(70) | $E2$ | |
| | | | 8 | 740.95(15) | 0.443(44)$^{\zeta}$ | −0.033(60) | $M1/E2$ | |
| | | | 8 | 1186.34(15) | | | $E2$ | 0.003(1) |
| | 2447 | 10 | 8 | 490.51(14) | | | $E2$ | |
| | | | 10 | 1231.54(16) | | 0.028(150) | $E2$ | 0.009(1) |
| | 2969 | 12 | 10 | 522.00(15) | | | $E2$ | |
| | | | 12 | 683.90(10) | | | $M1/E2$ | |
| | | | 10 | 1244.96(17) | | | $E2$ | 0.014(1) |
| | 3523 | 14 | 12 | 556.00(16) | | | $E2$ | |
| | | | 14 | 637.99(13) | | | $M1/E2$ | |
| | | | 12 | 1238.16(18) | | | $E2$ | |
| $\gamma$ (odd) | | | | | | | | |
| | 1022 | 3 | 4 | 617.73(8) | | | $M1/E2$ | |
| | | | 2 | 884.25(11) | | | $M1/E2$ | |
| | 1335 | 5 | 3 | 312.86(18) | | | $E2$ | |
| | | | 6 | 565.38(19) | | | $M1/E2$ | |
| | | | 4 | 931.14(13) | 0.59(5)$^{\zeta}$ | 0.04(6) | $M1/E2$ | 0.031(2) |
| | 1728 | 7 | 5 | 393.04(13) | | | $E2$ | |
| | | | 8 | 512.37(14) | | | $M1/E2$ | |
| | | | 6 | 958.11(13) | 0.451(30)$^{\zeta}$ | 0.02(10) | $M1/E2$ | 0.020(1) |
| | 2190 | 9 | 7 | 462.46(13) | | 0.093(20) | $E2$ | |
| | | | 10 | 466.52(15) | | | $M1/E2$ | |
| | | | 8 | 975.42(14) | 0.562(4)$^{\zeta}$ | 0.042(5) | $M1/E2$ | 0.014(1) |
| | 2711 | 11 | 9 | 520.07(13) | | 0.069(4) | $E2$ | |
| | | | 10 | 264.58(18) | | | $M1/E2$ | |
| | | | 10 | 986.61(17) | | | $M1/E2$ | 0.011(10) |
| | 3274 | 13 | 11 | 563.01(14) | | | $E2$ | |
| | | | 12 | 989.18(19) | | | $M1/E2$ | |
| | 3861 | 15 | 13 | 587.16(14) | | | $E2$ | |
| $^{160}$Yb | | | | | | | | |
| Ground | | | | | | | | |
| | 243 | 2 | 0 | 243.20(10) | | | $E2$ | |
| | 639 | 4 | 2 | 395.39(10) | | | $E2$ | |
| | 1148 | 6 | 4 | 508.73(10) | | | $E2$ | |
| | 1737 | 8 | 6 | 589.27(10) | | | $E2$ | |
| | 2374 | 10 | 8 | 637.03(10) | | | $E2$ | |
| | 2960 | 12 | 10 | 586.50(10) | | | $E2$ | |
| | 3364 | 14 | 12 | 404.02(10) | | | $E2$ | |
| | 3848 | 16 | 14 | 484.08(10) | | | $E2$ | |
| $0_2{}^+$ band | | | | | | | | |
| | 1293 | 2 | 2 | 1048.65(15) | | | $M1/E2$ | |
| | | | 0 | 1292.01(21) | | | $E2$ | |
| | 1592 | 4 | 2 | 299.33(21) | | | $E2$ | |
| | | | 4 | 953.34(15) | 0.95(12) | | $M1/E2$ | |
| | | | 2 | 1348.65(15) | | | $E2$ | 0.0037(10) |
| | 1958 | 6 | 4 | 365.60(11) | 1.10(18) | | $E2$ | |
| | | | 6 | 809.89(12) | 0.54(5) | | $M1/E2$ | |
| | | | 4 | 1318.74(11) | 0.92(9) | | $E2$ | 0.0047(10) |
| | 2365 | 8 | 6 | 406.81(10) | 1.20(11) | | $E2$ | |
| | | | 6 | 1216.91(11) | 0.97(10) | | $E2$ | 0.0036(10) |
| | 2841 | 10 | 8 | 476.22(11) | | | $E2$ | |
| | | | 8 | 566.18(10) | | | $E2$ | |
| | | | 8 | 1104.52(33) | | | $E2$ | 0.009(2) |

TABLE II. (*Continued.*)

| Nucleus/band name | $E_i$ | $I_i$ | $I_f$ | $E_\gamma$(keV) | DCO | $A_p$ | Assign | $(BE2)_{out}/(BE2)_{in}$ |
|---|---|---|---|---|---|---|---|---|
| $\gamma$ (even) | | | | | | | | |
| | 821 | 2 | 2 | 577.16(10) | 0.77(6) | −0.05(16) | $M1/E2$ | |
| | | | 0 | 820.44(10) | 0.98(10) | 0.84(25) | $E2$ | |
| | 1256 | 4 | 2 | 435.15(10) | 1.02(9) | | $E2$ | |
| | | | 4 | 616.71(10) | 0.78(7) | −0.15(12) | $M1/E2$ | |
| | | | 2 | 1012.67(11) | | −0.20(27) | $E2$ | 0.007(1) |
| | 1744 | 6 | 4 | 488.04(10) | 0.99(9) | | $E2$ | |
| | | | 6 | 596.37(10) | 0.72(6) | | $M1/E2$ | |
| | | | 4 | 1104.52(33) | | 0.17(40) | $E2$ | 0.0019(2) |
| | 2275 | 8 | 6 | 530.90(10) | 1.15(10) | 0.22(14) | $E2$ | |
| | | | 8 | 537.45(15) | | | $M1/E2$ | |
| | | | 6 | 1127.35(16) | | | $E2$ | |
| | 2790 | 10 | 8 | 425.55(10) | 0.80(9) | | $E2$ | |
| | | | 8 | 515.63(10) | 0.92(8) | | $E2$ | |
| | | | 8 | 1053.14(11) | | | $E2$ | 0.048(4) |
| | 3319 | 12 | 10 | 478.37(10) | 0.68(69) | | $E2$ | |
| | | | 10 | 528.84(10) | 0.98(9) | | $E2$ | |
| | 3870 | 14 | 12 | 550.79(10) | | | $E2$ | |
| $\gamma$ (odd) | | | | | | | | |
| | 1113 | 3 | 2 | 292.35(11) | 0.68(8) | −0.07(32) | $M1/E2$ | |
| | | | 4 | 474.15(11) | 0.72(7) | | $M1/E2$ | |
| | | | 2 | 869.61(10) | 0.69(6) | 0.07(12) | $M1/E2$ | |
| | 1574 | 5 | 3 | 461.33(10) | 1.02(12) | 0.58(14) | $E2$ | |
| | | | 4 | 318.05(11) | | | $M1/E2$ | |
| | | | 6 | 427.08(11) | 0.98(10) | | $M1/E2$ | |
| | | | 4 | 935.43(10) | 0.58(5) | 0.24(8) | $M1/E2$ | 0.00366(26) |
| | 2109 | 7 | 5 | 534.62(10) | 1.09(10) | | $E2$ | |
| | | | 6 | 365.55(12) | | | $M1/E2$ | |
| | | | 6 | 961.51(11) | | 0.44(15) | $M1/E2$ | 0.013(1) |
| | 2701 | 9 | 7 | 592.47(10) | | | $E2$ | |
| | | | 8 | 963.71(15) | | 0.44(15) | $M1/E2$ | 0.0086(11) |
| | 3331 | 11 | 9 | 629.71(10) | 1.03(9) | | $E2$ | |
| | 4017 | 13 | 11 | 686.00(12) | | | $E2$ | |
| $^{158}$Dy | | | | | | | | |
| Ground | | | | | | | | |
| | 99 | 2 | 0 | 98.58(10) | | | $E2$ | |
| | 317 | 4 | 2 | 217.98(10) | | | $E2$ | |
| | 637 | 6 | 4 | 320.34(10) | | | $E2$ | |
| | 1043 | 8 | 6 | 405.97(10) | | | $E2$ | |
| | 1519 | 10 | 8 | 475.75(10) | | | $E2$ | |
| | 2048 | 12 | 10 | 529.07(10) | | | $E2$ | |
| | 2611 | 14 | 12 | 563.28(10) | | | $E2$ | |
| | 3189 | 16 | 14 | 577.81(13) | | | $E2$ | |
| $0_2{}^+$ band | | | | | | | | |
| | 1086 | 2 | 4 | 769.2(4) | | | $E2$ | |
| | | | 2 | 987.1(5) | | | $M1/E2$ | |
| | | | 0 | 1086.1(2) | | | $E2$ | |
| | 1279 | 4 | 2 | 193.7(2) | | | $E2$ | |
| | | | 6 | 642.50(18) | | | $E2$ | |
| | | | 4 | 962.5(3) | | | $M1/E2$ | |
| | | | 2 | 1180.9(3) | | | $E2$ | 0.020(4) |
| | 1554 | 6 | 4 | 274.59(17) | | | $E2$ | |
| | | | 8 | 510.86(13) | | | $E2$ | |
| | | | 6 | 917.13(12) | | | $M1/E2$ | |
| | | | 4 | 1237.75(11) | | | $E2$ | 0.008(3) |
| | 1901 | 8 | 6 | 346.63(8) | | | $E2$ | |
| | | | 6 | 424.79(17) | | | $E2$ | |

TABLE II. (*Continued*.)

| Nucleus/band name | $E_i$ | $I_i$ | $I_f$ | $E_\gamma$(keV) | DCO | $A_p$ | Assign | $(BE2)_{\text{out}}/(BE2)_{\text{in}}$ |
|---|---|---|---|---|---|---|---|---|
| | | | 8 | 857.76(15) | | | $M1/E2$ | |
| | | | 6 | 1263.79(11) | | | $E2$ | 0.004(1) |
| | 2267 | 10 | 8 | 367.5(4) | | | $E2$ | |
| | | | 8 | 404.58(17) | | | $E2$ | |
| | | | 10 | 748.59(15) | | | $M1/E2$ | |
| | | | 8 | 1223.99(19) | | | $E2$ | 0.015(3) |
| | 2698 | 12 | 10 | 430.55(22) | | | $E2$ | |
| | | | 12 | 650.17(7) | | | $M1/E2$ | |
| | | | 10 | 1179.10(13) | | | $E2$ | |
| | 3259 | 14 | 12 | 561.01(13) | | | $E2$ | |
| | | | 12 | 1211.17(25) | | | $E2$ | |
| $\gamma$ (even) | | | | | | | | |
| | 946 | 2 | 4 | 629.70(20) | | | $E2$ | |
| | | | 2 | 847.74(15) | | | $M1/E2$ | |
| | | | 0 | 946.3(9) | | | $E2$ | |
| | 1163 | 4 | (2) | 216.69(11) | | | $E2$ | |
| | | | 3 | 118.8(10) | | | $M1/E2$ | |
| | | | 6 | 526.08(22) | | | $E2$ | |
| | | | 4 | 846.39(5) | | | $M1/E2$ | |
| | | | 2 | 1064.43(15) | | | $E2$ | 0.005(3) |
| | 1476 | 6 | 4 | 312.92(6) | | | $E2$ | |
| | | | 5 | 161.78(15) | | | $M1/E2$ | |
| | | | 6 | 839.00(4) | | | $M1/E2$ | |
| | | | 4 | 1159.31(20) | | | $E2$ | 0.003(1) |
| | 1863 | 8 | 6 | 386.69(6) | | | $E2$ | |
| | | | 7 | 188.1(1) | | | $M1/E2$ | |
| | | | 6 | 308.5(1) | | | $E2$ | |
| | | | 8 | 819.66(15) | | | $M1/E2$ | |
| | | | 6 | 1225.69(20) | | | $E2$ | 0.010(1) |
| | 2349 | 10 | 8 | 486.33(7) | | | $E2$ | |
| | | | 8 | 448.2(1) | | | $E2$ | |
| | | | 10 | 830.30(18) | | | $M1/E2$ | |
| | | | 8 | 1306.01(10) | | | $E2$ | 0.001(1) |
| | 2866 | 12 | 10 | 516.97(15) | | | $E2$ | |
| | | | 12 | 818.34(18) | | | $M1/E2$ | |
| $\gamma$ (odd) | | | | | | | | |
| | 1044 | 3 | (2) | 97.90(10) | | | $M1/E2$ | |
| | | | 4 | 727.63(9) | | | $M1/E2$ | |
| | | | 2 | 945.67(5) | | | $M1/E2$ | |
| | 1314 | 5 | 4 | 151.1(4) | | | $M1/E2$ | |
| | | | 3 | 269.90(7) | | | $E2$ | |
| | | | 6 | 677.22(5) | | | $M1/E2$ | |
| | | | 4 | 997.53(3) | | | $M1/E2$ | 0.034(2) |
| | 1675 | 7 | 5 | 360.39(4) | | | $E2$ | |
| | | | 6 | 198.61(13) | | | $M1/E2$ | |
| | | | 8 | 631.59(6) | | | $M1/E2$ | |
| | | | 6 | 1037.61(4) | | | $M1/E2$ | 0.020(1) |
| | 2111 | 9 | 7 | 436.85(4) | | | $E2$ | |
| | | | 10 | 592.75(15) | | | $M1/E2$ | |
| | | | 8 | 1068.44(5) | | | $M1/E2$ | 0.015(1) |
| | 2610 | 11 | 9 | 498.38(4) | | | $E2$ | |
| | | | 12 | 562.21(12) | | | $M1/E2$ | |
| | | | 10 | 1091.1(10) | | | $M1/E2$ | 0.013(1) |
| | 3147 | 13 | 11 | 537.59(15) | | | $E2$ | |
| | | | 12 | 1099.8(10) | | | $M1/E2$ | 0.003(1) |
| | 3685 | 15 | 13 | 537.5(2) | | | $E2$ | |
| | | | 14 | 1074.1(2) | | | $M1/E2$ | |

TABLE II. (*Continued.*)

| Nucleus/band name | $E_i$ | $I_i$ | $I_f$ | $E_\gamma$(keV) | DCO | $A_p$ | Assign | $(BE2)_{out}/(BE2)_{in}$ |
|---|---|---|---|---|---|---|---|---|
| $^{160}$Er | | | | | | | | |
| Ground | | | | | | | | |
| | 125 | 2 | 0 | 125.43(6) | | | $E2$ | |
| | 389 | 4 | 2 | 263.87(6) | | | $E2$ | |
| | 765 | 6 | 4 | 375.71(6) | | | $E2$ | |
| | 1229 | 8 | 6 | 464.08(6) | | | $E2$ | |
| | 1761 | 10 | 8 | 531.86(6) | | | $E2$ | |
| | 2340 | 12 | 10 | 579.22(6) | | | $E2$ | |
| | 2932 | 14 | 12 | 592.21(6) | | | $E2$ | |
| | 3466 | 16 | 14 | 534.04(6) | | | $E2$ | |
| $0_2{}^+$ band | | | | | | | | |
| | 1008 | 2 | 0 | 1008.0(1) | | | $E2$ | |
| | 1230 | 4 | 4 | 840.31(17) | | | $M1/E2$ | |
| | | | 2 | 1104.30(24) | | | $E2$ | |
| | 1542 | 6 | 4 | 312.48(20) | | | $E2$ | |
| | | | 6 | 777.2(3) | | | $M1/E2$ | |
| | | | 4 | 1152.64(12) | | | $E2$ | 0.003(2) |
| | 1921 | 8 | 6 | 379.20(11) | | | $E2$ | |
| | | | 6 | 1156.47(13) | | | $E2$ | 0.006(1) |
| | 2360 | 10 | 8 | 438.69(14) | | | $E2$ | |
| | | | 8 | 409.6(10) | | | $E2$ | |
| | | | 10 | 599.20(10) | | | $M1/E2$ | |
| | | | 8 | 1131.01(10) | | | $E2$ | 0.005(1) |
| | 2846 | 12 | 10 | 485.79(14) | | | $E2$ | |
| | | | 10 | 1084.99(10) | | | $E2$ | |
| | 3372 | 14 | 12 | 526.23(14) | | | $E2$ | |
| | 3966 | 16 | 14 | 594.07(12) | | | $E2$ | |
| | | | 14 | 1033.84(22) | | | $E2$ | |
| $\gamma$ (even) | | | | | | | | |
| | 854 | 2 | 2 | 728.9(10) | | | $M1/E2$ | |
| | | | 0 | 854.21(15) | | | $E2$ | |
| | 1129 | 4 | 2 | 274.1(10) | | | $E2$ | |
| | | | 4 | 739.13(5) | | | $M1/E2$ | |
| | | | 2 | 1003.09(9) | | | $E2$ | 0.005(3) |
| | 1499 | 6 | 4 | 370.66(8) | | | $E2$ | |
| | | | 6 | 734.26(5) | | | $M1/E2$ | |
| | 1950 | 8 | 6 | 451.18(10) | | | $E2$ | |
| | | | 7 | 209.6(20) | | | $M1/E2$ | |
| | | | 6 | 408.3(12) | | | $E2$ | |
| | | | 8 | 721.36(10) | | | $M1/E2$ | |
| | | | 6 | 1185.44(14) | | | $E2$ | 0.003(1) |
| | 2437 | 10 | 8 | 486.27(7) | | | $E2$ | |
| | | | 9 | 194.5(19) | | | $M1/E2$ | |
| | | | 8 | 515.3(25) | | | $E2$ | |
| | | | 10 | 675.82(11) | | | $M1/E2$ | |
| | | | 8 | 1207.63(14) | | | $E2$ | 0.003(1) |
| | 2998 | 12 | 10 | 561.52(8) | | | $E2$ | |
| | | | 10 | 1237.45(9) | | | $E2$ | 0.001(1) |
| | 3566 | 14 | 12 | 568.21(9) | | | $E2$ | |
| $\gamma$ (odd) | | | | | | | | |
| | 987 | 3 | 4 | 597.77(5) | | | $M1/E2$ | |
| | | | 2 | 861.73(11) | | | $M1/E2$ | |
| | 1316 | 5 | 3 | 329.21(9) | | | $E2$ | |
| | | | 4 | 187.41(39) | | | $M1/E2$ | |
| | | | 6 | 511.50(11) | | | $M1/E2$ | |
| | | | 4 | 926.99(5) | | | $M1/E2$ | 0.034(3) |
| | 1741 | 7 | 5 | 424.36(4) | | | $E2$ | |

TABLE II. (*Continued.*)

| Nucleus/band name | $E_i$ | $I_i$ | $I_f$ | $E_\gamma$(keV) | DCO | $A_p$ | Assign | $(BE2)_{out}/(BE2)_{in}$ |
|---|---|---|---|---|---|---|---|---|
| | | | 6 | 241.6(10) | | | $M1/E2$ | |
| | | | 8 | 511.50(11) | | | $M1/E2$ | |
| | | | 6 | 975.66(5) | | | $M1/E2$ | 0.019(1) |
| | 2242 | 9 | 7 | 501.35(5) | | | $E2$ | |
| | | | 8 | 291.72(25) | | | $M1/E2$ | |
| | | | 8 | 1013.09(6) | | | $M1/E2$ | 0.013(1) |
| | 2800 | 11 | 12 | 459.96(20) | | | $M1/E2$ | |
| | | | 9 | 557.91(6) | | | $E2$ | |
| | | | 10 | 1039.19(10) | | | $M1/E2$ | 0.010(1) |
| | 3363 | 13 | 11 | 562.92(9) | | | $E2$ | |
| | | | 12 | 1022.9(4) | | | $M1/E2$ | |

demonstrating the positive-parity bands in $^{160}$Yb are shown in Figs. 2(b)–2(d). The $0^+$ state shown dashed on the level scheme at 1086 keV is the $0_2{}^+$ level identified in $\beta$-decay [51,52]. The levels at 821 and 1113 keV, assigned as $I^\pi = 2^+$ and $3^+$ in the $\beta$-decay work, are placed in the $2_\gamma{}^+$ band, which is now extended to spin $I = 11\hbar$. Support for a positive-parity

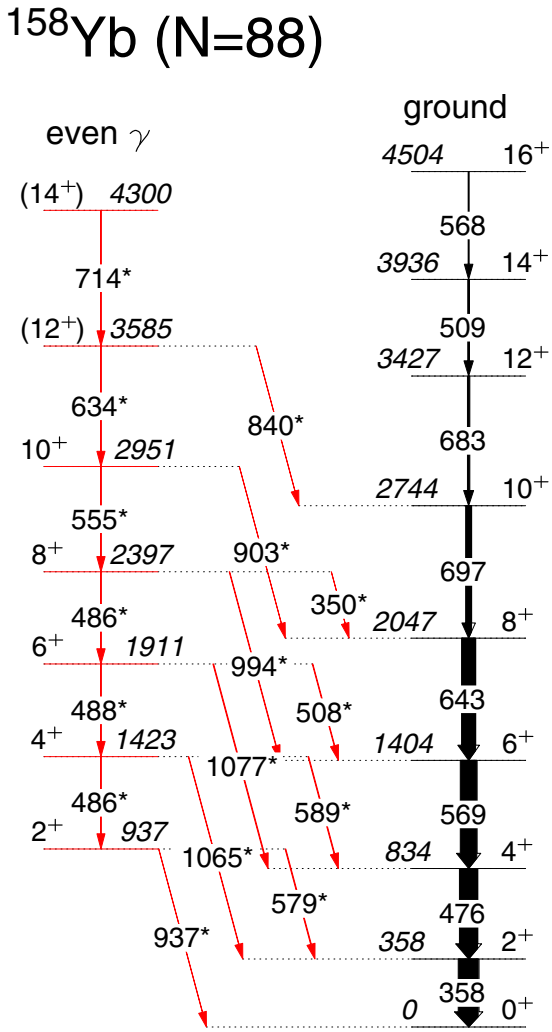


FIG. 1. Partial level scheme showing the ground band and the even spin member of the $2_\gamma{}^+$ band in $^{158}$Yb. Levels and transitions marked with asterisk (*) symbols and colored in red have been established in this work.

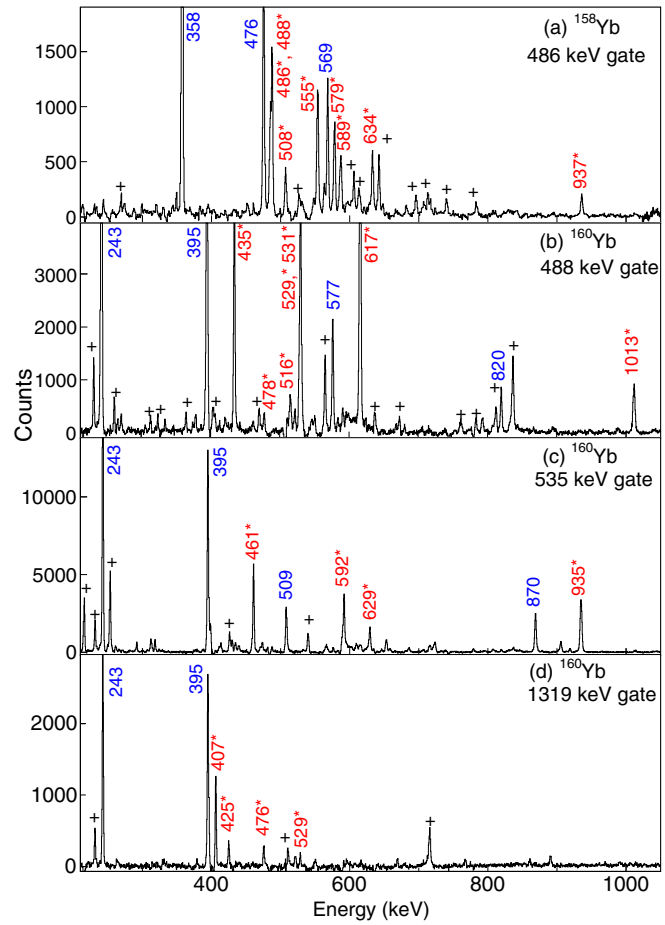


FIG. 2. Spectra showing transitions confirming the placements of the newly built structures in (a) $^{158}$Yb and [(b)–(d)] $^{160}$Yb. Photo peak energies marked with asterisk (*) symbols and colored in red represent new transitions established in this work; previously known $\gamma$ rays are highlighted in blue and unmarked. Plus symbols (+) are used for identifying contaminants from other reaction channels and/or other bands, not associated with the cascade of interest.

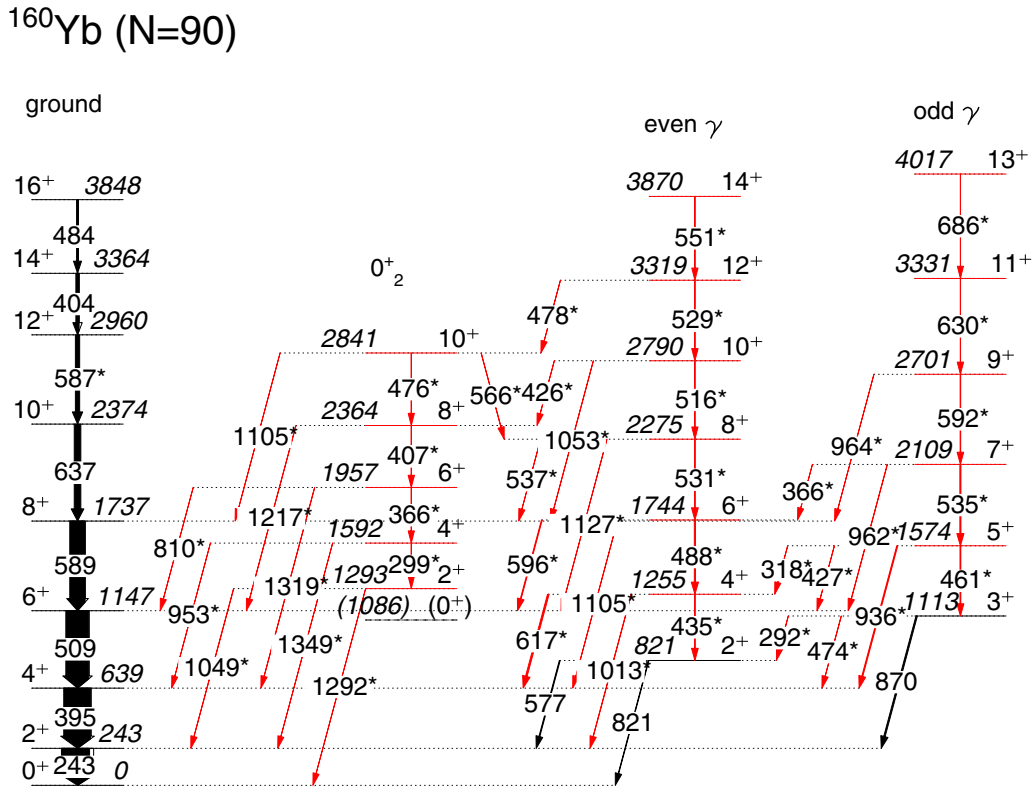


FIG. 3. Partial level scheme of $^{160}$Yb showing the ground, $0_2{}^+$, and $2_\gamma{}^+$ bands. Levels and transitions marked with asterisk (*) symbols and colored in red have been established in this work.

assignment arises from our limits on mixing ratios which have been extracted for some of the transitions depopulating the levels in the $2_\gamma{}^+$ band to the ground-state band. In particular, those for the 577- and 870-keV transitions are consistent with the pure $E2$ assignment favoured in the angular correlation analysis of Garrett *et al.* [51]. However, the level at 1256 keV in the $2_\gamma{}^+$ band was assigned spin and parity of $I^\pi = 3^-$ by Auer *et al.* [52], based on measured conversion coefficients for the 617 and 435 keV transitions. This assignment is rejected here because our DCO ratio for the 435-keV transition, 1.02(9) is consistent with a stretched $E2$ transition, and if a $I^\pi = 3^-$ assignment was adopted, $M2$ multipolarity would be required for the 318- and 366-keV transitions linking the signature partners of the $2_\gamma{}^+$ band. Also visible in Fig. 2(b) are the 566- and 478-keV transitions, which link the $0_2{}^+$ band to $2_\gamma{}^+$ band. Apparently, these transitions and the 426-keV transition are the result of mixing due to the near degeneracy of the levels at 2790 and 2841 keV. On this basis, the 2790-keV level of the $0_2{}^+$ band is assigned as a $I^\pi = 10^+$ state, which in turn fixes the spins and parities of all the members of the $0_2{}^+$ band, which is observed down to the $2^+$ state. Members of this band are also visible in Fig. 2(d), which shows the spectrum produced by gating on the 1319-keV line. Because of the loss of intensity through $I \to I - 2$ and $I \to I$ transitions to the ground band, the $0^+$ bandhead could not be observed. The assignment of the 1086 keV level to the bandhead is justified by the smooth continuation of states when it is plotted as a member of the band in Fig. 6(b), which shows the energies of the levels of the bands of $^{160}$Yb, minus a rigid rotor reference, as a function of spin.

### C. $N = 92$ isotones

The experimental levels and transition rates for $^{154}$Sm and $^{156}$Gd are extracted from Refs. [22,53,54], respectively.

Low-lying positive-parity states in $^{158}$Dy, deduced in this work, are presented in Fig. 4. According to the literature [55], the states built on the $0_2{}^+$ and even spin sequence of the $2_\gamma{}^+$ bands were known up to spins $I = 6$ and 8, with the $6^+$ member of the $0_2{}^+$ band placed at 1547 keV. However, this study positions the $6^+$ level at 1554 keV. In addition, five new in-band transitions (including the $\gamma$-ray depopulating the newly revised level) have been added to this structure. The $6^+$ and $8^+$ members of the even spin $2_\gamma{}^+$ band are listed in the data sheets at 1486 and 1893 keV [55]. This study has revised the positioning of both levels in the level scheme; they are now placed at 1476 and 1863 keV, respectively. The rearrangement of these levels is supported by the newly established interband transitions connecting both the odd and even spin members of the $2_\gamma{}^+$ band. Therefore, when taking into account the rearrangements made in this study, the latter has been extended by five rotational levels from $I = 4$ to $I = 14$. In addition, the odd spin sequence of the $2_\gamma{}^+$ band has also been extended by four in-band transitions from $I = 7$ to $I = 15$. Figure 5 shows a spectrum with interband transitions decaying out of the newly established rotational levels of

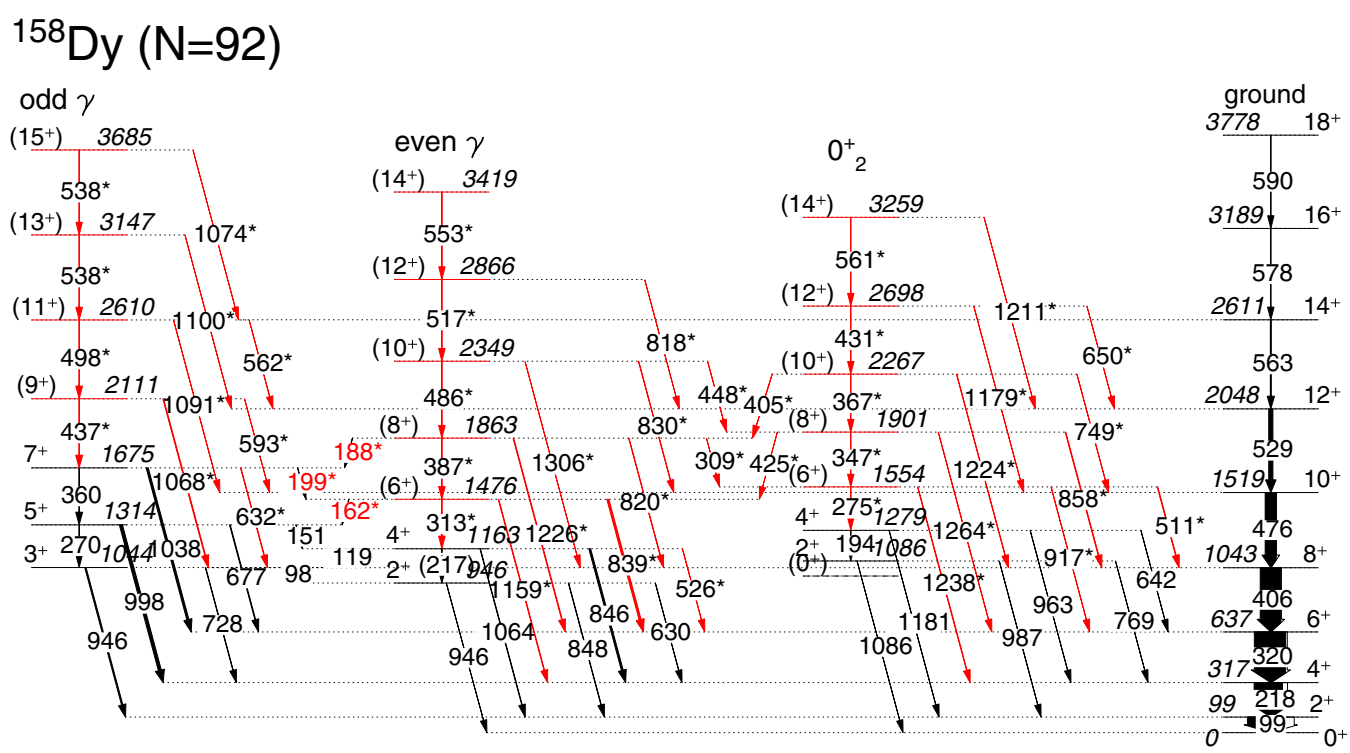


FIG. 4. Partial level scheme of $^{158}$Dy showing the low-lying positive-parity bands, namely the ground, $0_2{}^+$, and $2_\gamma{}^+$ bands. Levels and transitions marked with asterisk (*) symbols and colored in red have been established in this work.

$0_2{}^+$ and $2_\gamma{}^+$ bands, to the ground band of $^{158}$Dy. The DCO and polarization measurements could not be determined for the level scheme of $^{158}$Dy. The ordering of the transitions observed is solely based on the spin and parity selection rule, the interacting behavior between levels (from different bands) that lie energetically close together, and the systematics of the neighboring nuclei.

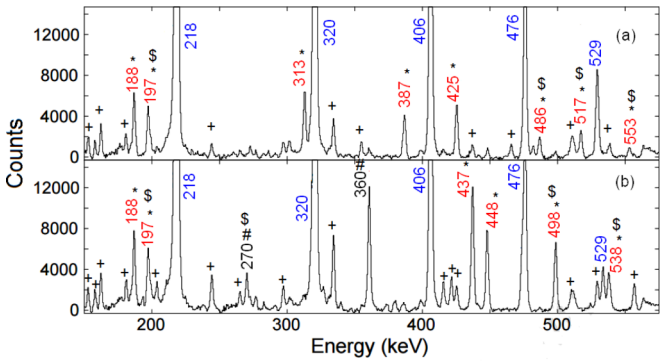


FIG. 5. Summed spectra showing peaks associated with some of the low-lying positive-parity bands in $^{158}$Dy, namely the (a) even and (b) odd $\gamma$ bands. Photo peak energies colored in red and marked with asterisk (*) symbols represent new transitions established in this work. The in-band members of the ground band are highlighted in blue and unmarked. Transitions belonging to $0_2{}^+$ and $2_\gamma{}^+$ bands, known from previous studies are highlighted in black and marked with a hash symbol (#). Transitions marked with a dollar sign ($) are among the transitions that were included in the gating that produced the coincident spectra. Plus symbols (+) are used for identifying contaminants from other reaction channels and/or other bands, not associated with the cascades of interest.

The low-lying positive-parity states in $^{160}$Er, deduced from this work, confirm all the placements that were reported in the in-beam works of Refs. [56,57], which studied the spectroscopy of this nucleus previously. In this study, we report for the first time the ratios of transition rates extracted for the decays out of the $0_2{}^+$ and $2_\gamma{}^+$ bands, which are listed in Table II. The $^{150}$Sm($^{16}$O, 4n)$^{162}$Yb reaction was recently performed at iThemba LABS, using the AFRODITE array. Though partial results of $^{162}$Yb are shown in this work, the complete spectroscopy pertaining to the low-lying positive-parity bands of this nucleus will be published elsewhere [58].

## IV. ENERGY SYSTEMATICS

The energy systematics of the lowest-lying positive-parity bands are summarized, in Fig. 6, by plotting the energies of the levels of the ground, $0_2{}^+$, and $2_\gamma{}^+$ bands, less a rigid-rotor reference. At higher spins ($I > 8\hbar$), the moments of inertia are altered by interactions with higher lying bands. To ascertain the level of mixing due to crossings with high-lying quasiparticle bands such as the $S$ band (attributed to the alignment of $i_{13/2}$ neutrons) [59], the ground bands (blue squares) have been plotted together with those of the $S$ band (black open diamonds). The maximum strength of the interaction $V$ at the first crossing of the ground band with the $S$ band is, in a two-band mixing approximation, given by half of the closest separation of the states of the observed bands. This is evidently limited to $E_x < 250$ keV in all cases, with the possible exception of the lighter $N = 92$ isotones,

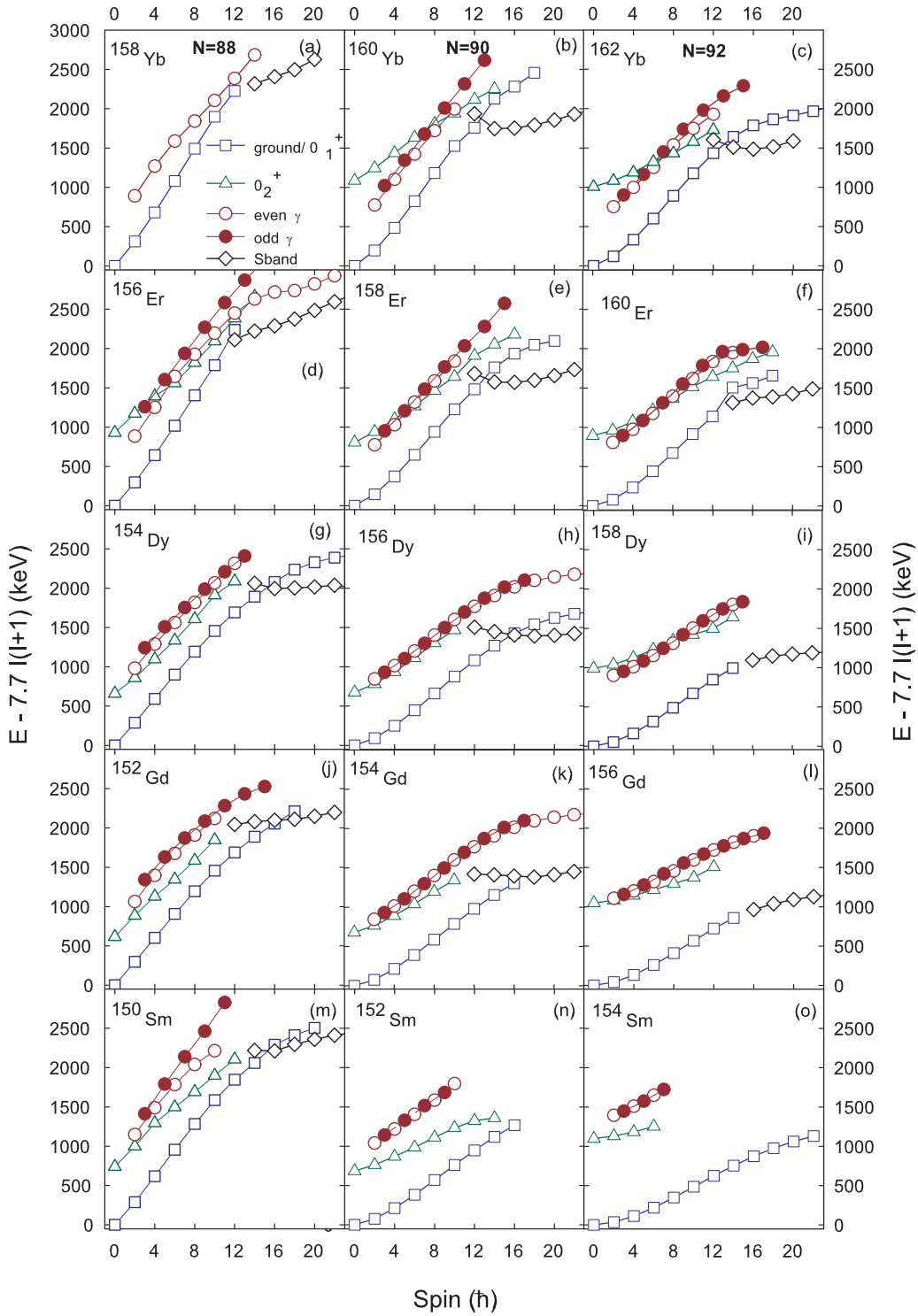


FIG. 6. Energies, less a rigid-rotor reference, of ground, $0_2^+$, $\gamma$, and $S$ bands for $N = 88$ to 92.

where the yrare states have not been confirmed and hence the interactions may be stronger. Using the band mixing equations listed in Ref. [60] and solving unperturbed states, the 250-keV limit implies a negligible perturbation of less than 10 keV at spin $8\hbar$ due to the crossing with the $S$ band.

In general, the slopes of the ground bands decrease with increasing $N$, indicating an increasing moment of inertia, and by implication, an increasing deformation. The opposite is true with increasing proton number, $Z$: The slope increases, implying a decreasing moment of inertia and a decreasing deformation.

In Fig. 7, the moment of inertia is examined quantitatively in the region below spin 10, which is relatively free of mixing with the $S$ band. The quantity $2\Im/\hbar^2$ has been calculated as

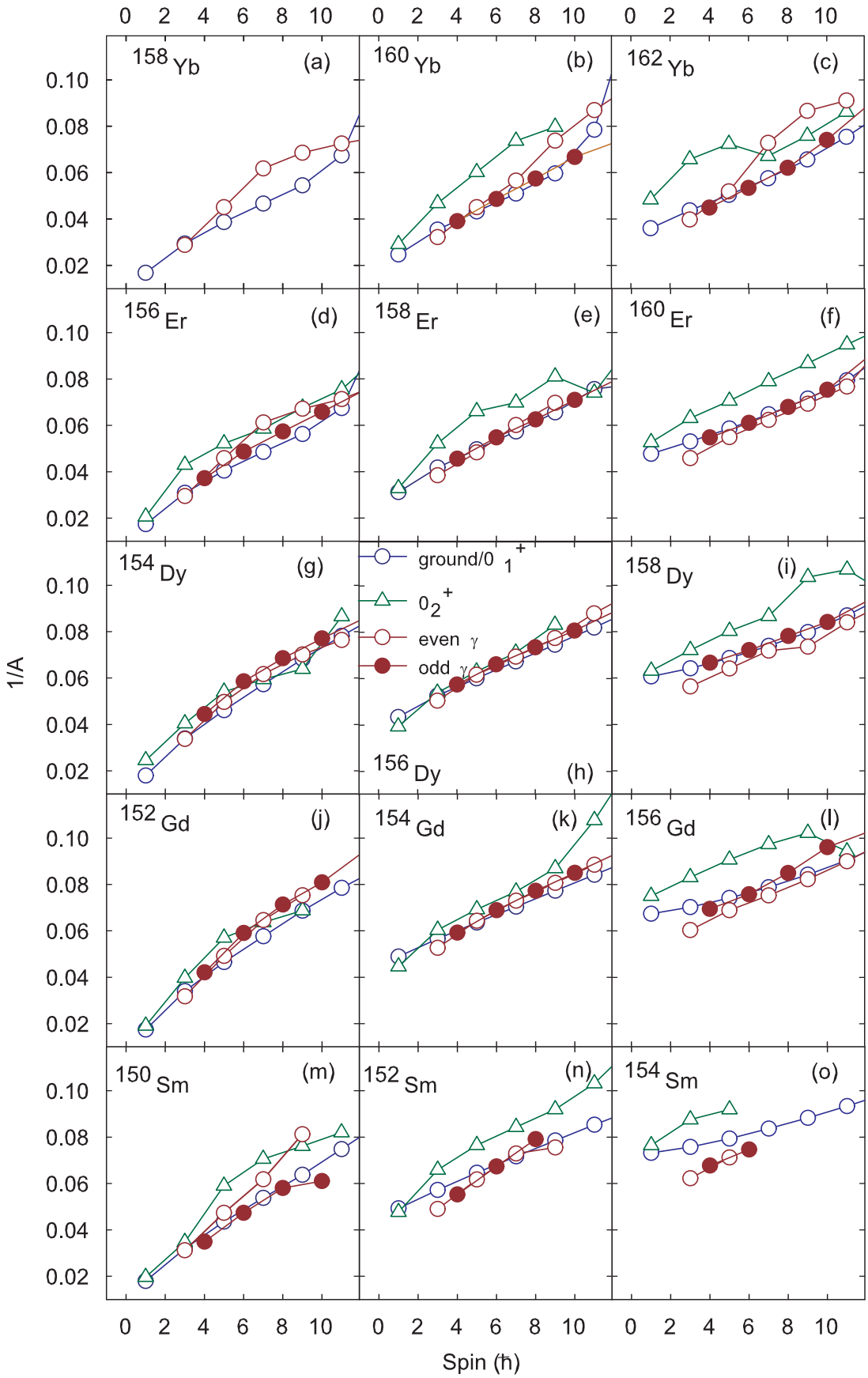


FIG. 7. Moment-of-inertia parameter, $1/A = 2\Im/\hbar^2$, as a function of spin, deduced from the experimental data.

a function of spin, using $2\Im/\hbar^2 = (4I + 2)/E_\gamma$, where $E_\gamma$ is the transition energy between states of spin $I + 1$ and $I - 1$. In agreement with the above discussion, $2\Im/\hbar^2$ increases with $N$ and decreases with $Z$. In Fig. 7, it can also be seen that the moments of inertia are not constant but increase with spin, which has been discussed in terms of Coriolis antipairing [59]. The next striking feature of the data is observed in the comparison of the $2_\gamma{}^+$ bands with the ground-state bands. As a general rule, the odd-spin members of the $2_\gamma{}^+$ bands track the ground bands as a function of spin, indicating similar moments of inertia. The $2_\gamma{}^+$ even-spin band members also have a similar moment of inertia to that of the ground bands, with the main exception being at $N = 88$, where the best agreement is in $^{154}$Dy and $^{152}$Gd. By contrast, the $0_2{}^+$ bands often have moments of inertia greater than their ground bands and the $2_\gamma{}^+$ bands (see Fig. 7). As a result, crossings are observed between the $2_\gamma{}^+$ and $0_2{}^+$ bands, particularly in Yb and Er isotopes, where the $0_2{}^+$ bands have the right bandhead energy to cause crossings with the even members of the $2_\gamma{}^+$ bands (Fig. 6).

Our assignment of the new rotational structure in $^{158}$Yb, shown in Fig. 1, to the even spin $2_\gamma{}^+$ band can now be understood in the context of the systematics presented in Fig. 6. First, the heads of all $2_\gamma{}^+$ bands have energies just below 1 MeV, consistent with the newly established structure, whereas the bandhead energy of the $0_2{}^+$ band appears to increase gradually in excitation energy, (with either $N$ or $Z$), such that its bandhead energy can be expected to be above 1 MeV in $^{158}$Yb. This is not compatible with an extrapolated $0_2{}^+$ energy close to 500 keV and therefore leaves the band in question as the ideal candidate for the $2_\gamma{}^+$ band in $^{158}$Yb. Finally, the moment of inertia for this band is similar to those of well established $2_\gamma{}^+$ bands observed in the neighboring Yb isotopes.

## V. ANALYSIS OF THE LOW-LYING SPECTROSCOPY USING A FIVE-DIMENSIONAL COLLECTIVE HAMILTONIAN BASED ON COVARIANT DENSITY FUNCTIONAL THEORY

The observed energy and moment-of-inertia systematics are the starting point for our theoretical analysis of the bands. The covariant density functional theory has been used as input to a five-dimensional collective Hamiltonian. The model is compared to the energies and the out-of-band to in-band branching ratios determined in our measurements. In addition, comparisons are also made for absolute and relative transition $E0$ and $E2$ strengths using experimental quantities obtained from the literature.

Here, we present a brief introduction to the five-dimensional collective Hamiltonian based on the covariant density functional theory (5DCH-CDFT), which could simultaneously treat the quadrupole vibrational and rotational excitations with the collective parameters self-consistently determined by the microscopic CDFT calculations [35]. The collective Hamiltonian is expressed in terms of the two deformation parameters $\beta$ and $\gamma$ and three Euler angles $(\phi, \theta, \psi) \equiv \Omega$ that define the orientation of the intrinsic principal axes in the laboratory frame,

$$\hat{H}_{\rm coll}(\beta,\gamma) = \hat{T}_{\rm vib}(\beta,\gamma) + \hat{T}_{\rm rot}(\beta,\gamma,\Omega) + V_{\rm coll}(\beta,\gamma). \quad (3)$$

The three terms in $\hat{H}_{\rm coll}(\beta,\gamma)$ are the vibrational kinetic energy

$$\begin{aligned}\hat{T}_{\rm vib} = -\frac{\hbar^2}{2\sqrt{wr}}\Bigg\{&\frac{1}{\beta^4}\Bigg[\frac{\partial}{\partial\beta}\sqrt{\frac{r}{w}}\beta^4 B_{\gamma\gamma}\frac{\partial}{\partial\beta} \\ &- \frac{\partial}{\partial\beta}\sqrt{\frac{r}{w}}\beta^3 B_{\beta\gamma}\frac{\partial}{\partial\gamma}\Bigg] \\ &+ \frac{1}{\beta\sin 3\gamma}\Bigg[-\frac{\partial}{\partial\gamma}\sqrt{\frac{r}{w}}\sin 3\gamma B_{\beta\gamma}\frac{\partial}{\partial\beta} \\ &+ \frac{1}{\beta}\frac{\partial}{\partial\gamma}\sqrt{\frac{r}{w}}\sin 3\gamma B_{\beta\beta}\frac{\partial}{\partial\gamma}\Bigg]\Bigg\}, \end{aligned} \quad (4)$$

the rotational kinetic energy

$$\hat{T}_{\rm rot} = \frac{1}{2}\sum_{k=1}^{3}\frac{\hat{J}_k^2}{\mathcal{I}_k}, \quad (5)$$

and the collective potential $V_{\rm coll}$, respectively. Here, $\hat{J}_k$ denote the components of the total angular momentum in the body-fixed frame and all the collective parameters, including the mass parameters $B_{\beta\beta}$, $B_{\beta\gamma}$, and $B_{\gamma\gamma}$, the moments of inertia $\mathcal{I}_k$, and the collective potential $V_{\rm coll}$, depend on the quadrupole deformation variables $\beta$ and $\gamma$. Two additional quantities that appear in the $\hat{T}_{\rm vib}$ term, $r = B_1B_2B_3$ and $w = B_{\beta\beta}B_{\gamma\gamma} - B_{\beta\gamma}^2$, determine the volume element in the collective space.

In the 5DCH-CDFT [35], which has provided successful descriptions for low-lying nuclear structure along with isotopic and isotonic chains in a variety of mass regions [61–63], the collective parameters of 5DCH are all determined from the triaxial CDFT calculations. In the present investigation, the moments of inertia are calculated with the Inglis-Belyaev formula [64,65] and the mass parameters with the cranking approximation [66]. The collective potential $V_{\rm coll}$ is obtained by subtracting the zero-point energy corrections [66] from the total energy of the constrained triaxial CDFT.

The eigenvalue problem of the Hamiltonian (3) is solved using an expansion of eigenfunctions in terms of a complete set of basis functions that depend on the five collective coordinates $\beta$, $\gamma$, and $\Omega$ [35]

$$\Psi_\alpha^{IM}(\beta,\gamma,\Omega) = \sum_{K\in\Delta I}\psi_{\alpha K}^I(\beta,\gamma)\Phi_{MK}^I(\Omega). \quad (6)$$

Then, the various observables can be calculated with the obtained collective wave functions, for example, the $E2$ transition probabilities

$$B(E2;\alpha I \to \alpha' I') = \frac{1}{2I+1}|\langle\alpha' I'||\hat{M}(E2)||\alpha I\rangle|^2, \quad (7)$$

where $\hat{M}(E2)$ is the electric quadrupole operator.

The analysis of low-lying states in this mass region starts by performing constrained self-consistent relativistic mean-field plus BCS (RMF+BCS) calculations for triaxial shapes (i.e., including both $\beta$ and $\gamma$ deformations). The energy density functional PC-PK1 [67] determines the effective interaction in the particle-hole channel and a finite-range force

that is separable in momentum space is used in the particle-particle channel [68]. The resulting self-consistent solutions (i.e., single-particle wave functions, occupation probabilities, and quasiparticle energies that correspond to each point on the potential energy surface) are used to calculate the parameters that determine the five-dimensional collective Hamiltonian: three mass parameters, three moments of inertia, and collective potential, as functions of the deformations $\beta$ and $\gamma$. The diagonalization of the Hamiltonian yields the excitation energies and collective wave functions that are used to calculate observables. Detailed formalism of the 5DCH based on covariant density functional theory can be found in Refs. [35,36]. The model has been extensively applied to describe the nuclear collective properties, such as the phase transitions, shape coexistence, and the low-lying spectra along the isotopic and isotonic chains in different mass regions [62,69–72]. It should be emphasized that the model includes the full quadrupole deformed configurations, namely, the whole $\beta$-$\gamma$ plane is adopted, and for each deformed configuration, the whole single-particle space is included. Therefore, *the model is parameter free* and accommodates transitional and shape-coexisting nuclei.

In the following, the theoretical calculations for the $N = 88$, $N = 90$, and $N = 92$ isotones are presented, including the potential energy surfaces (PESs) and the probability density distributions in the $\beta$-$\gamma$ plane, to obtain a better understanding of the calculated energy spectra and transition probabilities, and compared with the experimental data.

### A. Potential energy surfaces

Figure 8 displays the potential energy surfaces (PESs) of $N = 88$, $N = 90$, and $N = 92$ isotones in $\beta$-$\gamma$ plane calculated by constrained triaxial RMF+BCS with PC-PK1 density functional [67]. It can be seen that all the nuclei exhibit prolate-like shape in their ground states but show more or less different softness/rigidness in the $\beta$ and $\gamma$ directions. One can summarize the behavior as follows:

(1) For the $N = 88$ isotones, the global minima are all located at $\beta \approx 0.2$ and $\gamma \approx 0^\circ$. As the proton number increases, the PES around the global minimum becomes more rigid in the $\beta$ direction and a little bit softer in the $\gamma$ direction.
(2) For the $N = 90$ isotones, with increase in proton number, the global minima move to smaller prolate deformation, with $\beta \approx 0.3$ for $^{152}$Sm and $\beta \approx 0.25$ for $^{160}$Yb. The PES around the global minimum is rather soft in the $\beta$ direction and stiff in $\gamma$ direction in the $N = 90$ isotones, $^{152}$Sm, $^{154}$Gd, and $^{156}$Dy. This is consistent with the findings of Ref. [36], where both the microscopic calculations and the data show that there is an abrupt change of structure at $N = 90$, close to the proposed $X(5)$ critical point [73,74].
(3) For the $N = 92$ isotones, well-deformed prolate global minima are found in $^{154}$Sm, $^{156}$Gd, and $^{158}$Dy. As the proton number increases, the PES around the global minimum becomes softer in both $\beta$ and $\gamma$ directions.
(4) A secondary local minimum develops in the Er and Yb isotopes at $\beta \approx 0.45$ and $\gamma \approx 10^\circ$. These minima have a shape that corresponds to that of the well-known triaxial bands observed in nearby Lu isotopes, such as $^{163–165}$Lu [75,76]. It becomes very close in energy to the global minimum with the increase of neutron number, and therefore the effect of shape coexistence could be very important in $^{162}$Yb. The counterpart of the Yb minimum is present in the PES of the Er isotopes, although it is less well developed.

In total, for each isotopic chain, from $N = 88$ to 92, the quadrupole deformation $\beta$ of the global minimum increases and the PES around it becomes a little bit more rigid in the $\gamma$ direction. For each isotonic chain, from Sm to Yb, the PES around the global minimum becomes softer in the $\gamma$ direction, while in the $\beta$ direction it is largely influenced by the development of a secondary local minimum.

### B. Energy spectra

Based on the PESs and inertial parameters, one can construct a 5DCH Hamiltonian. Diagonalization of the Hamiltonian yields the excitation energies and collective wave functions that are used to calculate the observables such as $\langle r_c^2 \rangle^{1/2}$, $B(E0)$, $B(E2)$, and so on. For each nucleus, the collective band structure is constructed according to the calculated $E2$ transition probabilities between different states. Figures 9–11 display the comparison of the calculated energy spectra to the available experimental data for the $N = 88$, $N = 90$, and $N = 92$ isotones, respectively. Here, the comparisons have been performed for the band structures built on the ground state $0_1^+$, second state $0_2^+$, third $0_3^+$ state, and the $\gamma$ bands. Normally, in the classical picture of the collective model, the band built on the $0_2^+$ state is considered to be the $\beta$ vibrational band and the $0_3^+$ state is considered to be the second $\beta$ band. The bandhead of the $\gamma$ band is taken to be the second excited $2_\gamma^+$ state or the third excited $2_3^+$ state, depending on which has the larger $K = 2$ component in the 5DCH-CDFT calculations.

In Figs. 9–11, the theoretical energy levels, minus a rigid rotor reference $7.7I(I + 1)$ keV, are plotted for the $N = 88$, 90, and 92 isotones and compared to the corresponding experimental quantities. The most apparent observation is that the theoretical bands rise in energy more quickly than the experimental ones. This discrepancy is consistent with what is observed between the theoretical moments of inertia, plotted in Fig. 12, and their experimental counterpart in Fig. 7. These deviations may come from the assumption of adiabatic approximation of the collective Hamiltonian, where the collective parameters are calculated in the vicinity of zero collective angular momenta, such that the moments of inertia are calculated in the vicinity of zero rotational frequency [35,77].

It is worth noting that for the transitional nuclei like the $N = 88$, 90, and 92 isotones discussed here, whose soft potentials are susceptible to the increasing angular momentum, this approximation becomes less satisfying [63,78]. As shown in Ref. [63], one possibility to improve the agreement between theoretical results and experimental data is by introducing an

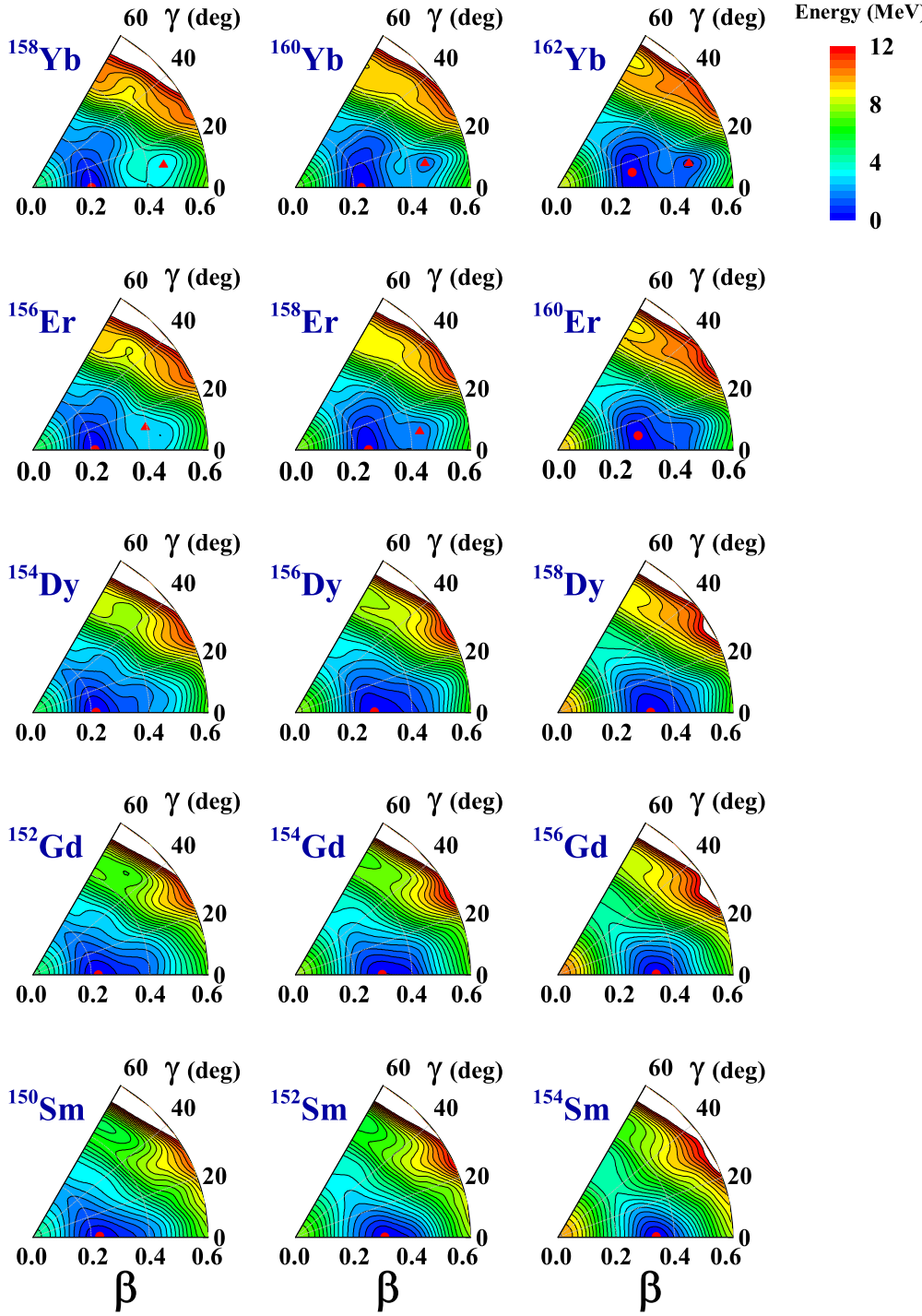


FIG. 8. Potential energy surfaces (PESs) of $N = 88$, $N = 90$, and $N = 92$ isotones in the $\beta$-$\gamma$ plane. Minima are marked with red symbols; circles and triangles represent the global and secondary minima, respectively. The energy spacing in the contour lines is 0.25 MeV.

empirical *ab* formula for the moments of inertia [79], which is responsible for the fourth-order effect of collective momentum in the collective Hamiltonian. Nevertheless, despite the minor discrepancies mentioned above, the overall agreement in the trends between the theoretical energy spectra and the available data is satisfactory.

The main features of the theoretical energy spectra are summarized as follows:

(1) Ground-state band: The trends of moments of inertia in both $N$ and $Z$ are consistent with the variation of the quadrupole deformation of the global minima in the PESs in Fig. 8. The larger deformations generally correspond to larger moments of inertia and result in a more compact ground-state band, rising more slowly in energy with spin. The general trends are in agreement with experiment.

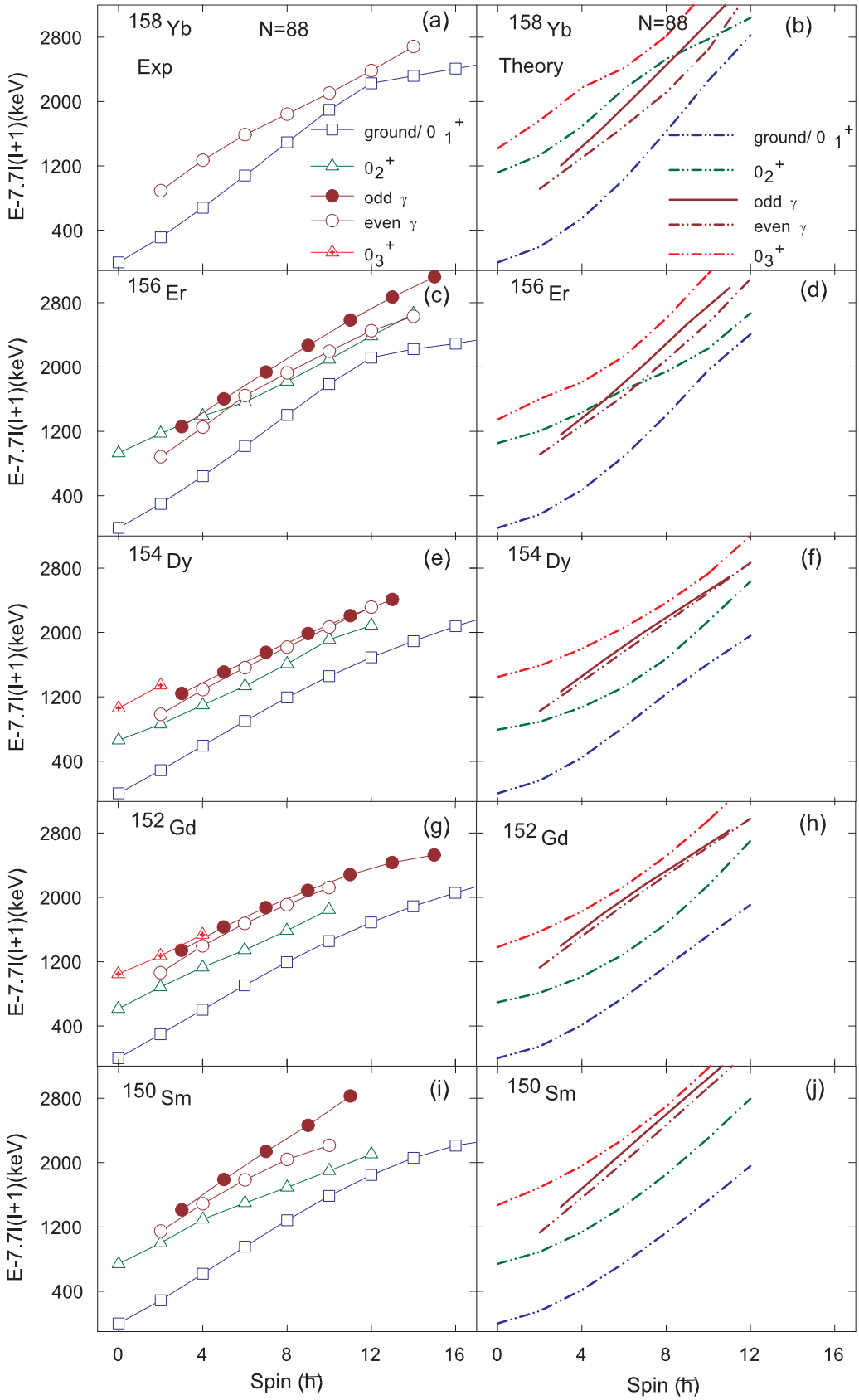


FIG. 9. The experimental energy spectra of the bands built on the ground state $0_1{}^+$, the second and third $0^+$ states, and the $\gamma$ bands for the $N = 88$ isotones (left panels), in comparison with the theoretical results (right panels). For the $\gamma$ bands, the odd- and even-spin sequences are shown with different symbols.

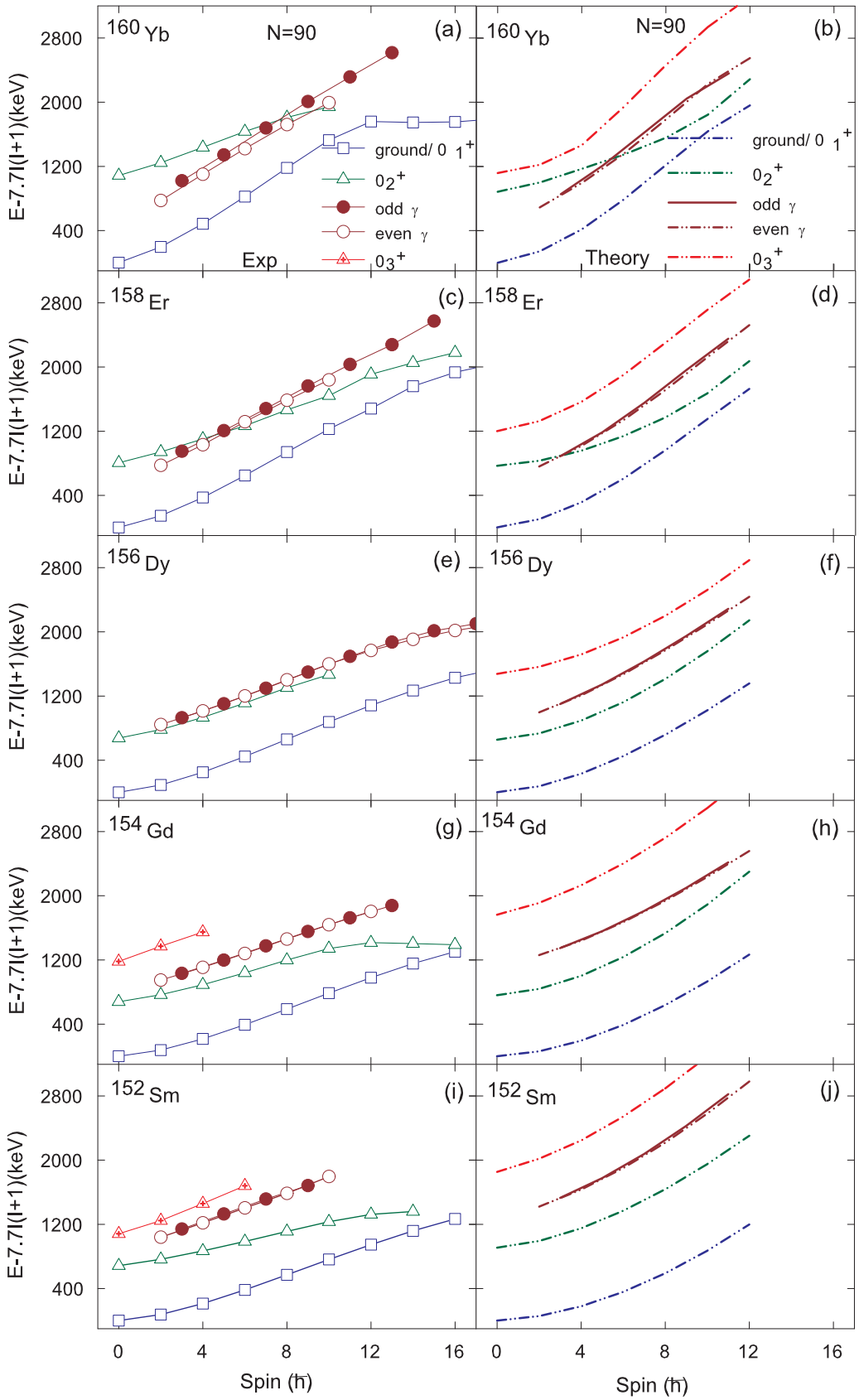


FIG. 10. The experimental energy spectra of the bands built on the ground state $0_1^+$, the second and third $0^+$ states, and the $\gamma$ bands for the $N = 90$ isotones (left panels), in comparison with the theoretical resutls (right panels). For the $\gamma$ bands, the odd- and even-spin sequences are shown with different symbols.

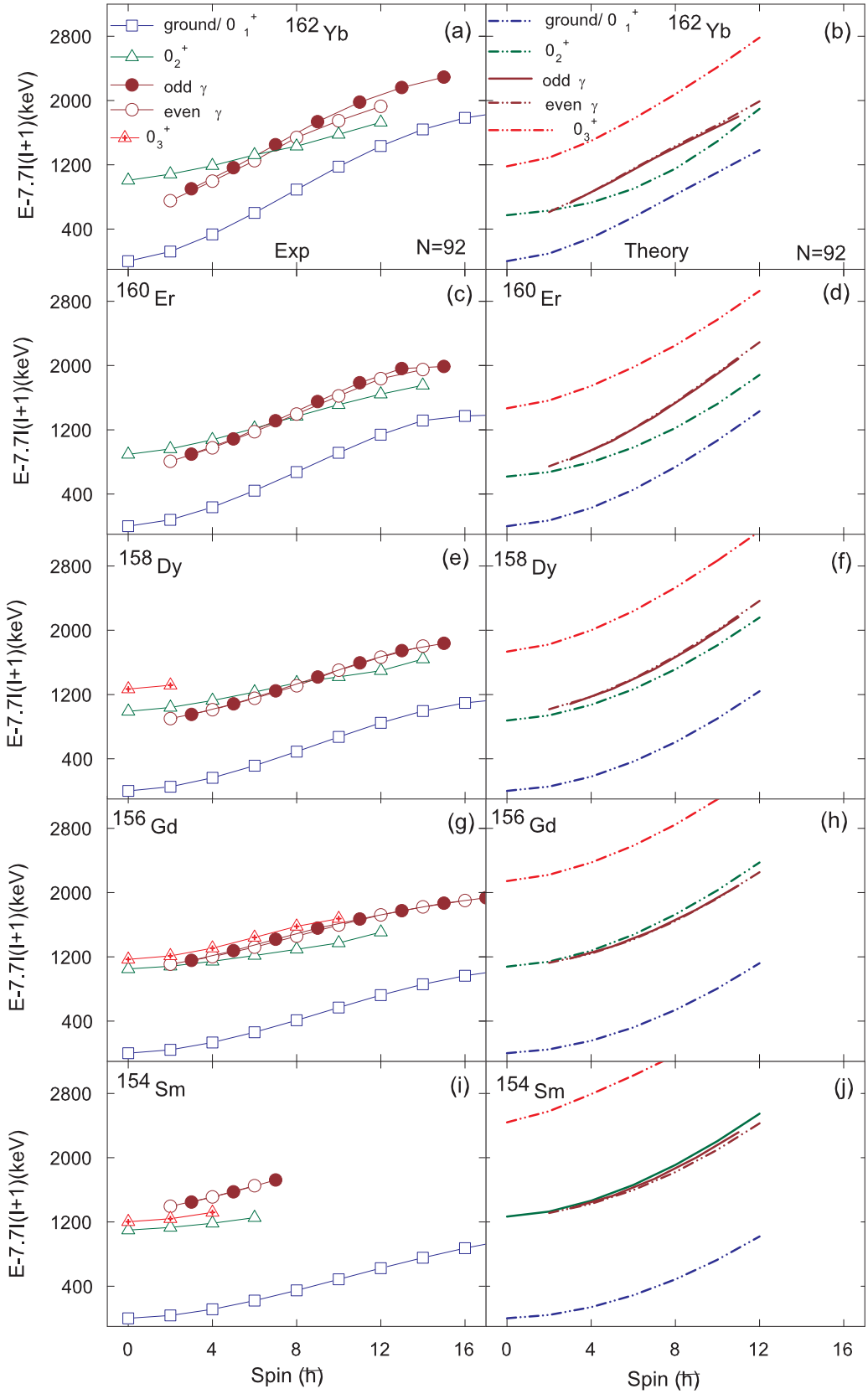


FIG. 11. The experimental energy spectra of the bands built on the ground state $0_1{}^+$, the second and third $0^+$ states, and the $\gamma$ bands for the $N = 92$ isotones (left panels), in comparison with the theoretical resutls (right panels). For the $\gamma$ bands, the odd- and even-spin sequences are shown with different symbols.

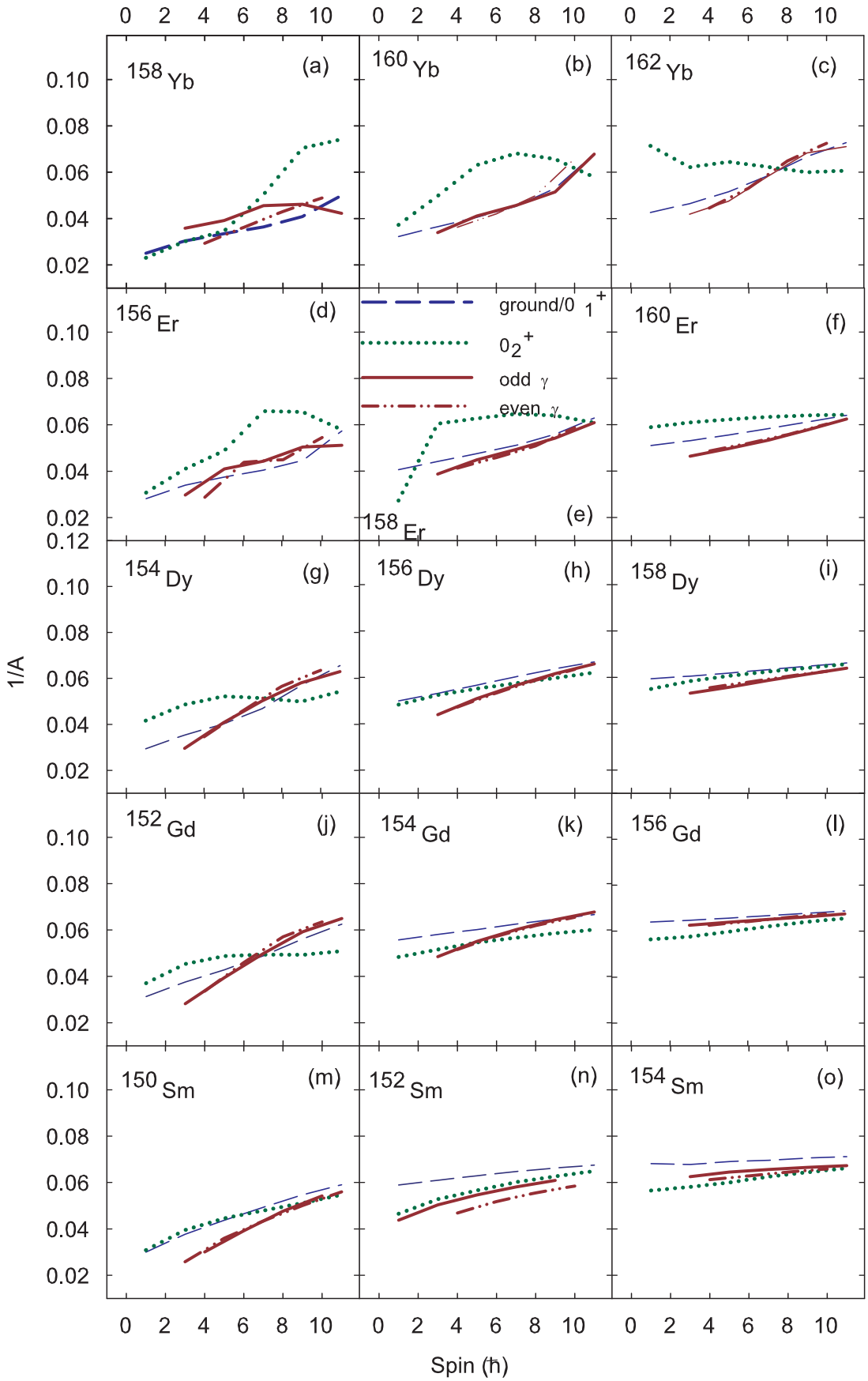


FIG. 12. Calculated values of $1/A = 2\Im/\hbar^2$ for the ground band (blue), $0_2{}^+$ band (green), and $2_\gamma{}^+$ band (brown). Solid lines have even spin.

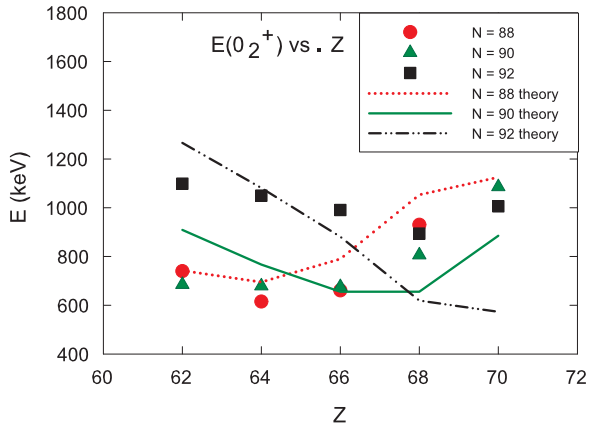


FIG. 13. Bandhead energies of the $2_\gamma{}^+$ bands as a function of $Z$.

(2) $\gamma$ band: The theoretical moments of inertia of the $\gamma$ band mimic the behavior of the experimental bands—their moments of inertia are very close to those of the ground bands. In Fig. 13, the theoretical and experimental bandhead energies of the $\gamma$ band are plotted and compared as a function of the atomic number. In both theory and experiment, the bandhead of the $\gamma$ band shifts toward lower energy as $Z$ increases, consistent with the observation that the PES around the global minimum becomes softer in the $\gamma$ direction from Sm to Yb for each isotonic chain.

(3) $0_2{}^+$ band: Like the data, the calculated moments of inertia of the $0_2{}^+$ band are often higher than those of the calculated ground-state band. The agreement for this feature between theory and experiment is moderate along $N = 88$ (see Figs. 7 and 12), best along $N = 90$, and moderate along the $N = 92$ isotonic chain. The experimental and calculated energies of the $0_2{}^+$ bandheads are plotted as a function of the proton number in Fig. 14. For each isotope, a minimum in experimental bandhead energy is found between $Z = 64$ and $Z = 68$. The calculated minima agree for $N = 88$ and $N = 90$, but for $N = 92$, the minimum is too soft, leading to the energy of the head of the $0_2{}^+$ band being underestimated by over 400 keV in $^{162}$Yb.

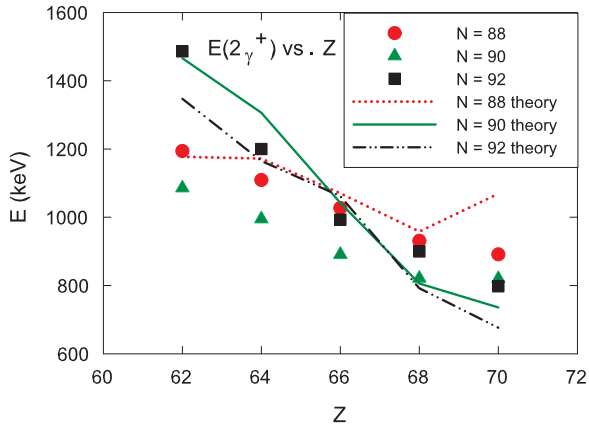


FIG. 14. Bandhead energies of the $0_2{}^+$ bands as a function of $Z$.

Nevertheless, the calculated bandhead energies and moments of inertia are accurate enough to reproduce most of the band crossings observed in the data. At $N = 88$ (Fig. 9), the $\beta$ band in $^{158}$Yb is predicted to lie above the $\gamma$ band and to cross it only at high spins. Experiment is consistent with this picture; the $0_2{}^+$ band is not observed, probably because it is too high in energy. In $^{156}$Er, in both theory and experiment, the $\beta$ band comes lower in energy and crosses the $\gamma$ band. In $^{154}$Dy and lighter isotones, the calculations correctly predict that the $\beta$ band lies lower than the $\gamma$ band; consequently, no crossings are observed. At $N = 90$ (Fig. 10), in agreement with the data, crossings are predicted in $^{160}$Yb and $^{158}$Er, and none in the lighter isotones, due to the $\beta$ band lying lower than the $\gamma$ band. At $N = 92$ (Fig. 11), experimental crossings are observed in all but $^{154}$Sm. The calculations predict that the $\gamma$ and $\beta$ bands should be close in energy as observed experimentally, but in the calculations, the moments of inertia of the two bands are too similar to reliably predict nuclei in which crossings occur. It is in Er and Yb isotopes that the theoretical moments of inertia of the $0_2{}^+$ bands are sufficiently different to cause crossings, see Fig. 12, while in Sm to Dy isotopes, the moments of inertia of the $0_2{}^+$ bands are very similar to those of the ground bands. As we shall see in the following sections, this points to a structural change in the predicted nature of the $0_2{}^+$ bands in Er and Yb isotopes. In these isotopes, the $0_2{}^+$ bands correspond to the superdeformed triaxial minima in Fig. 8, while in Sm to Dy, the $0_2{}^+$ bands align more closely to a vibrational excitation.

(4) $0_3{}^+$ band: In the Sm, Gd, and Yb isotopes, the calculated bandhead of the $0_3{}^+$ band is nearly twice that of the $0_2{}^+$ band, as would be expected for a two-phonon $\beta$ vibration. The 5DCH-CDFT calculations cannot reproduce the very low experimental excitation energy of the $0_3{}^+$ state in some nuclei, especially in $^{154}$Sm and $^{156}$Gd. This may suggest that the $0_3{}^+$ states observed in these nuclei are not collective quadrupole excitation states but based on other excitation modes, such as pairing isomers [20,28,42], which have not been taken into account in the present 5DCH-CDFT calculations. For Er and Yb isotopes, the calculated excitation energy of the $0_3{}^+$ band is much less than twice of that of the $0_2{}^+$ band. According to the PESs in Fig. 8, the triaxial local minimum plays an important role in the $0_2{}^+$ and $0_3{}^+$ states in these nuclei. In Sec. V E, the $0_2{}^+$ band is identified with superdeformed minimum while the $0_3{}^+$ band has mixed, vibrational character.

### C. Energy staggering in the $\gamma$ band

It is interesting to further investigate the odd-even energy staggering in the $\gamma$ bands, to probe the $\gamma$ deformation. The energy staggering is defined as

$$S(I) = \frac{[E(I) - E(I-1)] - [E(I-1) - E(I-2)]}{E(2_1{}^+)}. \quad (8)$$

Within the $\gamma$ band, $S(I)$ has been suggested as an important measure to distinguish soft or rigid triaxiality. For a $\gamma$-rigid rotor, the $\gamma$ band should exhibit pairs of levels close in energy, $(2^+, 3^+)$, $(4^+, 5^+)$, $(6^+, 7^+)$, … (even spins lower in energy) [80], while for a $\gamma$-soft collective structure a grouping of levels $2^+$, $(3^+, 4^+)$, $(5^+, 6^+)$, … (odd spins lower) should be observed [81]. Thus, in both cases $S(I)$ shows an odd-even staggering with the increase of spin, and $S(4) > 0$ in the former case while $S(4) < 0$ in the latter case. In addition, for an ideal axially symmetric rotor, this staggering parameter is a constant $S(I) = 0.33$, while for a harmonic vibrator, it exhibits a staggering behavior with an absolute value equal to 1.0 and $S(4) = -1$.

Figure 15 displays the experimental and theoretical energy staggering parameter $S(I)$ as a function of spin for the $\gamma$ bands in the $N = 88$, $N = 90$, and $N = 92$ isotones. The calculations can reproduce the experimental data not only for the staggering behavior but also for the variations in the absolute amplitude in the $N = 88$ and $N = 90$ isotones. For the $N = 92$ isotones, although the agreement between the calculated and experimental $S(I)$ is not as impressive as the $N = 88$ and $N = 90$ isotones, the amplitudes of $S(I)$ are close to each other.

For the $N = 88$ isotones, the $S(I)$ exhibits an obvious odd-even staggering with $S(4) \approx -1$, indicating a prominent vibrational character of the $\gamma$ bands. This is consistent with their potential energy surfaces with slightly quadrupole deformed minimum and $\gamma$-soft character. The amplitude of $S(I)$ decreases with spin $I$ for $^{152}$Gd and $^{154}$Dy but increases for $^{156}$Er and $^{158}$Yb which may reflect the delicate interplay with the second local minimum.

For the $N = 90$ and 92 isotones, with two or four more neutrons being added to $N = 88$ isotones, the odd-even staggering of $S(I)$ becomes very weak with a negative or positive $S(4)$ tending to 0, indicating large rotational compositions inside the $\gamma$ bands. This is consistent with their potential energy surfaces having relatively large deformed minimum and $\gamma$-stiff character. Further experimental and theoretical investigations may be needed for the small difference in the comparisons of $S(I)$ for the $N = 92$ isotones $^{154}$Sm, $^{158}$Dy, and $^{160}$Er.

### D. Transition ratios and probabilities

#### 1. *In-band* $B(E2)$

The experimental in-band $B(E2; I \to I-2)$ values for the yrast and $0_2{}^+$ bands in the $N = 88$, $N = 90$, and $N = 92$ isotones, taken from the literature [46,53–55,82–87] are summarized in Fig. 16. The calculations reproduce the increasing trend of the in-band $B(E2; I \to I-2)$ rates with spin for all the nuclei in the low spin region and also the evolution of $B(E2; 2 \to 0)$ with neutron number for all the isotopic chains. A decrease in the experimental $B(E2; I \to I-2)$ values in the high spin region can be seen in several nuclei, which is due to the influence of the band crossings and goes beyond the scope of present 5DCH-CDFT calculations. It should be emphasized that the calculation is completely parameter free, an important advantage of using collective models based on self-consistent mean-field single-particle solutions. Here, physical observables, such as transition probabilities and spectroscopic quadrupole moments, are calculated in the full configuration space and there is no need for effective charges. Considering this, the systematic agreement between the theoretical $B(E2; I \to I-2)$ values and the available data is reasonably good.

There are relatively few experimental data points for the in-band $B(E2; I \to I-2)$ values of the $0_2{}^+$ bands. These values are reasonably reproduced by the microscopic calculations, with the exception of the measured values for the Gd isotopes. The 5DCH-CDFT calculations predict much larger in-band $B(E2; I \to I-2)$ values for the $0_2{}^+$ bands compared to the ground bands in $^{156,158,160}$Er, and $^{160,162}$Yb. This supports the interpretation that the deformations of the two bands are rather different, pointing to possible shape coexistence in these nuclei. To this end, in the future more lifetime measurements for these nuclei would be welcome.

#### 2. *B(E2) branching ratios*

A systematic comparison between theory and experiment is also made for the branching ratios of both the $0_2{}^+$ and $\gamma$ bands with respect to the ground-state bands; see Figs. 17–20. As can be seen in Figs. 17 and 18, the systematic comparison for the $0_2{}^+$ bands in the $N = 88$, 90, and 92 isotones, shows a very good agreement between the experimental and theoretical branching ratios for the out-of-band to in-band transitions.

A striking feature of the branching ratio shown in Fig. 17 is the rapid increase of the predicted $B(E2; I_{0_2{}^+} \to (I-2)_g)/B(E2; I_{0_2{}^+} \to (I-2)_{0_2{}^+})$ ratios, around spin $I \approx 10\hbar$, in $^{154}$Dy, $^{156,158}$Er, and $^{160}$Yb. It indicates configuration mixing between the ground and $0_2{}^+$ bands, which can also be clearly seen as the band interaction in the calculated energy spectra of these nuclei in Figs. 9 and 10. Such a rapid increase of the $B(E2; I_{0_2{}^+} \to (I-2)_g)/B(E2; I_{0_2{}^+} \to (I-2)_{0_2{}^+})$ ratio is seen experimentally in $^{160}$Er, but in this spin region ($I > 10\hbar$), mixing with the $S$ band is likely to also play a role. Evidence of such an increase can also be found experimentally in $^{158}$Er and $^{160}$Yb, but more experimental data are needed to confirm the observations.

Figure 19 displays the out-of-band to in-band branching ratios $B(E2; I_\gamma \to (I-2)_g)/B(E2; I_\gamma \to (I-2)_\gamma)$ for even $I$ and $B(E2; I_\gamma \to (I-1)_g)/B(E2; I_\gamma \to (I-2)_\gamma)$ for odd $I$, for the $\gamma$ bands in the $N = 88, 90$, and 92 isotones. Figure 20 further displays the branching ratios $B(E2; I_\gamma \to I_g)/B(E2; I_\gamma \to (I-2)_\gamma)$ for these $\gamma$ bands. The vertical lines in Fig. 19 correspond to a range of possible $B(E2)$ ratios depending on the actual value of the mixing ratio $\delta$ associated with the $I_\gamma \to (I-1)_g$ transitions. The lowest value of the vertical lines correspond to $\delta = 1$ while the highest correspond to pure $E2$. In general, the agreement between the experimental and theoretical results is impressive. In all cases, the ratios appear to be within the same order of magnitude and this suggests *structural similarities among these nuclei*. In addition, in both the experimental and theoretical results, there is also a fair amount of staggering between

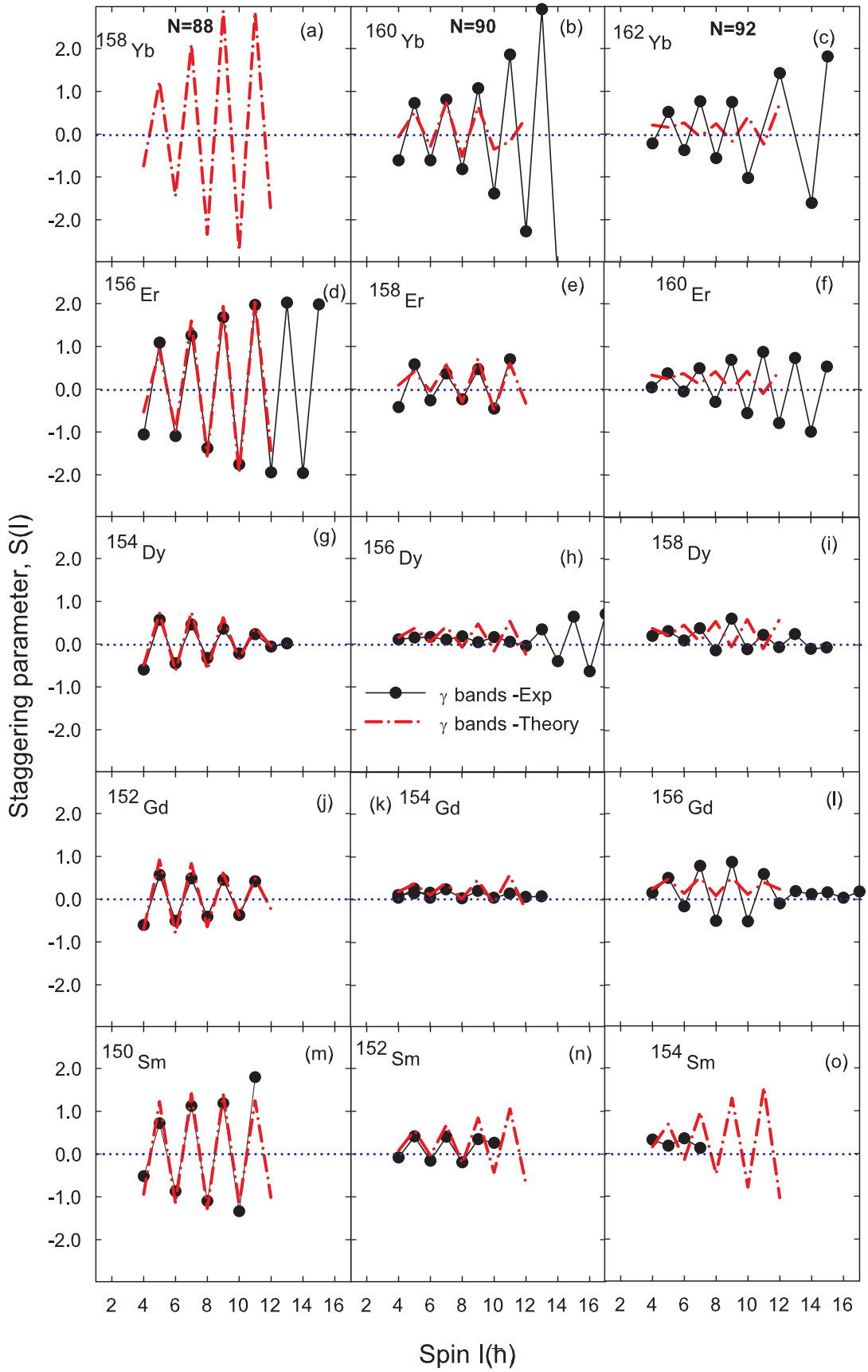


FIG. 15. The experimental staggering parameter $S(I)$ for the $\gamma$ bands in the $N = 88$, $N = 90$, and $N = 92$ isotones (solid circles), in comparison with the calculated results by the 5DCH-CDFT (dash-dotted lines).

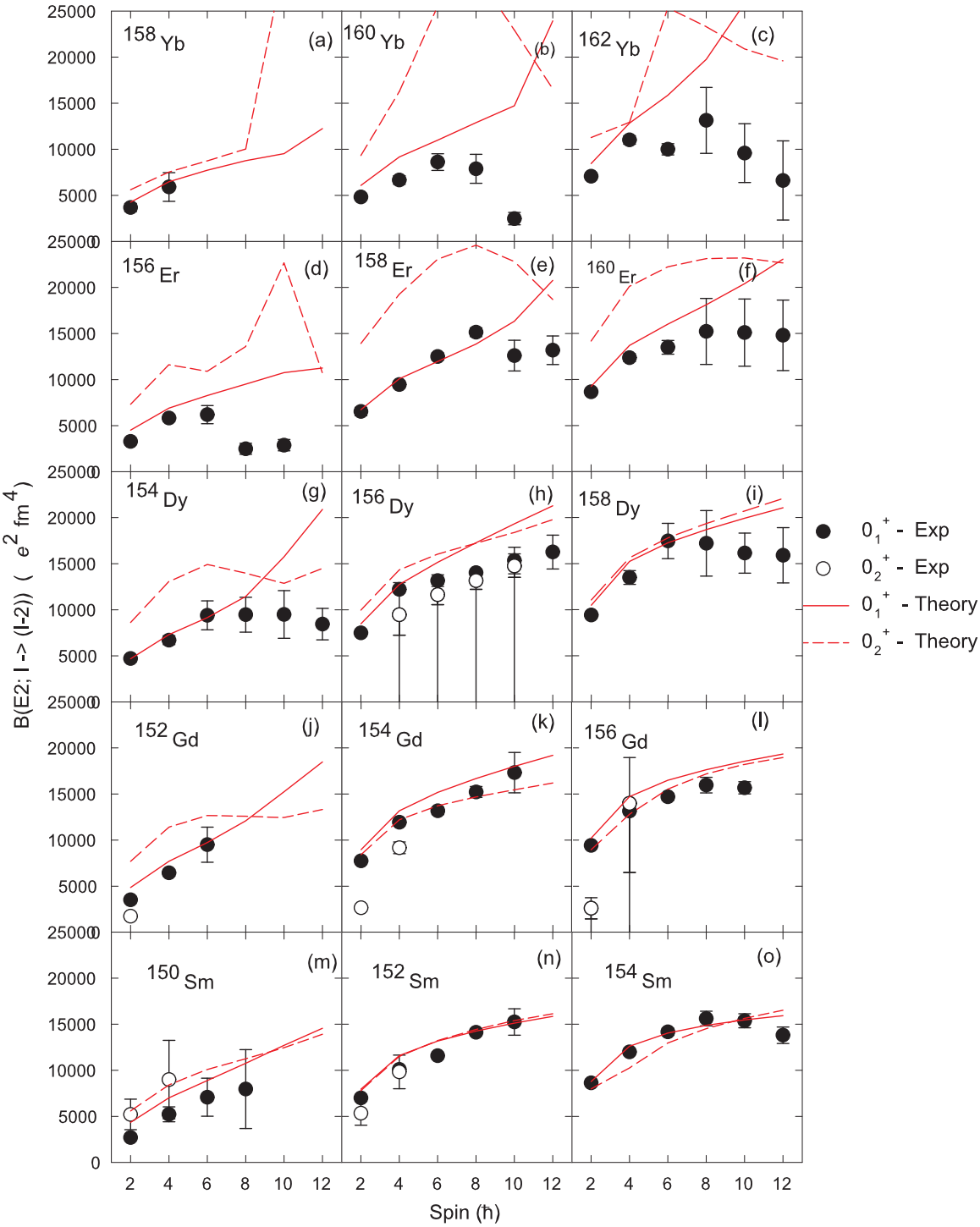


FIG. 16. In-band $B(E2; I \to I-2)$ values for the yrast (solid lines) and $0_2^+$ bands (dashed lines) in the $N = 88$, $N = 90$, and $N = 92$ isotones, calculated with PC-PK1 (lines), in comparison with the available data, shown as filled circles for the yrast bands and as empty circles for the $0_2^+$ bands [46,53–55,82–87].

$B(E2; I_\gamma \to (I-1)_g)/B(E2; I_\gamma \to (I-2)_\gamma)$ for odd $I$ and $B(E2; I_\gamma \to (I-2)_g)/B(E2; I_\gamma \to (I-2)_\gamma)$ for even $I$.

One of the most decisive observables that can be used to characterize the first excited $K^\pi = 0_2^+$ bands is $B(E2; I_2 \longrightarrow I_g + 2)$. In Table III, the experimental $\frac{B(E2; I_2 \longrightarrow I_g+2)}{B(E2; I_2 \longrightarrow I_2-2)}$ ratios deduced from this work are compared with those from previous studies. The experimental data are well reproduced by the calculations.

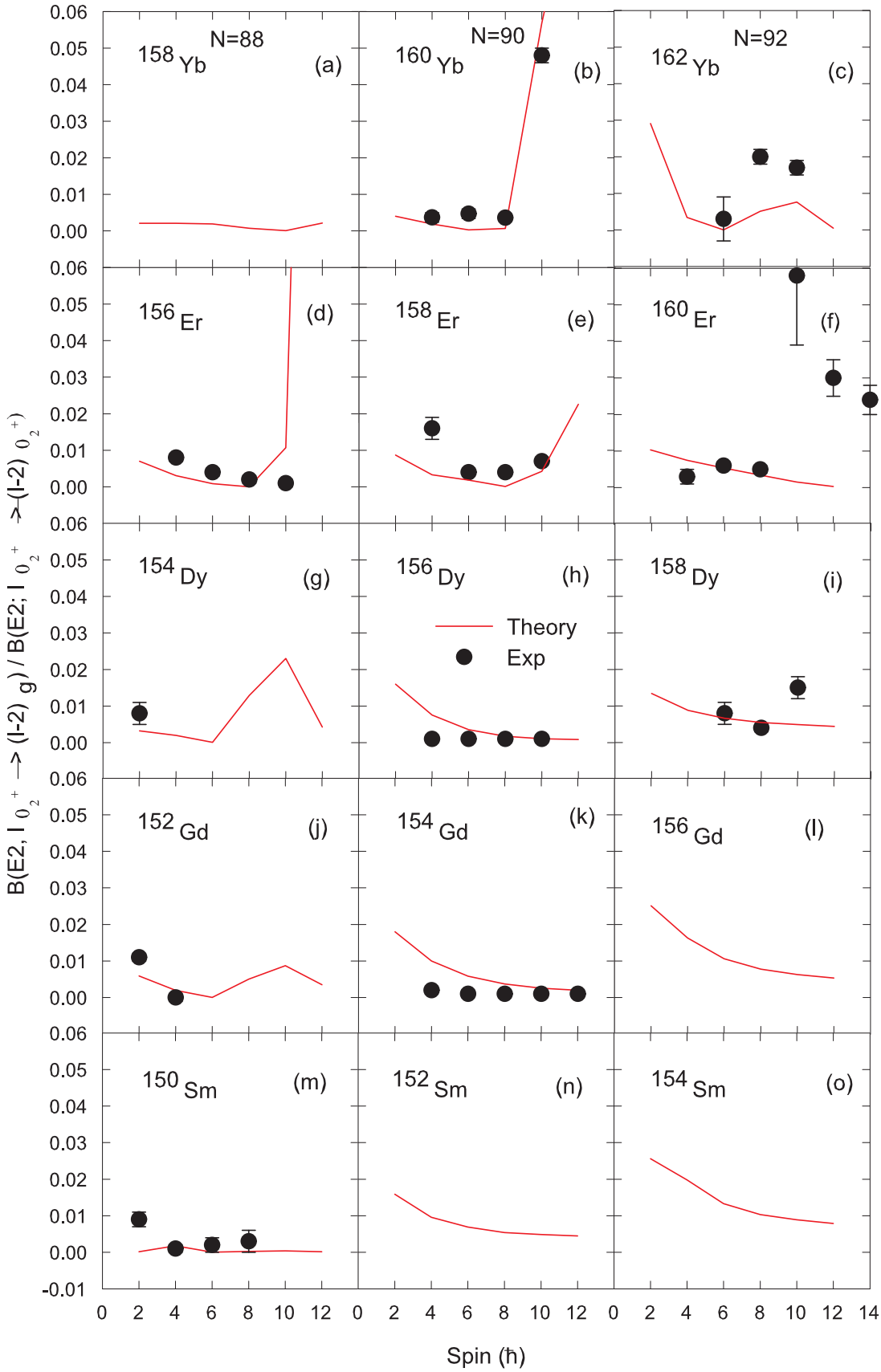


FIG. 17. The calculated branching ratios for out-of-band to in-band transitions, $B(E2; I_{0_2^+} \rightarrow (I-2)_g)/B(E2; I_{0_2^+} \rightarrow (I-2)_{0_2^+})$, for the $0_2^+$ bands in the $N = 88$, $N = 90$, and $N = 92$ isotones, in comparison with the available data.

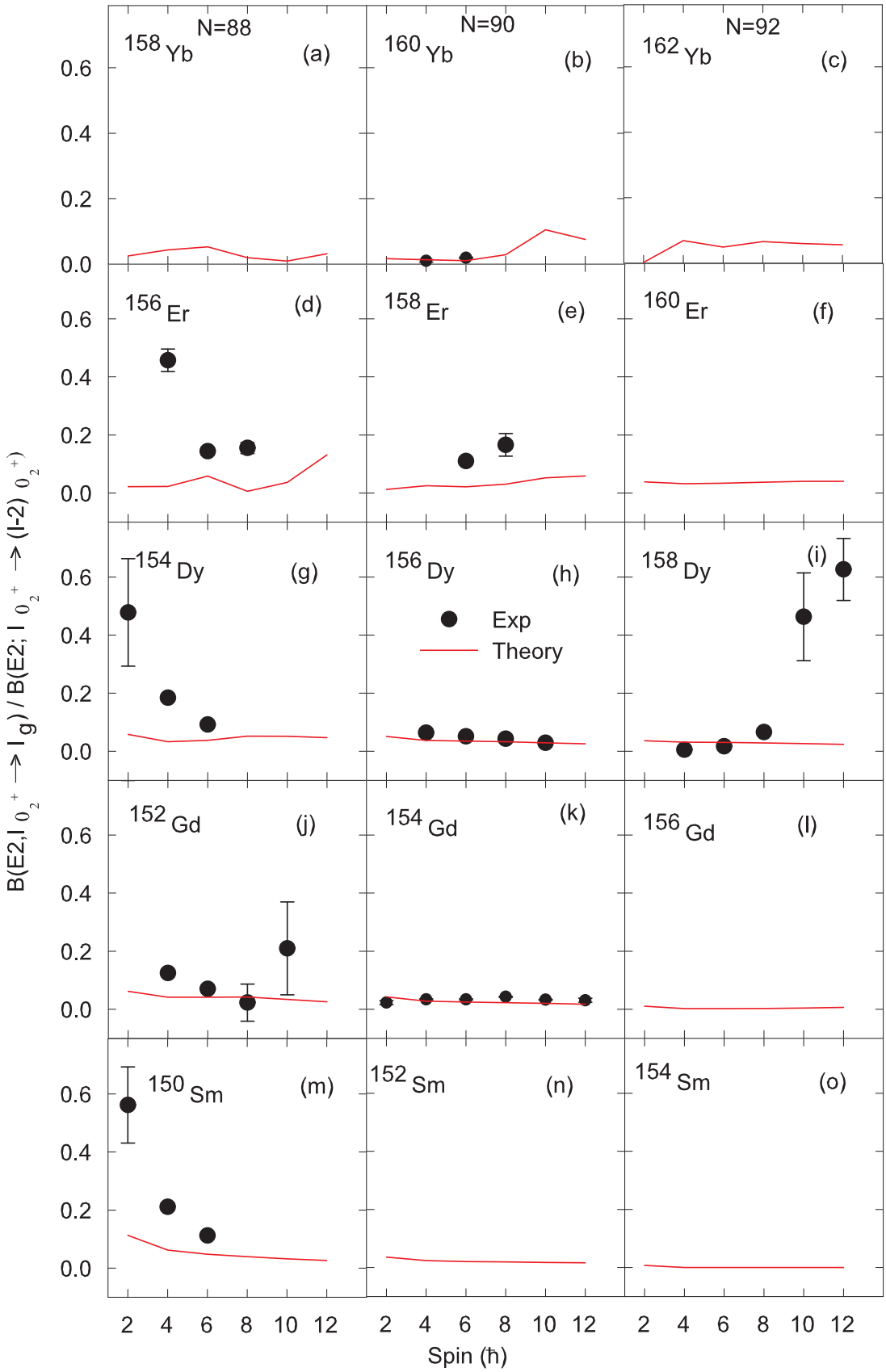


FIG. 18. The calculated branching ratios for out-of-band to in-band transitions, $B(E2; I_{0_2^+} \rightarrow I_g)/B(E2; I_{0_2^+} \rightarrow (I-2)_{0_2^+})$, for the $0_2^+$ bands in the $N = 88$, $N = 90$, and $N = 92$ isotones, in comparison with the available data.

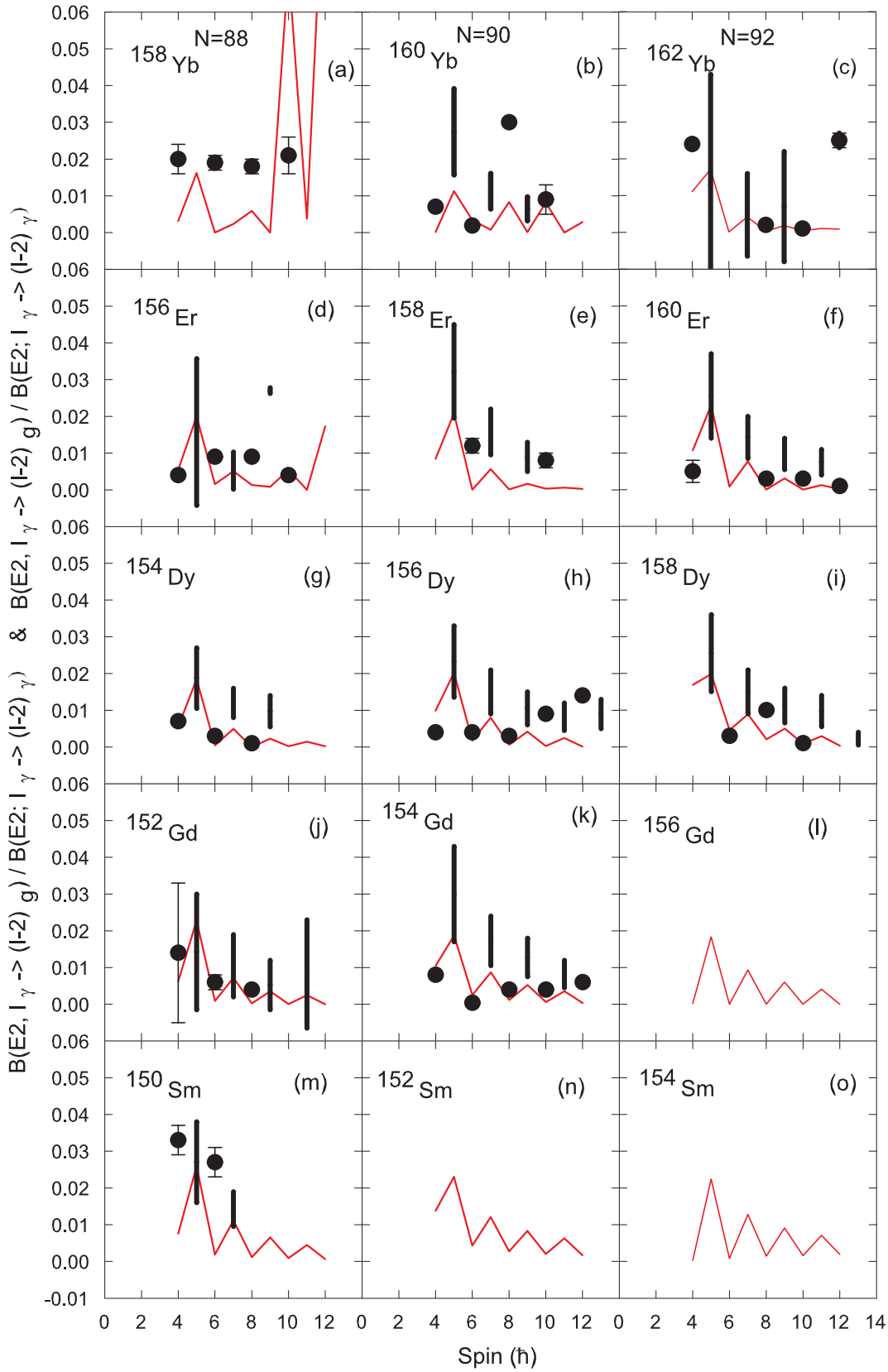


FIG. 19. The calculated branching ratios for out-of-band to in-band transitions, $B(E2; I_\gamma \rightarrow (I-2)_g)/B(E2; I_\gamma \rightarrow (I-2)_\gamma)$ for even $I$ and $B(E2; I_\gamma \rightarrow (I-1)_g)/B(E2; I_\gamma \rightarrow (I-2)_\gamma)$ for odd $I$, for the $\gamma$ bands in the $N = 88$, $N = 90$, and $N = 92$ isotones, in comparison with the available data. The lowest values of the vertical lines, for $B(E2)$ values of odd-spin members of the $\gamma$ bands correspond to $\delta = 1$ while the highest correspond to a pure $E2$.

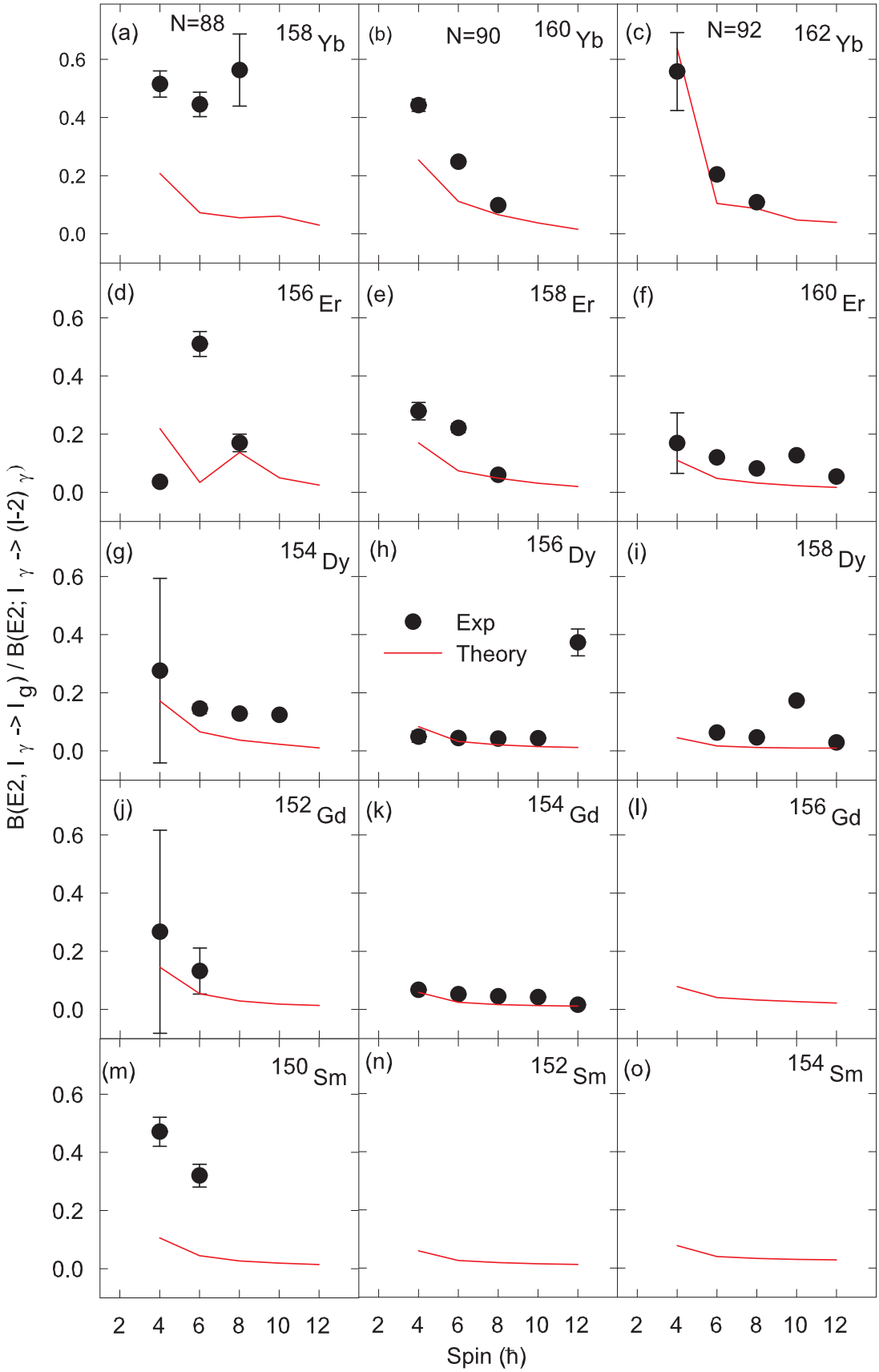


FIG. 20. The calculated branching ratios for out-of-band to in-band transitions, $B(E2; I_\gamma \rightarrow (I)_g)/B(E2; I_\gamma \rightarrow (I-2)_\gamma)$, for the $\gamma$ bands in the $N = 88$, $N = 90$, and $N = 92$ isotones, in comparison with the available data.

TABLE III. Results of the 5DCH-CDFT calculations for the $\frac{B(E2;I_2\longrightarrow I_g+2)}{B(E2;I_2\longrightarrow I_2-2)}$ ratios are shown below and they are compared with the experimental ratios deduced from the current and previous works, as per reference. The ratios deduced from Nucler Data Sheets (NDS) for both $^{152}$Sm and $^{154}$Gd are from Refs. [46,53], respectively.

| Nucleus | $I_i$ | Current work | NDS [46,53] | 5DCH |
|---|---|---|---|---|
| $^{152}$Sm | $2_2$ | | 0.106(10) | 0.0948 |
| | $4_2$ | | 0.063(15) | 0.0570 |
| $^{154}$Gd | $2_2$ | 0.071(21) | 0.20(3) | 0.1277 |
| | $4_2$ | 0.098(6) | 0.076(7) | 0.0845 |
| $^{156}$Dy | $4_2$ | 0.025(9) | | 0.1206 |

#### *3. Electric monopole transitions*

Strong electric monopole transitions are often considered to be indicative of shape coexistence and configuration mixing between different deformations [21]. The absolute transition strength of the $E0$ transitions between $0_2{}^+ \rightarrow 0_1{}^+$ states can be defined as

$$\rho(E0; 0_2{}^+ \rightarrow 0_1{}^+) = \left| \frac{\langle 0_2{}^+ | \hat{T}(E0) | 0_1{}^+ \rangle}{eR^2} \right|, \tag{9}$$

where $R = 1.2A^{1/3}$ fm, $\hat{T}(E0) = \sum_k e_k r_k^2$ is the electric monopole transition operator, with $e_k$ being the electric charge of the $k_{th}$ nucleon and $r_k$ being its relative position in the center-of-mass frame. The absolute transition strengths of other $E0$ transitions can be calculated in a similar way.

In Figs. 21 and 22, the calculated transition strengths $\rho^2(E0; I_{0_2{}^+} \rightarrow I_{\rm gs})$ and the relative transition strengths between $E0$ and $E2$ transitions $X(E0/E2)$ [88] as a functions of the spin $I$ are plotted for the $N = 88$, $N = 90$, and $N = 92$ isotones, respectively, in comparison with the available data [21,22,46,53,54,85,86,88,89]. The values from the 5DCH-CDFT calculations are overall larger than the available data for $\rho^2(E0; I_{0_2{}^+} \rightarrow I_{\rm gs})$ and $X(E0/E2)$. This suggests that the experimental $0_2{}^+$ levels may involve other configurations, such as two-quasiparticle excitations or pairing isomers [20,28,42], which are not included in the present 5DCH-CDFT calculations.

The detailed trend of the calculated transition strength $\rho^2(E0; I_{0_2{}^+} \rightarrow I_{\rm gs})$ with increase of spin can be qualitatively understood by the collective wave functions in the $(\beta, \gamma)$ plane of the initial $I_{0_2{}^+}$ and final $I_{\rm gs}$ states. For example, it is found that due to a relatively soft potential in $^{152}$Gd, the centers of the collective wave functions of the $I_{0_2{}^+}$ and $I_{\rm gs}$ states move to large quadrupole deformation with the increase of spin from $0^+$ to $8^+$. On the contrary, due to a relatively rigid potential in $^{154}$Gd, the centers of collective wave functions of the $I_{0_2{}^+}$ and $I_{\rm gs}$ states are nearly stable in the $(\beta, \gamma)$ plane with the increase of spin. As a result, the $E0$ strength increases with the increase of spin from $0^+$ to $8^+$ in $^{152}$Gd while it remains constant with spin in $^{154}$Gd.

Another trend visible, at $N = 90$ and $N = 92$, is the increase in $E0$ strength with $Z$. The $E0$ strength becomes especially strong in $^{158,160}$Er and $^{160,162}$Yb, where the secondary minimum lies lowest in energy, supporting the picture in which the $I_{0_2{}^+}$ bands are actually shape-coexisting triaxial bands. To study this possibility further, we study the calculated wave functions in the next section.

### E. Probability density distribution

To analyze the configuration mixing in the collective excitation states, one can evaluate the probability density distributions in the $\beta$-$\gamma$ plane, which are defined by

$$\rho_{I\alpha}(\beta, \gamma) = \sum_{K \in \Delta I} \left| \psi^I_{\alpha K}(\beta, \gamma) \right|^2 \beta^3, \tag{10}$$

with the normalization

$$\int_0^\infty \beta d\beta \int_0^{2\pi} \rho_{I\alpha} |\sin 3\gamma| d\gamma = 1. \tag{11}$$

The probability density distributions for the ground states, $0_2{}^+$ states, $0_3^+$ states, and bandheads of $\gamma$ bands for the $N = 88$, $N = 90$, and $N = 92$ isotones are plotted in Figs. 23–26, respectively.

It is clearly seen in Fig. 23 that the probability density distributions of the ground states for the $N = 88$, $N = 90$, and $N = 92$ isotones all concentrate on the prolate sides with one pronounced peak. The location of the peak for each nucleus is consistent with the global energy minimum of the nucleus shown in Fig. 8. The feature that the density distributions are very concentrated means that the ground states are almost pure with little configuration mixing with other states. Furthermore, the probability density distributions extend along the $\beta$ and $\gamma$ directions in accordance with the softness of PESs around the ground states, i.e., the PES around the global minimum becomes $\gamma$ softer with the increase of the proton number and becomes more rigid with the increase of the neutron number. Note that the probability density distributions of the ground states for $^{162}$Yb and neighboring nuclei are influenced by the local minimum developing in the PES.

In Figs. 24 and 25, the probability density distributions are shown for the $0_2^+$ and $0_3^+$ states, respectively. For most nuclei that are investigated, such as Sm, Gd, and Dy isotopes, the density distributions of the $0_2{}^+$ and $0_3{}^+$ states possess two and three maxima respectively along the $\beta$ direction in the $\beta$-$\gamma$ plane. In Bohr's rotation vibration model, the $0_2{}^+$ and $0_3{}^+$ states are considered as the bandheads of the $\beta$ and the second $\beta$ bands, which correspond to one-phonon and two-phonon vibrational excitations in the $\beta$ collective degree of freedom. Therefore, the behavior of the density distributions suggests that for most nuclei investigated, the $0_2{}^+$ and $0_3{}^+$ states originate mainly from the one-phonon and two-phonon $\beta$ vibrations and could be regarded as the bandheads of the $\beta$ and the second $\beta$ bands.

Exceptional cases are found in the Er and Yb isotopes. The density distributions of $0_2{}^+$ states in $^{156}$Er and $^{158,160}$Yb are different from those discussed above. For $^{156}$Er and $^{158}$Yb, there also exist two maxima, but for $^{156}$Er the distribution with larger deformation is much more extended in the $\beta$ and $\gamma$ directions, while for $^{158}$Yb the maximum with larger deformation no longer concentrates on the prolate side but has considerable triaxial deformation. For $^{160}$Yb, there appear three maxima in the density distributions of $0_2{}^+$ state. The density distributions of $0_3{}^+$ states in all the Er and Yb isotopes

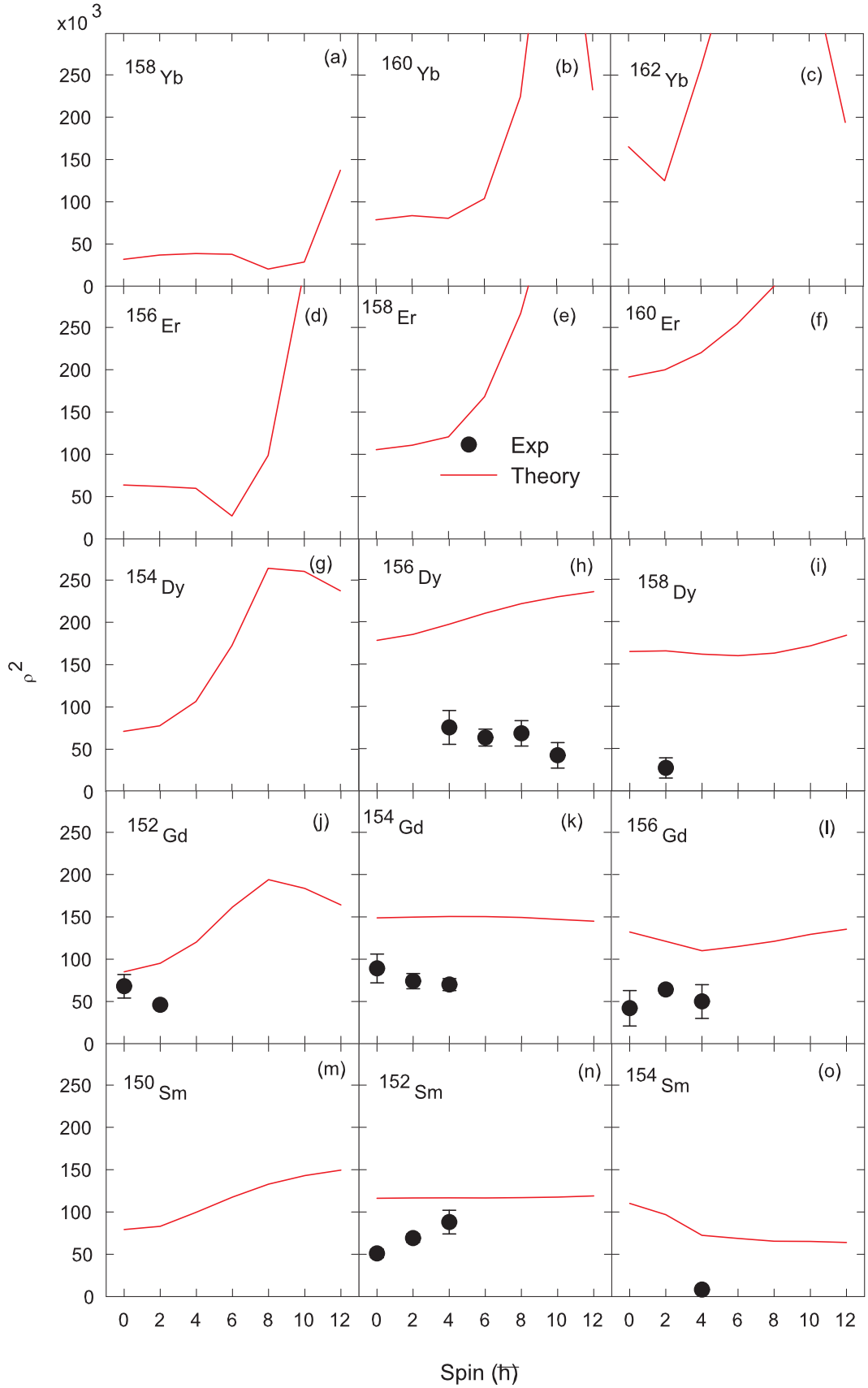


FIG. 21. Absolute transition strengths of $E0$ transitions $\rho^2(E0; I_{0_2^+} \rightarrow I_{gs})$ in the $N = 88$, $N = 90$, and $N = 92$ isotones obtained by the 5DCH-CDFT calculations, in comparison with the available data in Refs. [21,22,46,53,54,85,86,88,89,91].

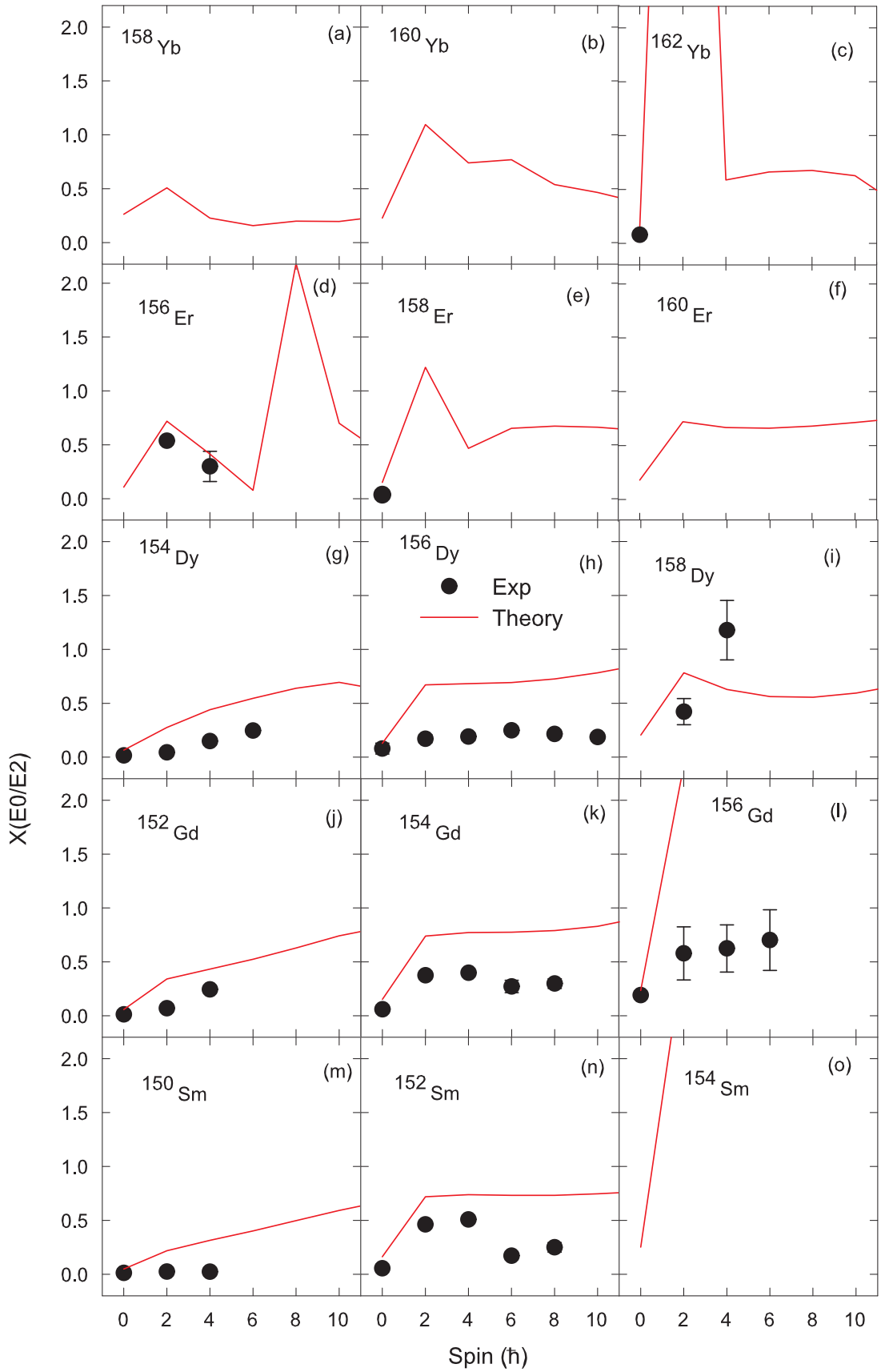


FIG. 22. The relative transition strength between $E0$ and $E2$ transitions in the $N = 88$, $N = 90$, and $N = 92$ isotones obtained by the 5DCH-CDFT calculations, in comparison with the data in Refs. [21,22,46,53,54,85,86,88–91].

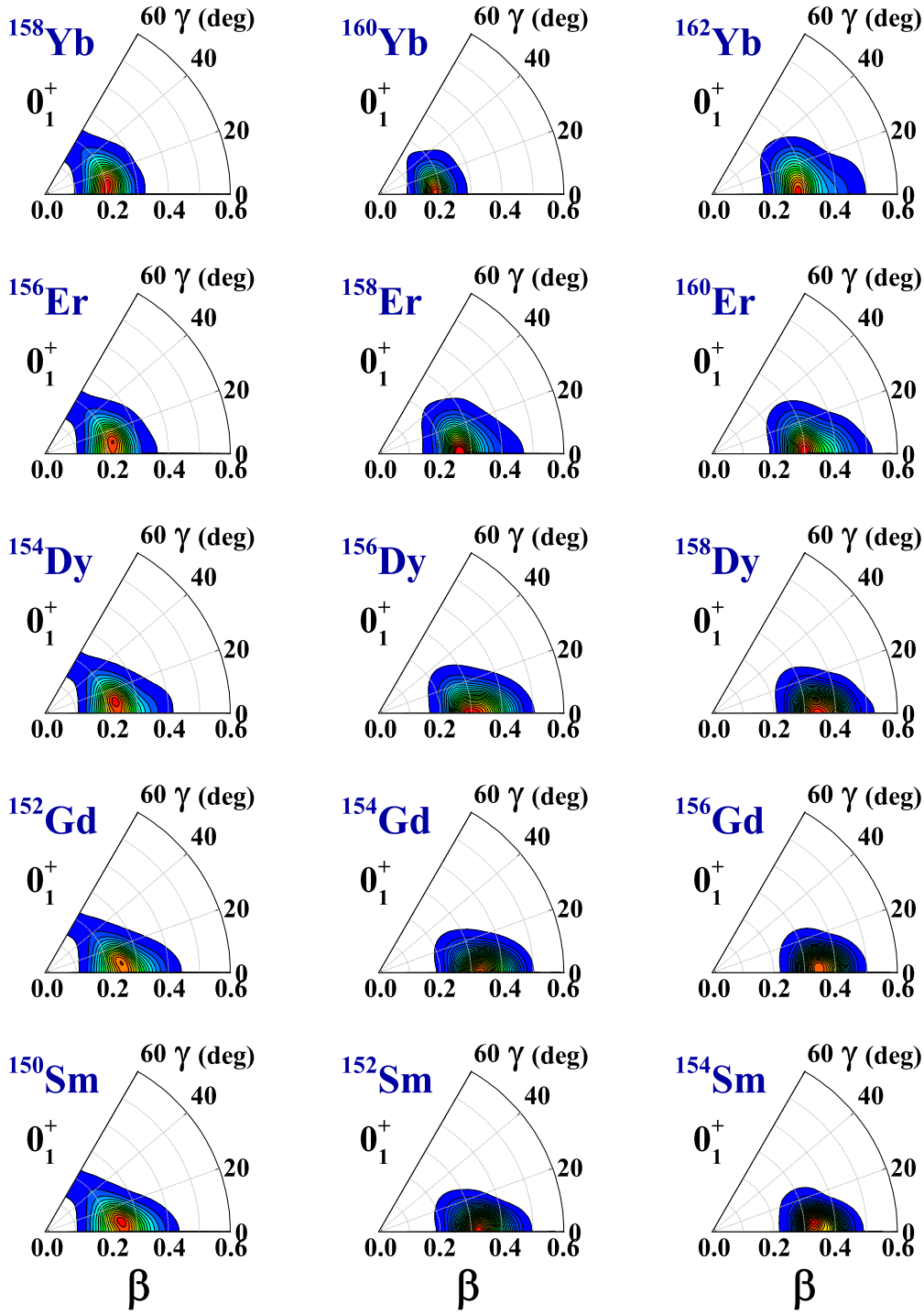


FIG. 23. Probability density distribution in the $\beta$-$\gamma$ plane for the ground states of $N = 88$, $N = 90$, and $N = 92$ isotones, predicted by PC-PK1 density functional.

investigated are somewhat different from the general feature of two-phonon $\beta$ vibration, where a maximum with considerable triaxial deformation is shown. As discussed above, the PESs of the Er and Yb isotopes are softer than those of the Sm, Gd, and Dy isotopes, and meanwhile a local triaxial minimum starts to emerge with the increase of the proton number and manifests itself obviously in $^{158,160,162}$Yb. The exceptional probability density distributions of the Er and Yb isotopes can be therefore understood as arising from the softer potential and the influence of the local triaxial minimum. In this sense, the $0_2^+$ states in $^{156}$Er and $^{158,160}$Yb and the $0_3^+$ states in all the Er and Yb isotopes investigated cannot be simply interpreted as the one-phonon and two-phonon $\beta$ vibrations, which is also consistent with the fact that the calculated energy

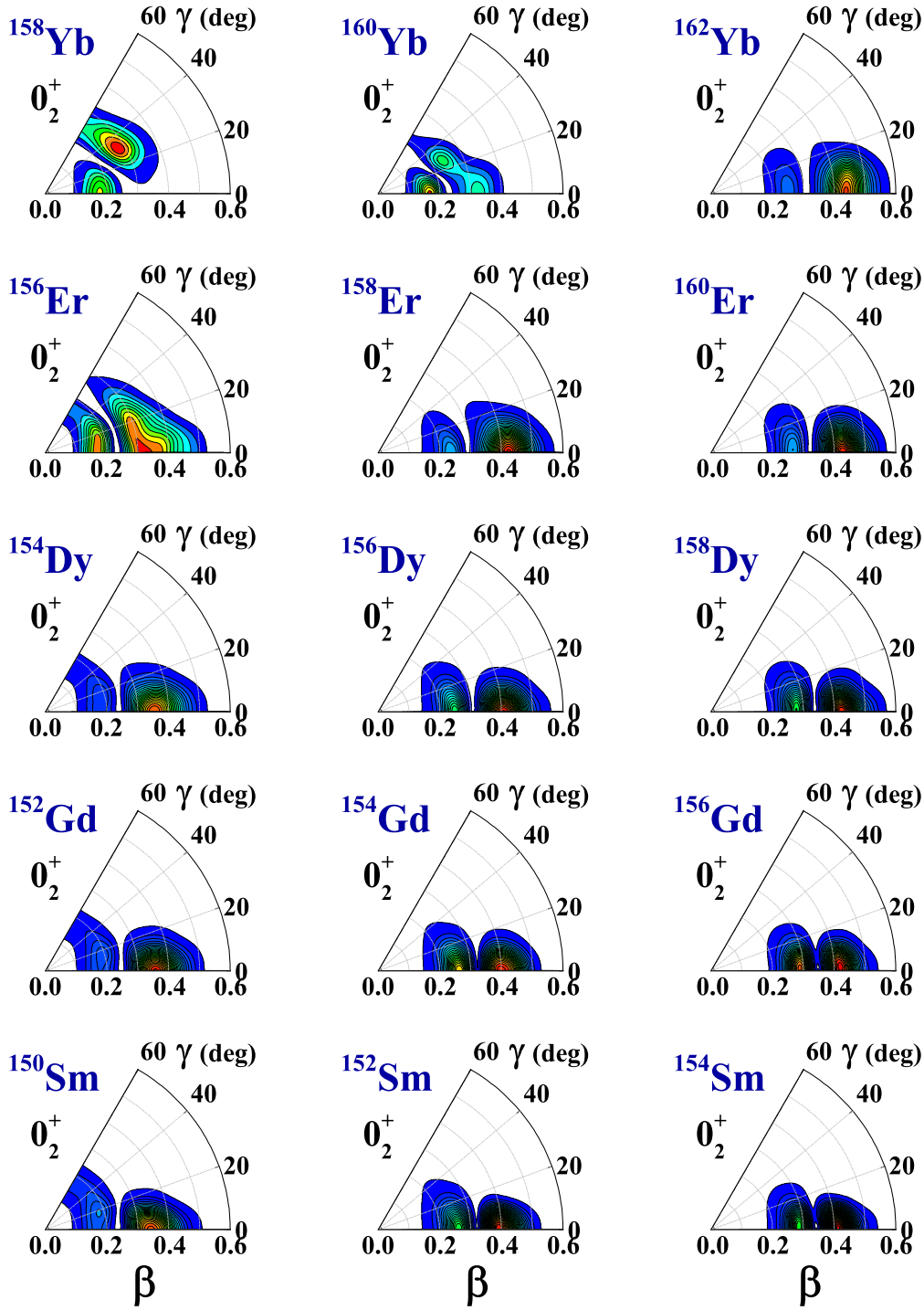


FIG. 24. Probability density distribution in the $\beta$-$\gamma$ plane for the $0_2{}^+$ states of $N = 88$, $N = 90$, and $N = 92$ isotones, predicted by PC-PK1 density functional.

differences between $0_3{}^+$ and $0_2{}^+$ states are much smaller than those between $0_2{}^+$ and $0_1{}^+$ states in the isotopes like $^{156,158}$Er and $^{158,160}$Yb.

In Fig. 26, the probability density distributions for the bandhead of $\gamma$ bands are presented. It is noted that in some nuclei the head of the $\gamma$ band is the second $2^+$ state while in the other nuclei it corresponds to the third $2^+$ state. It can be seen in Fig. 26 that generally the probability density distributions for the bandhead of $\gamma$ bands have a peak with a considerable triaxiality. In the $N = 88$ isotones, the distributions all concentrate around $\beta \approx 0.25$ and $\gamma \approx 25°$. In $^{150}$Sm, due to the configuration mixing with the $2_2{}^+$ state, there also exists a little peak around $\beta \approx 0.4$, $\gamma \approx 0°$. With the increase of proton number, such distribution is not obvious in $^{152}$Gd and $^{154}$Dy and disappears in $^{156}$Er and $^{158}$Yb. In the $N = 90$ isotones, the probability density distributions are quite

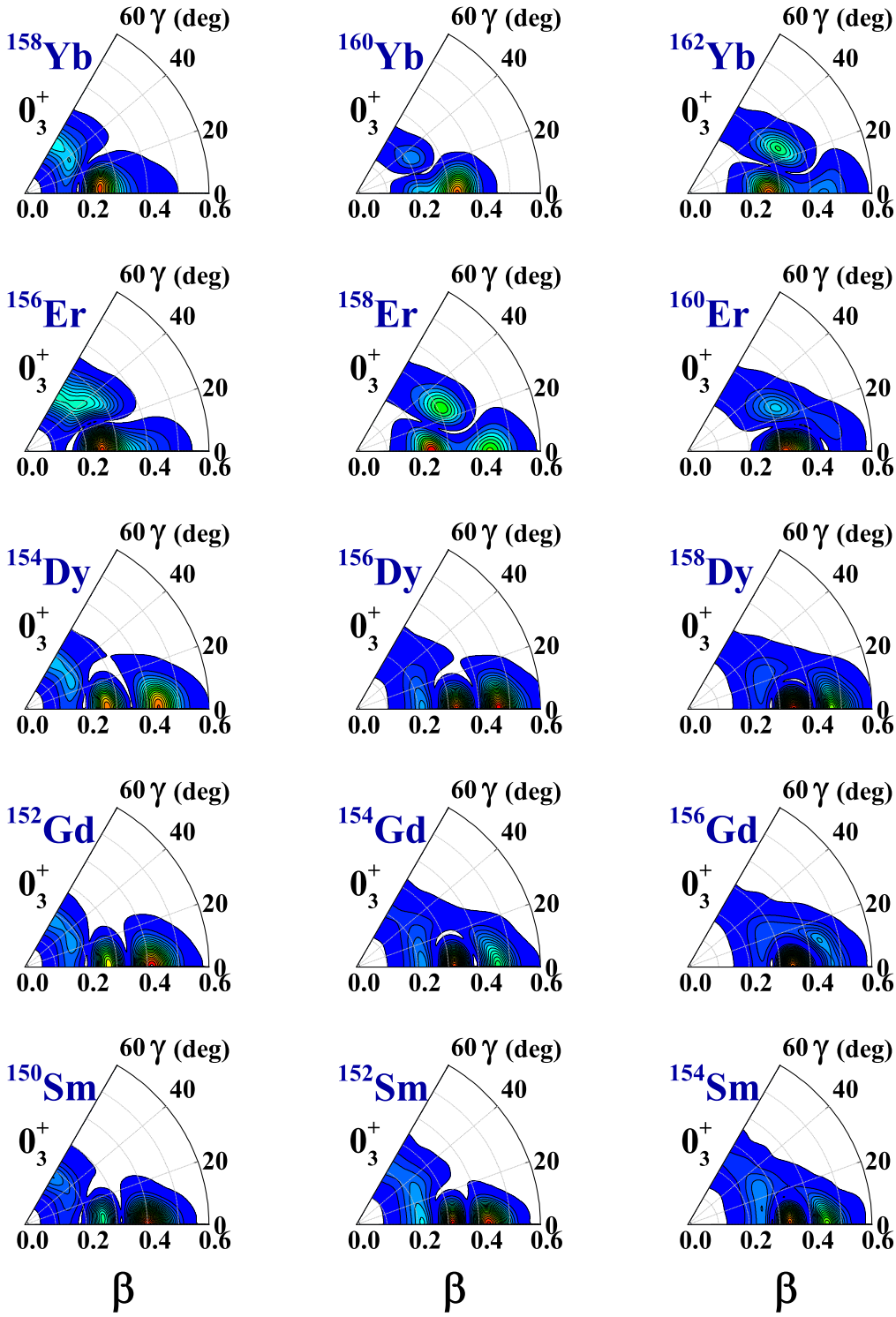


FIG. 25. Probability density distribution in the $\beta$-$\gamma$ plane for the $0_3{}^+$ states of $N = 88$, $N = 90$, and $N = 92$ isotones, predicted by PC-PK1 density functional.

similar to those in the $N = 88$ isotones. The distributions are all concentrated around $\beta \approx 0.3$, $\gamma \approx 20^\circ$. With the increase of proton number, the density distributions become more concentrated. In the $N = 92$ isotones, apart from $^{162}$Yb, the probability density distributions are all concentrated around $\beta \approx 0.35$, $\gamma \approx 15^\circ$. This is to say, with the increase of neutron number from $N = 88$ to 92, the probability density distributions for the bandhead of $\gamma$ bands become closer to prolate side, which reflects the shape transition from the near-spherical to well-deformed cases. In $^{162}$Yb, besides the

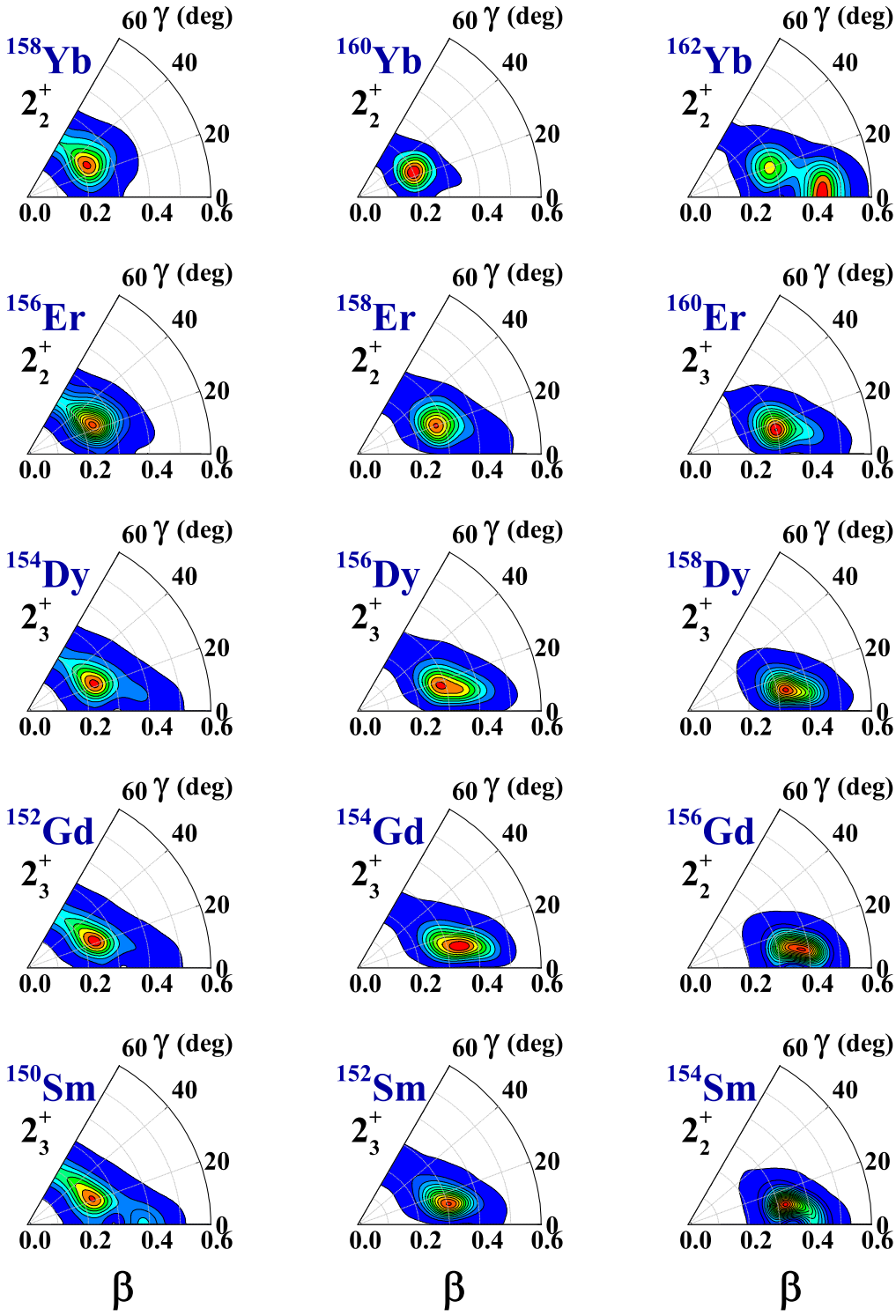


FIG. 26. Probability density distribution in the $\beta$-$\gamma$ plane for the $\gamma$-bandhead states of $N = 88$, $N = 90$, and $N = 92$ isotones, predicted by PC-PK1 density functional.

peak around $\beta \approx 0.3$, $\gamma \approx 20^\circ$, there is another peak near $\beta \approx 0.4$, $\gamma \approx 0^\circ$. This can be understood from the well-developed shape coexistence in this nucleus where two minima in the PES are very close in energy as shown in Fig. 8.

In Fig. 27, for the shape coexistence nucleus $^{162}$Yb, we further plot the probability density distributions in the $\beta$-$\gamma$ plane for the ground-state, $\gamma$, $0_2{}^+$, and $0_3{}^+$ bands. These bands are organized according to the calculated electromagnetic transitional probabilities. It can be seen that due to the existence of the second minimum in the PES, the levels in ground-state bands have important contributions from the second minimum with a large deformation ($\beta_2 \approx 0.45$), which becomes

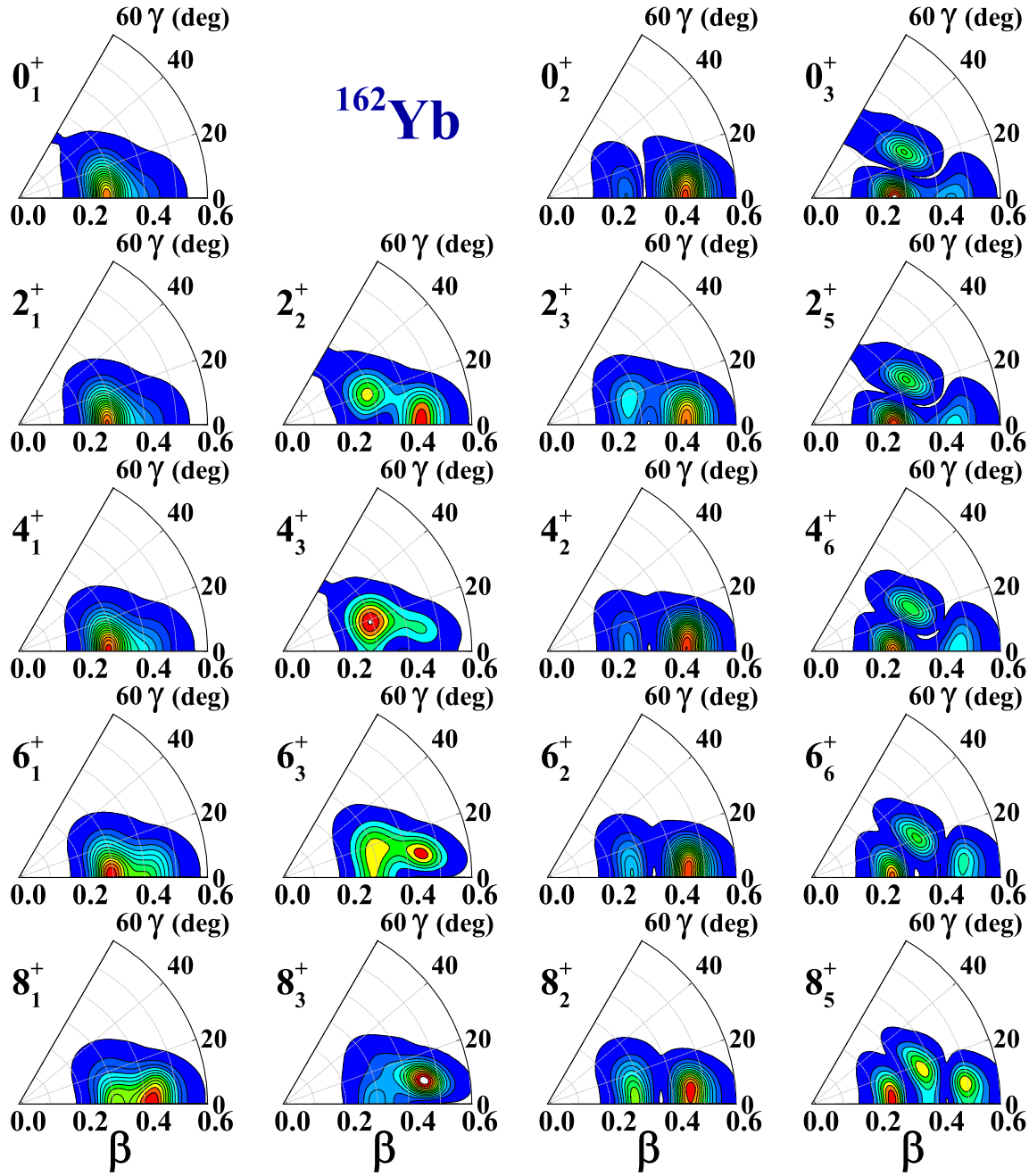


FIG. 27. Probability density distributions in the $\beta$-$\gamma$ plane for the ground-state band ($0_1{}^+$, $2_1{}^+$, $4_1{}^+$, $6_1{}^+$, and $8_1{}^+$), $\gamma$ band ($2_2{}^+$, $4_3{}^+$, $6_3{}^+$, and $8_3{}^+$), $0_2{}^+$ band ($0_2{}^+$, $2_3{}^+$, $4_2{}^+$, $6_2{}^+$, and $8_2{}^+$) and $0_3{}^+$ band ($0_3{}^+$, $2_5{}^+$, $4_6{}^+$, $6_6{}^+$, and $8_5{}^+$) in $^{162}$Yb, obtained by the 5DCH-CDFT calculations with PC-PK1 density functional.

more important with the increase of spin $I$ (there is a crossing near spin 8). The levels in $\gamma$ bands also have two important contributions from both the global and the second minima, and the latter contribution becomes more important with the increase of spin $I$. The probability distributions for the levels in the $0_2{}^+$ band exhibit two maxima along the prolate side, the characteristic of a $\beta$ vibration, and meanwhile the maximum with large deformation is predominant, reflecting the mixing with the second minimum. The probability distributions for the levels in the $0_3{}^+$ band exhibit three maxima: two maxima along the prolate side and the other with obvious triaxial degree of freedom. Such distributions are different from the typical distribution of a $\beta$ vibration with two phonons for a well-deformed nucleus.

## VI. SUMMARY AND CONCLUSION

An extensive set of data on the low-lying positive-parity bands in even-even nuclei for $N = 88$, $N = 90$, and $N = 92$

from Sm to Yb has been collected. The following observations can be made:

(1) The $0_2^+$ bands all have the same or larger moment of inertia as the ground-state bands. By contrast, the $\gamma$ bands, particularly the odd-spin members, track the ground band as a function of spin. This appears to be a general feature throughout the $A = 150$ to 160 mass region.
(2) The splitting $S(I)$ of the $\gamma$ bands varies considerably over the nuclides studied.
(3) The even-spin $0_2^+$ bands cross the $\gamma$ bands in Er and Yb isotopes.

Overall, the comparison of the data to the results obtained using the 5DCH-CDFT calculations with PC-PK1 density functional yields a satisfactory agreement. The trends in energy and moment of inertia of all bands are well reproduced, including the staggering $S(I)$ of the $2_\gamma^+$ bands. The model does well with electromagnetic transition rates and branching ratios, with the exception of the $E0$ rates, which are generally overestimated. Within the model, the following conclusions can be drawn:

(1) The potential energy surfaces of the CDFT calculations indicate $\gamma$-soft nuclei at $N = 88$ becoming $\gamma$ rigid along $N = 90$ and $N = 92$. This is in agreement with the staggering $S(I)$ of the levels in the $\gamma$ bands.
(2) The nature of the $0_2^+$ band changes with atomic number. In the isotopes of Sm to Dy, they can be understood as $\beta$ vibrations, but in the Er and Yb isotopes, the $0_2^+$ bands can be understood as having large components in a triaxial superdeformed minimum. They are better understood as shape-coexisting states.
(3) Shape coexistence has been suggested to describe the nuclei in the vicinity of $^{152}$Sm. The present calculations predict a soft potential in the $\beta$ direction but do not find two coexisting minima. This is reminiscent of $^{152}$Sm exhibiting an $X(5)$ behavior.
(4) In the Sm, Gd, and Dy isotopes, the model predicts that the $0_3^+$ bands are of two-phonon nature, having an energy of twice the $0_2^+$ band. This is in contradiction with the experimental data and implies that other excitation modes must be invoked to explain their origin.

## ACKNOWLEDGMENTS

We would like to thank the iThemba LABS technical staff for their support in these experiments. This work is supported by the National Research Foundation of South Africa under grants (No. 109711, No. 92791, No. 106012, No. 92792, No. 90741, No. 109134, No. 96829, No. 93531, and No. 116666); the National Natural Science Foundation of China under grants (No. 11461141002, No. 11375015, No. 11875225, and No. 11875075); the US National Science Foundation under Grants No. PHY-1401574 (USNA) and No. PHY-0754674 (FSU), and No. PHY-1502092 (USNA); the National Research, Development and Innovation Fund of Hungary under Grant No. K128947; and the European Regional Development Fund, under grant (No. GINOP-2.3.3-15-2016-00034). JYFL research is supported by the Academy of Finland under the Finnish Centre of Excellence Programme 2006-2011, Contract No. 213503. The authors also acknowledge the support of GAMMAPOOL for the loan of the JUROGAM detectors.

[1] A. Bohr, Mat. Fys. Medd. Dan. Vid. Selsk. **26**, 14 (1952).
[2] A. Bohr and B. R. Mottelson, Mat. Fys. Medd. Dan. Vid. Selsk. **27**, 16 (1953).
[3] D. R. Bes and R. A. Broglia, Nucl. Phys. **80**, 289 (1966).
[4] O. Mikoshiba, Nucl. Phys. A **101**, 202 (1967).
[5] A. Kuliev and N. I. Pyatov, Nucl. Phys. A **106**, 689 (1968).
[6] S. T. Belyaev and B. A. Rumiantsev, Phys. Lett. B **30**, 444 (1969).
[7] J. V. Maher, J. R. Erskine, A. M. Friedman, J. P. Schiffer, and R. H. Siemssen, Phys. Rev. C **5**, 1380 (1972).
[8] P. Kleinheinz, R. K. Sheline, M. R. Maier, R. M. Diamond, and F. S. Stephens, Phys. Rev. Lett. **32**, 68 (1974).
[9] J. J. Kolata and M. Oothoudt, Phys. Rev. C **15**, 1947 (1977).
[10] M. H. Mortensen, R. R. Betts, and C. K. Bockelman, Phys. Rev. C **21**, 2275 (1980).
[11] S. W. Yates, I. Y. Lee, N. R. Johnson, E. Eichler, L. L. Riedinger, M. W. Guidry, A. C. Kahler, D. Cline, R. S. Simon, P. A. Butler *et al.*, Phys. Rev. C **21**, 2366 (1980).
[12] D. R. Zolnowski, M. B. Hughes, J. Hunt, and T. T. Sugihara, Phys. Rev. C **21**, 2556 (1980).
[13] A. Bohr and B. R. Mottelson, Phys. Scr. **25**, 28 (1982).
[14] P. E. Garrett, M. Kadi, M. Li, C. A. McGrath, V. Sorokin, M. Yeh, and S. W. Yates, Phys. Lett. B **400**, 250 (1997).
[15] P. E. Garrett, J. Phys. G: Nucl. Part. Phys. **27**, R1 (2001).
[16] H. F. Wirth, G. Graw, S. Christen, D. Cutoiu, Y. Eisermann, C. Günther, R. Hertenberger, J. Jolie, A. I. Levon, O. Möller *et al.*, Phys. Rev. C **69**, 044310 (2004).
[17] N. Pietralla and O. M. Gorbachenko, Phys. Rev. C **70**, 011304(R) (2004).
[18] D. Bucurescu, G. Graw, R. Hertenberger, H.-F. Wirth, N. L. Iudice, A. V. Sushkov, N. Y. Shirikova, Y. Sun, T. Faestermann, R. Krücken *et al.*, Phys. Rev. C **73**, 064309 (2006).
[19] E. A. McCutchan, D. Bonatsos, N. V. Zamfir, and R. F. Casten, Phys. Rev. C **76**, 024306 (2007).
[20] W. D. Kulp, J. L. Wood, P. E. Garrett, C. Y. Wu, D. Cline, J. M. Allmond, D. Bandyopadhyay, D. Dashdorj, S. N. Choudry, A. B. Hayes *et al.*, Phys. Rev. C **77**, 061301(R) (2008).
[21] K. Heyde and J. L. Wood, Rev. Mod. Phys. **83**, 1467 (2011).
[22] J. Smallcombe, P. J. Davies, C. J. Bartona, D. G. Jenkins, L. L. Andersson, P. A. Butler, D. M. Cox, R.-D. Herzberg, A. Mistry, E. Parr *et al.*, Phys. Lett. B **732**, 161 (2014).
[23] F.-Q. Chen and J. L. Egido, Phys. Rev. C **93**, 064313 (2016).
[24] F.-Q. Chen and J. L. Egido, Phys. Rev. C **95**, 024307 (2017).
[25] W. D. Kulp, J. L. Wood, P. E. Garrett, J. M. Allmond, D. Cline, A. B. Hayes, H. Hua, K. S. Krane, R. M. Larimer, J. Loats *et al.*, Phys. Rev. C **71**, 041303(R) (2005).

[26] W. D. Kulp, J. L. Wood, J. M. Allmond, J. Eimer, D. Furse, K. S. Krane, J. Loats, P. Schmelzenbach, C. J. Stapels, R.-M. Larimer *et al.*, Phys. Rev. C **76**, 034319 (2007).
[27] I. Ragnarsson and R. A. Broglia, Nucl. Phys. A **263**, 315 (1976).
[28] J. F. Sharpey-Schafer, T. E. Madiba, S. P. Bvumbi, E. A. Lawrie, J. J. Lawrie, A. Minkova, S. M. Mullins, P. Papka, D. G. Roux, and J. Timár, Eur. Phys. J. A **47**, 6 (2011).
[29] S. K. Abdulvagabova, S. P. Ivanova, and N. I. Pyatov, Phys. Lett. **38**, 215 (1972).
[30] R. E. Griffin, A. D. Jackson, and A. B. Volkov, Phys. Lett. B **36**, 281 (1971).
[31] W. I. Van Rij and S. H. Kahana, Phys. Rev. Lett. **28**, 50 (1972).
[32] J. F. Sharpey-Schafer, R. A. Bark, S. P. Bvumbi, T. R. S. Dinoko, and S. N. T. Majola, Eur. Phys. J. A **55**, 15 (2019).
[33] J. L. Wood, A.-M. Oros-Peusquens, R. Zaballa, J. M. Allmond, and W. D. Kulp, Phys. Rev. C **70**, 024308 (2004).
[34] J. M. Allmond, R. Zaballa, A. M. Oros-Peusquens, W. D. Kulp, and J. L. Wood, Phys. Rev. C **78**, 014302 (2008).
[35] T. Nikšić, Z. P. Li, D. Vretenar, L. Próchniak, J. Meng, and P. Ring, Phys. Rev. C **79**, 034303 (2009).
[36] Z. P. Li, T. Nikšić, D. Vretenar, J. Meng, G. A. Lalazissis, and P. Ring, Phys. Rev. C **79**, 054301 (2009).
[37] G. Duchene, Nucl. Instrum. Methods **432**, 90 (1999).
[38] J. F. Sharpey-Schafer, Nucl. Phys. News **14**, 5 (2004).
[39] S. P. Bvumbi, J. F. Sharpey-Schafer, P. M. Jones, S. M. Mullins, B. M. Nyakó, K. Juhász, R. A. Bark, L. Bianco, D. M. Cullen, D. Curien *et al.*, Phys. Rev. C **87**, 044333 (2013).
[40] G. L. Zimba, J. F. Sharpey-Schafer, P. Jones, S. P. Bvumbi, L. P. Masiteng, S. N. T. Majola, T. S. Dinoko, E. A. Lawrie, J. J. Lawrie, D. Negi *et al.*, Phys. Rev. C **94**, 054303 (2016).
[41] S. N. Majola, D. J. Hartley, L. L. Riedinger, J. F. Sharpey-Schafer, J. M. Allmond, C. Beausang, M. P. Carpenter, C. J. Chiara, N. Cooper, D. Curien *et al.*, Phys. Rev. C **91**, 034330 (2015).
[42] J. F. Sharpey-Schafer, T. E. Madiba, S. P. Bvumbi, E. A. Lawrie, J. J. Lawrie, A. Minkova, S. M. Mullins, P. Papka, D. G. Roux, and J. Timár, Eur. Phys. J. A **47**, 5 (2011).
[43] R. A. Bark, Z. P. Li, S. N. T. Majola, J. F. Sharpey-Schafer, Z. Shi, and S. Q. Zhang, EPJ Web Conf. **178**, 02012 (2018)
[44] J. F. Sharpey-Schafer, R. A. Bark, S. P. Bvumbi, E. A. Lawrie, J. J. Lawrie, T. E. Madiba, S. N. T. Majola, A. Minkova, S. M. Mullins, P. Papka *et al.*, Nucl. Phys. A **834**, 45c (2010).
[45] G. L. Zimba, S. P. Bvumbi, L. P. Masiteng, P. Jones, J. F. Sharpey-Schafer, S. N. T. Majola, T. S. Dinoko, O. Shirinda, J. J. Lawrie, J. E. Easton *et al.*, Eur. Phys. J. A **54**, 59 (2018).
[46] M. J. Martin, Nucl. Data Sheets **114**, 1497 (2013).
[47] D. J. Hartley, L. L. Riedinger, R. V. F. Janssens, S. N. T. Majola, M. A. Riley, J. M. Allmond, C. W. Beausang, M. P. Carpenter, C. J. Chiara, N. Cooper *et al.*, Phys. Rev. C **95**, 014321 (2017).
[48] S. Jehangir, G. H. Bhat, J. A. Sheikh, S. Frauendorf, S. N. T. Majola, P. A. Ganai, and J. F. Sharpey-Schafer, Phys. Rev. C **97**, 014310 (2018).
[49] T. S. Dinoko *et al.* (unpublished).
[50] R. A. Bark, J. F. Sharpey-Schafer, S. M. Maliage, T. E. Madiba, F. S. Komati, E. A. Lawrie, J. J. Lawrie, R. Lindsay, P. Maine, S. M. Mullins *et al.*, Phys. Rev. Lett. **104**, 022501 (2010).
[51] C. Garrett, S. Rastikerdar, W. Gelletly, and D. D. Warner, Phys. Lett. B **118**, 292 (1982).
[52] H. Auer, J. Fernandez-Niello, H. Puchta, and F. Riess, Z. Phys. A **318**, 323 (1984).
[53] C. W. Reich, Nucl. Data Sheets **110**, 2257 (2009).
[54] C. W. Reich, Nucl. Data Sheets **113**, 2537 (2012).
[55] R. G. Helmer, Nucl. Data Sheets **101**, 325 (2004).
[56] K. Dusling, N. Pietralla, G. Rainovski, T. Ahn, B. Bochev, A. Costin, T. Koike, T. C. Li, A. Linnemann, S. Pontillo, and C. Vaman, Phys. Rev. C **73**, 014317 (2006).
[57] J. Ollier, J. Simpson, M. A. Riley, E. S. Paul, X. Wang, A. Aguilar, M. P. Carpenter, I. G. Darby, D. J. Hartley, R. V. F. Janssens *et al.*, Phys. Rev. C **83**, 044309 (2011).
[58] L. Mdletshe *et al.*, Eur. Phys. J. A **54**, 176 (2018).
[59] F. S. Stephens and R. S. Simon, Nucl. Phys. A **179**, 753 (1972).
[60] P. J. Brussaard and P. W. Glaudemans, *Shell Model Applications in Nuclear Spectroscopy* (Elsevier, Amsterdam, 1977).
[61] Z. P. Li, C. Y. Li, J. Xiang, J. M. Yao, and J. Meng, Phys. Lett. B **717**, 470 (2012).
[62] Z. P. Li, T. Nikšić, D. Vretenar, P. Ring, and J. Meng, Phys. Rev. C **81**, 064321 (2010).
[63] Y. Y. Wang, Z. Shi, Q. B. Chen, S. Q. Zhang, and C. Y. Song, Phys. Rev. C **93**, 044309 (2016).
[64] D. R. Inglis, Phys. Rev. **103**, 1786 (1956).
[65] S. T. Beliaev, Nucl. Phys. **24**, 322 (1961).
[66] M. Girod and B. Grammaticos, Nucl. Phys. A **330**, 40 (1979).
[67] P.-W. Zhao, Z. P. Li, J.-M. Yao, J. Meng *et al.*, Phys. Rev. C **82**, 054319 (2010).
[68] J. Xiang, Z. P. Li, Z. X. Li, J. M. Yao, and J. Meng, Nucl. Phys. A **873**, 1 (2012).
[69] Z. P. Li, T. Nikšić, D. Vretenar, and J. Meng, Phys. Rev. C **80**, 061301(R) (2009).
[70] Z. P. Li, T. Nikšić, D. Vretenar, and J. Meng, Phys. Rev. C **81**, 034316 (2010).
[71] Z. P. Li, J. M. Yao, D. Vretenar, T. Nikšić, H. Chen, and J. Meng, Phys. Rev. C **84**, 054304 (2011).
[72] S. Quan, Q. Chen, Z. P. Li, T. Nikšić, and D. Vretenar, Phys. Rev. C **95**, 054321 (2017).
[73] F. Iachello, Phys. Rev. Lett. **87**, 052502 (2001).
[74] F. Iachello, Phys. Rev. Lett. **85**, 3580 (2000).
[75] Ødegård, G. B. Hagemann, M. Bergström, B. Herskind, D. R. Jensen, G. Sletten, J. Wilson, K. Spohr, H. Hübel, A. Bracco *et al.*, Nucl. Phys. A **682**, 427 (2001).
[76] G. Schönwaßer, H. Hübel, G. B. Hagemann, H. Amro, R. M. Clark, M. Cromaz, R. M. Diamond, P. Fallon, B. Herskind, G. Lane *et al.*, Eur. Phys. J. A **15**, 435 (2002).
[77] M. Baranger, Ann. Phys. **114**, 123 (1978).
[78] J. J. Sun, Z. Shi, X. Q. Li, H. Hua, C. Xu, Q. B. Chen, S. Q. Zhang, C. Y. Song, J. Meng, X. G. Wu *et al.*, Phys. Lett. B **734**, 308 (2014).
[79] C. S. Wu and J. Y. Zeng, Commun. Theor. Phys. **8**, 51 (1987).
[80] A. S. Davydov and G. F. Filippov, Nucl. Phys. **8**, 237 (1958).
[81] L. Wilets and M. Jean, Phys. Rev. **102**, 788 (1956).
[82] O. Möller, A. Dewald, P. Petkov, B. Saha, A. Fitzler, K. Jessen, D. Tonev, T. Klug, S. Heinze, J. Jolie *et al.*, Phys. Rev. C **74**, 024313 (2006).
[83] N. R. Johnson, I. Y. Lee, F. K. McGowan, T. T. Sugihara, S. W. Yates, and M. W. Guidry, Phys. Rev. C **26**, 1004 (1982).
[84] M. P. Fewell, N. R. Johnson, F. K. McGowan, J. S. Hattula, I. Y. Lee, C. Baktash, Y. Schutz, J. C. Wells, L. L. Riedinger, M. W. Guidry, and S. C. Pancholi, Phys. Rev. C **37**, 101 (1988).
[85] C. W. Reich, Nucl. Data Sheets **105**, 557 (2005).

[86] C. W. Reich, Nucl. Data Sheets **108**, 1807 (2007).
[87] D. Tonev, A. Dewald, T. Klug, P. Petkov, J. Jolie, A. Fitzler, O. Möller, S. Heinze, P. von Brentano, and R. F. Casten, Phys. Rev. C **69**, 034334 (2004).
[88] T. Kibedi and R. H. Spear, At. Data Nucl. Data Tables **89**, 77 (2005).
[89] J. L. Wood, E. E. Zganjar, C. De Coster, and K. Heyde, Nucl. Phys. A **651**, 323 (1999).
[90] N. Blasi, L. Guerro, A. Saltarelli, O. Wieland, and L. Fortunato, Phys. Rev. C **88**, 014318 (2013).
[91] S. K. Basu and A. A. Sonzogn, Nucl. Data Sheets **114**, 435 (2013).